# Polymer-Metallodrug Conjugates for Cancer Diagnostics and Therapy

INAUGURAL DISSERTATION

submitted to the faculty of

Heinrich-Heine-Universität Düsseldorf
Institut für Anorganische Chemie und Strukturchemie
Lehrstuhl I: Bioanorganische Chemie and Katalyse

in partial fulfillment of the requirements for the degree of

*Dr. rer. nat.*

submitted by

Nadine E. Brückmann

Düsseldorf, November 2010

Printed with permission of the
Mathematisch-Naturwissenschaftliche Fakultät
Heinrich-Heine-Universität Düsseldorf

Graduate referee: Prof. Dr. Dr. W. Kläui

Co-referee: Prof. Dr. C. Ganter

Date of graduate thesis defense: 13.01.2011

## Presentations, Publications and Awards:

Presentations (talks and posters):

Nadine E. Brückmann, Peter C. Kunz, *New Polymer-Metallodrug Conjugates for Cancer Diagnostics*, **2008**, XI$^{th}$ International Seminar for Ph.D. Students on Organometallic and Coordination Chemistry, Sayda, Germany.

Peter C. Kunz, Nadine E. Brückmann, *Bioorganometallics going Polymer: Using the EPR-Effect for Organometallic Drug Targeting*, **2008**, XI$^{th}$ Symposium on Medicinal Organometallic Chemistry, St. Martin in der Pfalz, Germany.

Nadine E. Brückmann, Peter C. Kunz, *Hunting for Tumours with Fluorescent Polymers*, **2009**, 11$^{th}$ JCF - Spring Symposium, Essen, Germany.

Nadine E. Brückmann, Peter C. Kunz, *Fluorescent Polymers for Tumour Diagnostics*, **2010**, ISBOMC 10 - 5$^{th}$ International Symposium on Bioorganometallic Chemistry, Ruhr-Universität Bochum, Germany.

Publications:

Peter C. Kunz, Nadine E. Brückmann, and Bernhard Spingler, *Towards Polymer Diagnostic Agents - Copolymers of N-(2-Hydroxypropyl)-methacrylamide and Bis(2-pyridylmethyl)-4-vinylbenzylamine: Synthesis, Characterisation and Re(CO)$_3$-Labelling*, Eur. J. Inorg. Chem., **2007**, 394-399.

Peter C. Kunz, Michael Berghahn, Nadine E. Brückmann, Marcus Dickmeis, Markus Kettel and Bernhard Spingler, *Functionalised Tris(pyrazolyl)methane Ligands and Re(CO)$_3$ Complexes Thereof*, Z. Anorg. Allg. Chem., **2009**, 635, 471-478.

Nadine E. Brückmann, Susanne Kögel, Alexandra Hamacher, Matthias U. Kassack and Peter C. Kunz, *Fluorescent Polylactides with Rhenium(bisimine)-cores for Tumour Diagnostics*, Eur. J. Inorg. Chem., **2010**, in press.

Awards:

1st poster prize (*Hunting for Tumours with Fluorescent Polymers*, **2009**, 11$^{th}$ JCF - Spring Symposium)

3rd poster prize (*Fluorescent Polymers for Tumour Diagnostics*, **2010**, ISBOMC 10)

*To my beautiful daughter Celine,*

*may her world always be one of curiosity and wonder*

# Acknowledgments

It has been a pleasure working with the faculty, staff and students at the Institute of Inorganic Chemistry I during my tenure as a doctoral student. My thanks go to Professor Dr. Dr. Wolfgang Kläui for the freedom I was given to pursue my research interests and to Dr. Peter Kunz, my long-time advisor and friend for mentoring and advice. Thanks also go to Prof. Dr. Christian Ganter for taking the time to evaluate this dissertation as the co-referee.

Many thanks to my fellow (former) doctoral students Steffen Alfs, Melanie Bongartz, Wilhelm Huber, Arndt Karschin, Dr. Monika Lindner, Mareike Meyer and Corinna Wetzel, graduate student Anna Louisa Noffke, as well as Dr. Udo Beckmann, who made the sometimes tedious research a lot of fun by offering their help and advice and generally creating a wonderful work environment.

Furthermore, I owe my thanks to the staff of the analytical services, Peter Behm (NMR), Dr. Peter Tommes and Ralf Bürgel (mass spectrometry), Dietmar Frunzke (IR spectroscopy), as well as to Dr. Stefanie Weidtkamp-Peters (confocal fluorescence microscopy) from the Institute of Molecular Physical Chemistry, Patricia Bach (GPC analysis) and Bernd Müller (DLS) from the Institute of Organic Chemistry and Macromolecular Chemistry, as well as Denis Dörr (flourescence spectroscopy) from the Institute of Physical Chemistry and Electrochemistry II. For experimental help I thank DAAD exchange student Matthew Merriman, who spent two months in Germany working on rhenium lactide conjugates.

Invaluable for all things concerning cell cultures and microbiology was the cooperation with the Department of Pharmacological Chemistry: Prof. Dr. Matthias U. Kassack, Dr. Alexandra Hamacher, Susanne Kögel and Daniel Esser.

And finally, without the constant encouragement, support and unshattering belief in me, given selflessly by my family and friends, I would not be where I am today. You know who you are. Thank you.

*"The greatest compliment that was ever paid me was when one asked me what I thought, and attended to my answer. I am surprised, as well as delighted, when this happens, it is such a rare use he would make of me, as if he were acquainted with the tool."* - Henry David Thoreau

# Abstract

Polymeric carrier systems have the capability of transporting pharmaceuticals specifically to tumour tissue, where they accumulate due to the so called EPR-effect.[1, 2] By incorporation of cleavable linkers, the drugs can be released at the target site. Polymer-drug conjugates are too large to pass through blood vessel walls and are therefore restricted to the vascular system. This prevents the drugs from distributing throughout the body and causing drug-related side effects. Using this approach, early tumour detection can be greatly improved, because the signal to background noise ratio is enhanced when radiopharmaceuticals are specifically transported to the tumour tissue. Tumour therapy can be similarly improved, since the amount of applied drug at the tumour site in relation to the total applied dose is significantly increased compared to low molecular chemotherapy drugs. In this work, design, synthesis and application related properties of two types of drug conjugates are presented: a multimodal conjugate, incorporating properties for *in vitro* (fluorescence microscopy) and *in vivo* (SPECT) diagnostic imaging as well as therapeutic properties and a conjugate solely for the purpose of cancer and inflammation therapy. Both carrier systems consist of a non-toxic polyhydroxypropylmethacrylate (HPMA) backbone with cleavable polylactide side chains. Degradation of the side chain to lactide acid molecules, which occur naturally in the body, releases the attached drug. Suitable ligand end groups were incorporated in the side chains to function as binding sites for the bioactive metallodrugs.

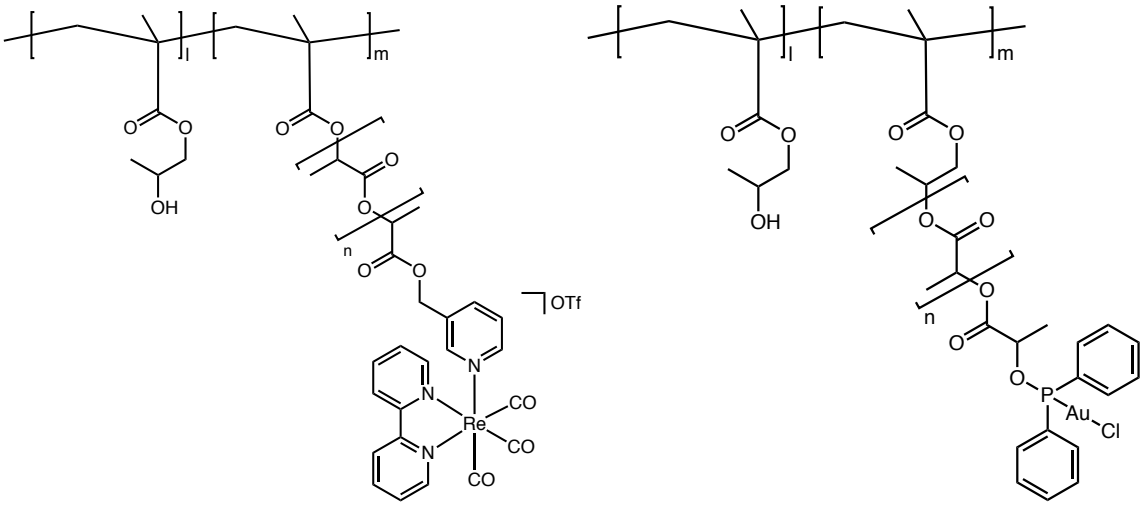


(a) (b)

Polymeric carrier systems with metallodrugs: (a) HPMA-rhenium conjugate (b) HPMA-gold conjugate

The multimodal conjugate bears rhenium tricarbonyl moieties as the bioactive unit. Bisimine ligands were coordinated to the rhenium cores, because they are known to

introduce fluorescence to rhenium tricarbonyl complexes. Three bisimine ligands were investigated: 2,2'-bipyridine (bipy), 1,10-phenanthroline (phen) and dipyrido[3,2-a:2',3'-c]phenazine (dppz), the first two of which were shown to have fluorescence properties useful for *in vitro* diagnostic imaging. Selecting the radioactive $\beta$-emitter $^{186/188}$Re instead of the non radioactive $^{185/187}$Re isotope results in conjugates useful for radiotherapy, selecting the radioactive $\gamma$-emitter of the lower homologue $^{99m}$Tc leads to conjugates useful for radiodiagnostics. The other polymeric carrier system was designed to bear gold(I) cores, which were bound to the carrier by phosphane type ligands. Gold(I)phosphane complexes have shown promising anti-tumour as well as anti-inflammatory activity.[3] The resulting polymer-gold(I) conjugates could thus prove useful not only in cancer therapy but also in the therapy of diseases associated with chronic inflammation such as autoimmune diseases, glaucoma or Alzheimer's. Both types of polymer-metallodrug conjugates were investigated in light of their applicability for drug transport and release. The molecular masses of the conjugates exceed 40 kDa and is thus high enough for the polymers to accumulate in tumour tissue. Polylactide scission kinetics were calculated, showing degradation half lives from 90 minutes to up to 25 hours, depending on the chain length. Since accumulation in the tumour tissue occurs within one hour, the release kinetics are useful for *in vivo* drug release. The degradation products are small enough, with molecular masses of less than 50 kDa, to be excreted by the kidneys. The fluorescence properties of the rhenium conjugates were determined and live cell confocal fluorescence microscopy images taken. The large Stokes shifts of about 11100 cm$^{-1}$ of the bipy and phen rhenium tricarbonyls make identification of the compounds easy, even in a biological context, because they are distinguishable from tissue autofluorescence. Furthermore, toxicity was determined using cytotoxicity assays, viability tests, as well as membrane integrity tests on the A2780 tumour cell line. The compounds show some cytotoxicity (with $IC_{50}$ values in the magnitude of 10 $\mu$M) and do not compromise cell membrane integrity, which is suitable for pharmaceutical purposes.

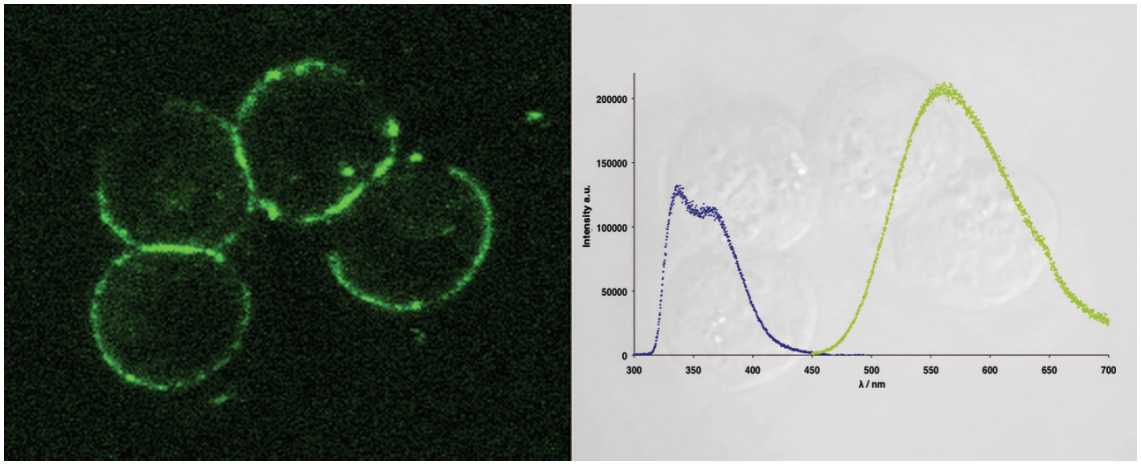


Confocal fluorescence images of $Re(CO)_3$(phen)-polylactide conjugate on A2780 live cells and corresponding fluorescence data: absorption spectrum (blue), emission spectrum (green).

# Abstract

Polymere Trägersysteme sind in der Lage Wirkstoffe gezielt zu tumoralem Gewebe zu transportieren, wo sie aufgrund des sogenannten EPR-Effektes akkumulieren.[1, 2] Verwendet man spaltbare Seitenketten, an welche der Wirkstoff gebunden ist, so lässt sich der Wirkstoff am Zielort freisetzen. Polymer-Wirkstoff-Konjugate haben den großen Vorteil, dass sie Blutgefäßwände nicht passieren können, sie sind auf das vaskuläre System beschränkt. Der Wirkstoff verteilt sich demnach nicht im gesamten Körper, wie es kleine Wirkstoffmoleküle üblicherweise tun, wodurch wirkstoffbezogene Nebenwirkungen vermieden werden können. Macht man sich polymere Trägersysteme in der Krebsdiagnostik zunutze, so dass Radiopharmaka direkt ins Tumorgewebe transportiert werden, erhöht sich das Signal zu Rauschen Verhältnis und selbst kleine Tumore können frühzeitig entdeckt werden. In der Krebstherapie kann man auf diese Weise, verglichen mit niedermolekularen Chemotherapeutika, das Verhältnis der am Wirkort vorhandene Dosis zur verabreichten Dosis erhöhen. In dieser Dissertation werden Design, Synthese und anwendungsbezogene Eigenschaften von zwei Polymer-Wirkstoff-Konjugaten vorgestellt: ein multimodales Konjugat, das sowohl Eigenschaften für *in vitro* (Fluoreszenzmikroskopie) und *in vivo* Diagnostik (SPECT) als auch für therapeutische Anwendungen in sich vereinigt und ein weiteres Konjugat, welches ausschließlich für therapeutische Zwecke einsetzbar ist. Beide Trägersysteme bestehen aus einem ungiftigem Polyhydroxypropylmethacrylat (HPMA) Rückgrat mit spaltbaren Polylactid Seitenketten. Abbau der Seitenkette zu kleinen Milchsäuremolekülen, wie sie ohnehin im Körper vorkommen, setzt den Wirkstoff frei. Geeignete Ligandsysteme, die den Wirkstoff an das Transportsystem binden, wurden als Endgruppen an den Seitenketten eingeführt.

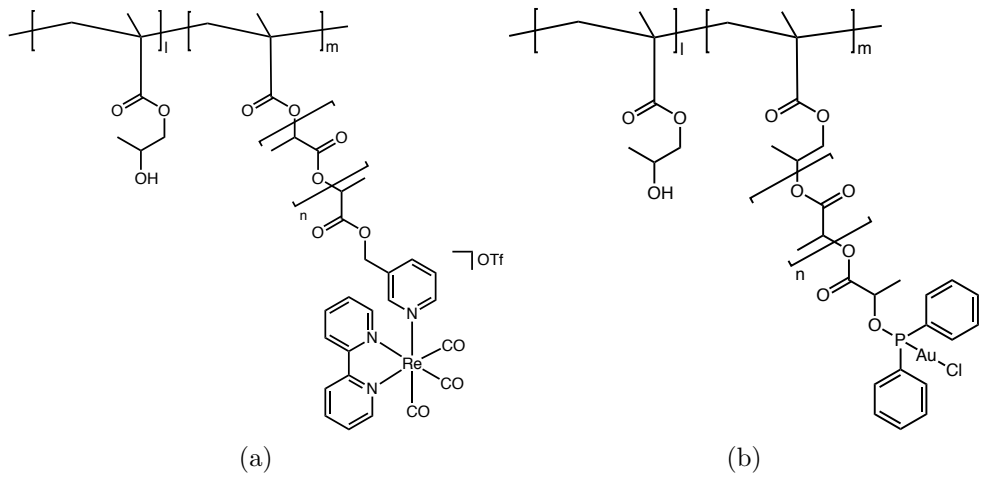


(a) (b)

Polymere Trägersysteme mit Metall-Wirkstoffen: (a) HPMA-Rhenium Konjugat (b) HPMA-Gold Konjugat

Das multimodale Konjugat trägt Rheniumtricarbonyl Einheiten als aktiven Wirkstoff. Bisiminliganden wurden an Rhenium koordiniert, um Fluoreszenzeigenschaften einzubrin-

gen. Drei Bisiminliganden wurden untersucht: 2,2'-Bipyridin (bipy), 1,10-Phenanthrolin (phen) und Dipyrido[3,2-a:2',3'-c]phenazin (dppz). Es konnte gezeigt werden, dass die Komplexe mit bipy und phen Liganden für die Fluoreszenzmikroskopie geeignet sind. Wählt man den radioaktiven $\beta$-Emitter $^{186/188}$Re an Stelle des stabilen $^{185/187}$Re Isotops, so erhält man Konjugate für die Strahlentherapie. Wählt man den radioaktiven $\gamma$-Emitter $^{99m}$Tc, so erhält man Konjugate, die für die Computertomographie geeignet sind. Das andere Polymer-Konjugat wurde entwickelt, um Gold(I)-Komplexe zu transportieren, welche mit Hilfe von Phosphan- bzw. Phosphinitliganden an das Polymer gebunden werden. Gold(I)phosphan-Komplexe haben in ersten Studien vielversprechende Antitumoraktivität gezeigt[3] und wirken zudem Entzündungshemmend. Die dargestellten Polymer-Gold(I)-Konjugate könnten demnach Erfolg versprechend in der Therapie nicht nur von Krebs, sondern auch von Krankheiten mit chronischen Entzündungen wie Autoimmunerkrankungen, Glaukom oder Alzheimer eingesetzt werden. Die dargestellten Konjugate wurden im Bezug auf ihre Verwendbarkeit als Wirkstofftransporter untersucht. Das Molekulargewicht der Konjugate überschreitet 40 kDa, was für eine Akkumulation im Tumorgewebe ausreicht. Die Abbau-Kinetik der Polylactid Seitenketten wurde berechnet, Halbwertszeiten betragen von 90 Minuten bis zu 25 Stunden, je nach Kettenlänge - die Akkumulation im Zielgewebe dauert etwa eine Stunde, so dass der Wirkstoff im Tumor freigesetzt werden kann. Die übrigbleibenden Fragmente haben Molekulargewichte unter 50 kDa und sollten über die Nieren ausgeschieden werden können. Des Weiteren wurden die Fluoreszenzeigenschaften der Rhenium-Konjugate bestimmt und konfokalmikroskopische Aufnahmen durchgeführt. Die großen Stokes Verschiebungen von etwa 11100 $cm^{-1}$ der Rheniumtricarbonyle mit bipy bzw. phen Liganden machen eine Identifikation der fluoreszierenden Polymere einfach, da sich ihre Fluoreszenz leicht von der Eigenfluoreszenz des Gewebes unterscheiden lässt. Zusätzlich wurde die Toxizität der Verbindungen mit Hilfe von Zytotoxizitäts- und Viabilitätstests sowie Tests zur Membranintegrität an der Tumorzelllinie A2780 bestimmt. Die Verbindungen zeigen eine gewisse Zytotoxizität ($IC_{50}$ Werte in der Größenordnung von 10 $\mu$M) und beeinträchtigen die Membranintegrität nicht, was für die pharmazeutische Anwendung geeignet sein sollte.

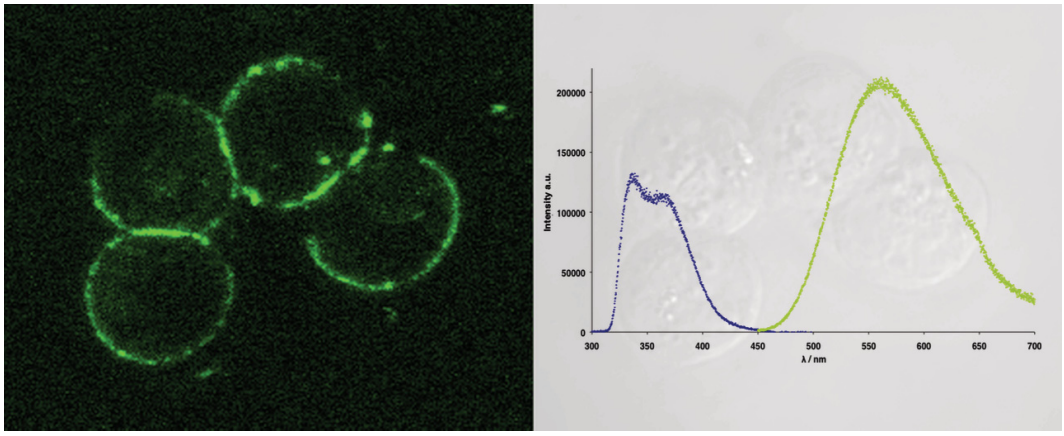


Konfokalmikroskopische Aufnahmen von $Re(CO)_3$(phen)-polylactid Konjugate auf A2780 Zellen und zugehörige Fluoreszenzdaten: Absorptionsspektrum (blau), Emissionsspektrum (grün).

# Contents

# Abbreviations

| | |
|---|---|
| AIBN | 2,2'-azobis(2-methylpropionitrile) |
| bipy | 2,2'-bipyridine |
| CTA | chain transfer agent |
| DMF | dimethyl formamide |
| DMSO | dimethyl sulfoxide |
| DLS | dynamic light scattering |
| dppz | dipyrido[3,2-a:2',3'-c]phenazine |
| EPR | enhanced permeability and retention |
| GPC | gel permeation chromatography |
| HMP | hydroxymethyl pyridine |
| HOMO | highest occupied molecular orbital |
| HPMAn | N-(2-hydroxypropyl)methacrylamide |
| HPMAo | N-(2-hydroxypropyl)methacrylate |
| IR | infrared spectroscopy |
| i.v. | intravenous |
| LUMO | lowest unoccupied molecular orbital |
| MALDI-TOF | matrix assisted laser desorption ionisation - time of flight |
| MLCT | metal-to-ligand charge transfer |
| MTT | 3-(4,5-dimethylthiazol-2-yl)-2,5-diphenyltetrazolium bromide |
| MMA | methyl methacrylate |
| NMR | nuclear magnetic resonance |
| OTf | trifluoromethanesulfonate |
| Ph | phenyl |
| phen | 1,10-phenanthroline |
| PLA | polylactide |
| py | pyridyl |
| RAFT | reversible addition-fragmentation chain transfer |
| ROP | ring-opening polymerisation |
| SPECT | single photon emission computed tomography |
| THF | tetrahydrofuran |
| tht | tetrahydrothiophene |
| triflate | trifluoromethanesulfonate |
| tpm | tris(pyrazolyl)methane |
| tppa | tris(pyrazolyl)propyl alcohol |

# Part I.

# Introduction

# 1. The application of polymers in medicine

Conventional chemotherapy is usually a series of injections of highly toxic drugs, which are small enough to leave the vascular system by passing through pores in the blood vessel walls. Therefore, they are distributed throughout the body. These drugs owe what little selectivity they have for cancer cells to their higher proliferation rates. This can lead to increased toxicities against normal tissues that also show enhanced proliferative rates, such as the bone marrow, gastrointestinal tract and hair follicles. The resulting severe side effects often restrict the frequency and size of dosages, much to the detriment of tumour inhibition.[4, 5]

The selective toxicity of an anticancer drug can be increased by either increasing the dose of the drug that reaches the diseased tissue or by decreasing the dose that reaches normal tissues. Several approaches for improving the selective toxicity of anticancer therapeutics are being pursued at present, one of them being the conjugation of anticancer-drugs to macromolecular carrier systems.

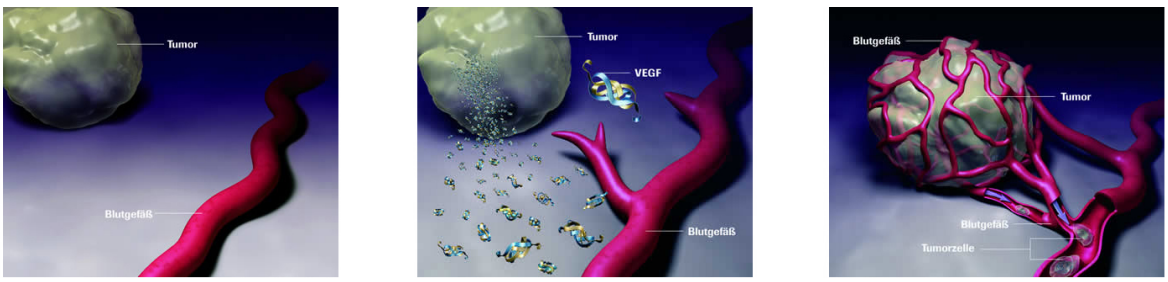


Figure 1.1.: Pathological angiogenesis through the release of VEGFs by solid tumours[6].

Conjugated to polymers, drugs are limited to the vascular system, which prevents them from distributing throughout the body and causing side effects. The conjugated drugs can be transported directly to the area of drug effect. Passive targeting by polymers is possible because macromolecular systems accumulate in tumour tissue due to the so called 'enhanced permeability and retention effect' (EPR-effect), first described and investigated by Maeda *et al.*[1, 2]

Small tumours are sustained by diffusion of nutrients and oxygen. Tumours that reach a size of about 2 millimetres in diameter, however, need to be supplied by active transport of oxygen and nutrients for further growth. To that end, they induce pathological

neoangiogenesis by releasing vascular endothelial growth factors (VEGFs) into the extracellular space (see fig. 1.1). VEGFs bind to and activate receptors located on the membrane of endothelial cells, triggering the corresponding intracellular pathways which lead to the transcription of angiogenesis-related genes, resulting in the growth of blood vessels that interpenetrate the tumour tissue. Moreover, VEGFs increase vascular permeability by weakening inter-endothelial cell contacts and destabilising the pre-existing vessels.[7]

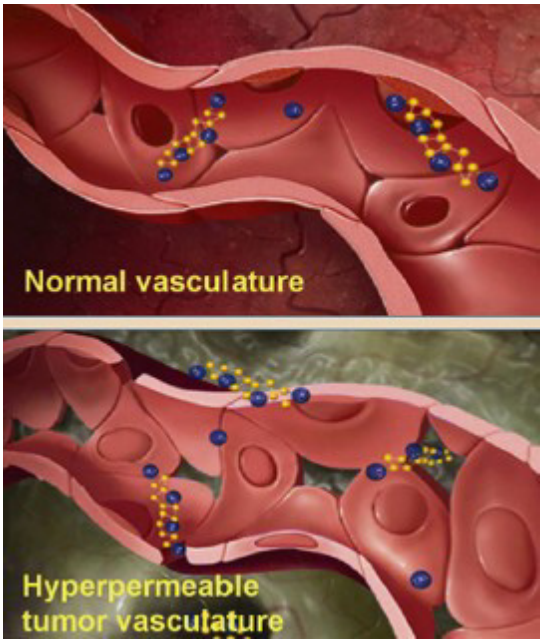


Figure 1.2.: Vasculature of healthy in comparison to tumour tissue[8].

The resulting blood vessels are lacking the tight junctions that are normally present between adjacent vascular endothelial cells, which leaves holes an order of magnitude greater than normal vascular pores (healthy tissue has pores of 5 to 8 nm, tumour tissue can have pores of about 50 nm and interendothelial junctions of about 500 nm). These defects allow for the extravasation of polymers into the tumour interstitium (see fig. 1.2). Since tumours are not part of the lymphatic system, polymer that is present extracellularly cannot be removed and returned to the blood compartment, which explains why polymers accumulate in tumour tissue. This significantly increases the amount of drug delivered to solid tumours relative to the free drug. At the same time, peak drug levels and distribution of the drugs to normal tissues is decreased, leading to fewer side effects, and sometimes even drug resistances can be circumvented.[9] Studies done by Maeda showed that macromolecules above a molecular weight threshold of 40 kDa are retained in the tumour interstitium for more than three to four weeks.[10]

Once inside the tumour interstitium, polymers are taken up by the cells via endocytosis pathways, depicted in figure 1.3. During endocytosis a significant drop in the pH value takes place from the physiological value of pH 7.2-7.4 in the extracellular space to pH 6.5-5.0 in the endosomes and to around pH 4.0 in primary and secondary lysosomes. A great number of lysosomal enzymes, such as phosphatases, nucleases, proteases and esterases, become active in the acidic environment of these vesicles. This can be used for on site drug release when the active drug is bound to the polymer via a cleavable linker.[11]

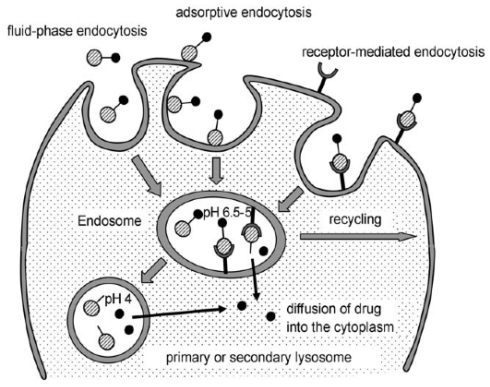


Figure 1.3.: Endocytotic cellular uptake of macromolecules[11].

The concept of polymer-anticancer conjugates was first proposed in 1975 by Helmut Ringsdorf. These macromolecular prodrugs consist of a minimum of three components: polymeric carrier, biodegradable polymer-drug linker and the antitumour agent (see fig. 1.4).[12, 13]

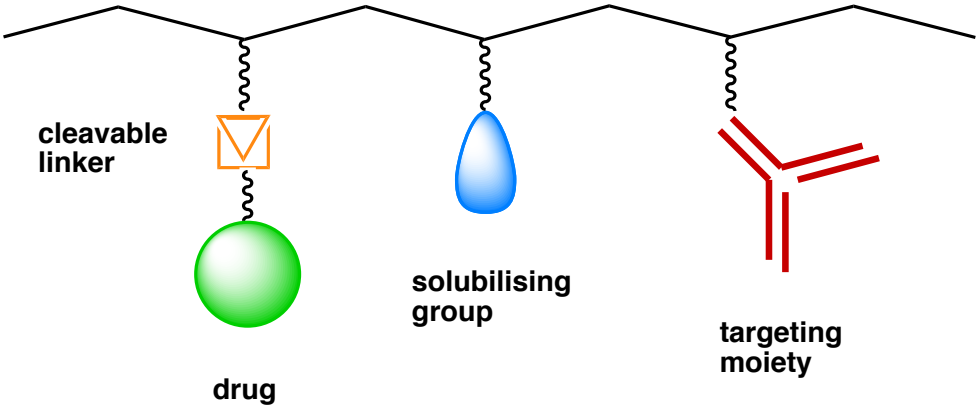


Figure 1.4.: Concept of multimodal linear carrier systems with active targeting functionality, adapted from[11].

In order to be effective, systemically administered polymer-drug conjugates must reach cancer cells in sufficient quantities to elicit a response and assume their active form within the tumour. Systemically administered nanomedicines should have diameters ranging from 10 to 200 nm. This size range is prescribed by human anatomy - the polymers must be larger than 10 nm in diameter to avoid first-pass elimination through the kidneys and smaller than 200 nm to avoid sequestration by the reticuloendothelial system in liver and spleen.[14] Furthermore, there are criteria to be met for the application of such carrier systems in the clinic:[15]

- The carrier must not increase overall toxicity or induce an immune response
- It must be suitable for industrial-scale manufacture
- Polymer molecular weight should be high enough to ensure long circulation and accumulation at the area of effect
- For non-biodegradable polymeric carriers the molecular weight (Mw) must be less than 50 kDa to enable renal elimination of the carrier following drug delivery
- The polymer must have sufficient drug loading capacity to show a therapeutic effect
- Controlled release of the active drug at the target site, tailored by the stability of the linker

The choice of an appropriate water-soluble polymer is crucial for systemic administration. The linear or branched polymer chain usually functions as the structural component of a conjugate. Most of the clinically tested polymer-drug and polymer-protein conjugates have the typical structure consisting of polymer backbone, a linker and the bioactive unit.
However, much more elaborate multicomponent compositions now exist, with additional functionalities for cell-specific targeting or nuclear localisation (see fig. 1.4). They also allow the administration of drug combinations simply by attaching several different bioactive molecules to one drug carrier. Modern polymer chemistry is developing increasingly intricate polymer carriers, such as multivalent, branched or graft polymers as well as micelles, dendrimers and the like. Their potential advantages include a more defined chemical composition, tailored surface multivalency and creation of three-dimensional architectures.[16] An overview over such structures is shown in figure 1.5.

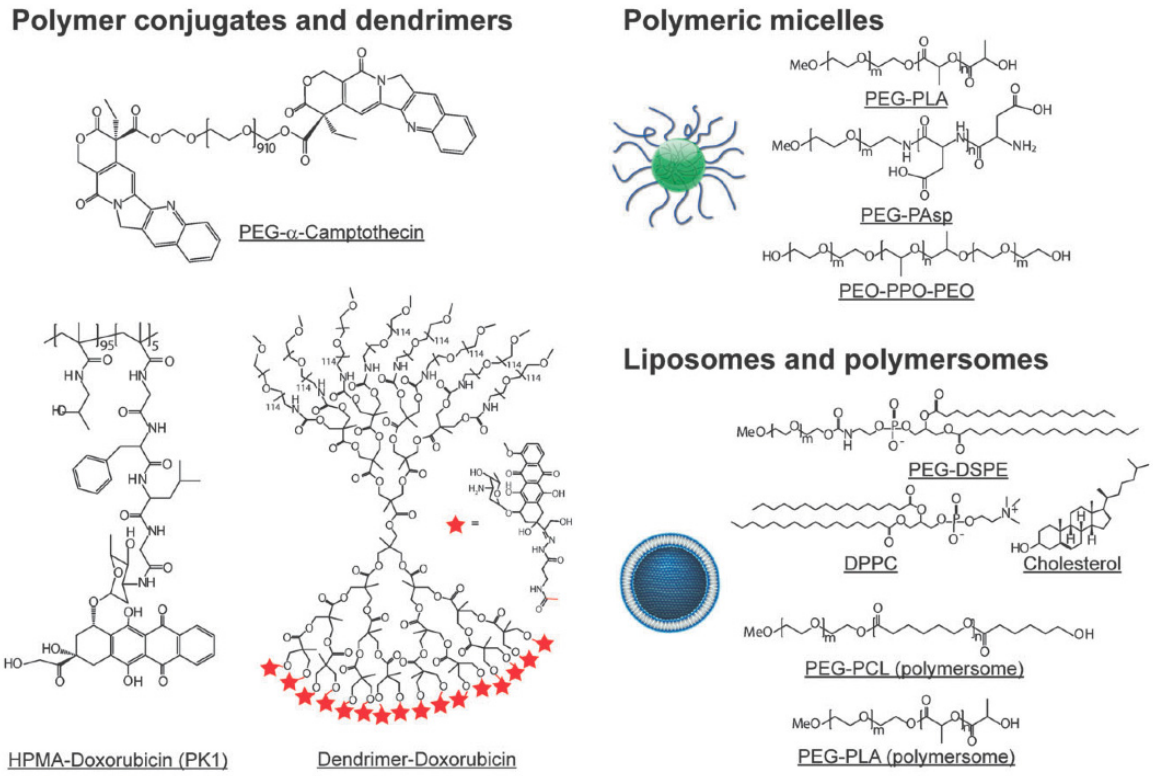


Figure 1.5.: Realised architectures for polymeric conjugates and carrier systems including linear polymers, dendrimers, micelles, liposomes and polymersomes[16].

So far, polymers with a linear, random-coil structure have been used to synthesise the polymer therapeutics that have been transferred to the clinic. These include synthetic polymers such as PEG, HPMA (N-(2-hydroxypropyl) methacrylamide) or PVP poly(vinyl pyrrolidone), natural polymers like dextran or chitosan and pseudosynthetic

polymers such as poly(amino acids).[17] By their very nature, polymers present specific challenges for pharmaceutical development. A manufactured drug substance should be homogeneous and composed of a single, defined species. By contrast, all polymers are inherently heterogeneous. Pharmacokinetics vary depending on chain length, which makes the development of carriers with low dispersity and their careful characterisation of the conjugates particularly important. The average molecular weight is described by the terms 'weight average molecular weight' ($M_w$) and 'number average molecular weight' ($M_n$), and the ratio $M_w/M_n$ gives a measure of the polydispersity.

$$M_n = \frac{\sum M_i N_i}{\sum N_i} \qquad M_w = \frac{\sum M_i^2 N_i}{\sum M_i N_i} \tag{1.1}$$

Polymers extracted from natural sources and synthetic polymers made by radical polymerisation are particularly polydisperse ($M_w/M_n \sim 2$). However, depending on the mechanism of polymerisation, narrower size distributions of the polymer chain lengths ($M_w/M_n = 1.3$ to 1.1) can be realised. New synthetic methods and dendrimer chemistry are even moving towards the production of macromolecules that are monodisperse ($M_w/M_n = 1$) like proteins.[17]

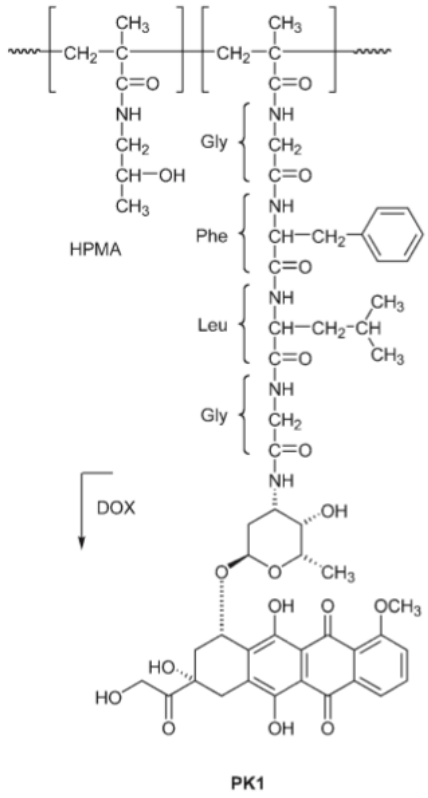


Figure 1.6.: HPMA-doxorubicin conjugate with tetrapeptide linker (PK1), in Phase II clinical trials[11].

A lot of research has been done recently to covalently attach chemotherapy drugs to polymeric carrier systems in order to change pharmacokinetic properties. For liberation of the attached bioactive molecule at the tumour site, careful tailoring of the cleavable linker is required. Linkers that are too stable prevent drug liberation and access to the pharmacological target, linkers that degrade too quickly lead to premature drug release and drug-related side effects. Peptidyl polymer-drug linkers were successfully incorporated in HPMA copolymer-Gly-Phe-Leu-Gly-doxorubicin conjugates. This tetrapeptide linker is stable in the circulation, but is cleaved by the lysosomal thiol-dependent protease cathepsin B following endocytic uptake of conjugate from the tumour interstitium.[18] Other enzymatically cleavable and hydrolysable linkers, such as polyesters and polyamides, as well as pH-sensitive functionalities such as cis-aconityl, hydrazone and acetal linkages have also been incorporated in polymeric carrier systems.[19, 20, 21]

The proton pumps present in the endosomal and lysosomal membranes create an acidic intravesicular environment (pH 6.5-4.0), which means that drug liberation is triggered following internalisation of the conjugate into the cells. A HPMA copolymer conjugate containing doxorubicin bound via hydrazone linkages for example has recently shown significantly improved antitumour activity against lymphoma *in vivo*, compared to the corresponding tetrapeptide conjugate.[22]

Most of the polymer-drug conjugates that have been tested clinically have used HPMA copolymers as the polymer backbone. Poly-HPMA was originally developed by Kopecek *et al.*[23, 24] It is a water-soluble, non-immunogenic, synthetic polymer, which shows no long term toxicity *in vivo*.[25] Collaborative research with Duncan *et al.* in the early 1980s produced two HPMA copolymer-doxorubicin conjugates (PK1, depicted in fig. 1.6, and PK2) that progressed into Phase I/II evaluation.[26, 27] The development of HPMA-drug conjugates was an important milestone for the use of polymers as nanocarriers, since it brought the new concept into clinical trials for the first time. This novel, non-biodegradable polymer had never before been administered to patients. HPMA copolymer molecular weight (Mw $\sim 30,000$ g/mol) was optimised to ensure renal elimination, while allowing tumour targeting at the same time. Then, the potential toxicity of the HPMA copolymer itself and each individual anticancer conjugate that was subsequently derived from it was carefully examined.[28, 29] By now, HPMA is approved by the FDA as a polymer suitable for medical application.

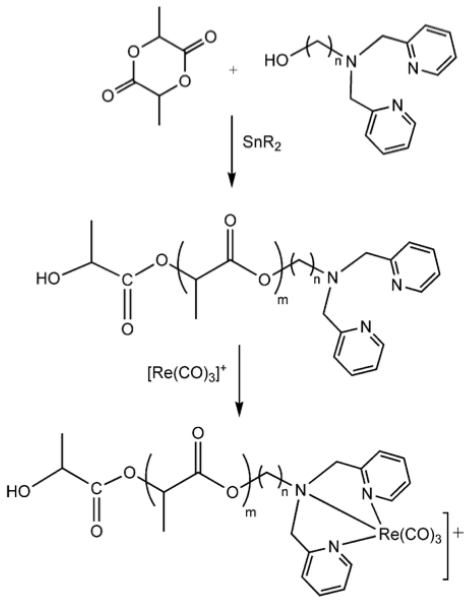


Figure 1.7.: Bis(2-picolylamine) functionalised polylactide and metal coordination[30].

Recently, Saatchi and Häfeli described the concept of using the hydroxy functionalised tridentate bis(2-picolyl)ethanolamine ligand as initiator for the ring opening polymerisation of lactides.[30] This way, polylactides can be synthesised bearing the tridentate ligands. Polylactides are hydrolytically and enzymatically degradable. The resulting ligand functionalised polymers can be used to coordinate specific metal ions, such as rhenium or technetium tricarbonyl moieties, which are useful for radiotherapy and nuclear imaging. The drawback of these polylactides is that they are water-insoluble and have a drug loading capacity of one molecule per carrier. However, ligand functionalised lactides could be useful as cleavable side chains, incorporated in larger macromolecules. This way, solubility can be adjusted using water-soluble backbones and drug loading capacity can be drastically increased.

# 2. Metallodrugs for radiotherapy and nuclear imaging

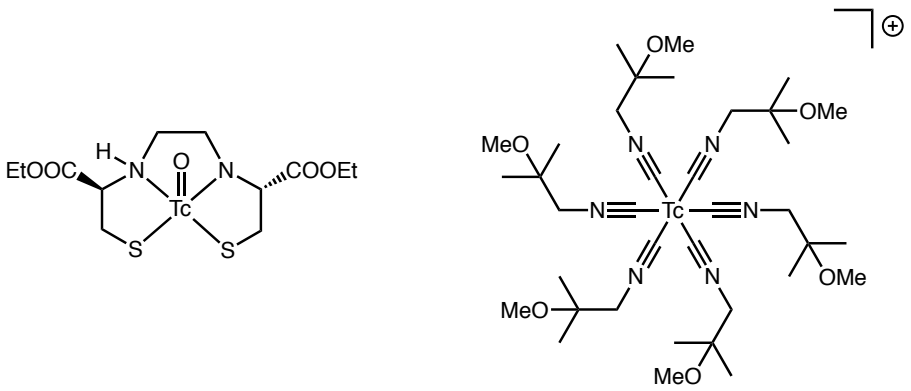


Figure 2.1.: Technetium radiopharmaceuticals: Tc-bicisate and Tc-sestamibi

In the past few decades, attachment of chemotherapy drugs to polymers has been studied intensively. Research into the development of radiotherapy and nuclear imaging nanomedicines, so called radiopharmaceuticals, however, have been few and far between. Improving imaging is particularly important, since cancer is a highly heterogeneous disease caused by genetic instability and accumulation of multiple molecular alterations. Lack of effective diagnostic methods at its early onset is a major reason for unsuccessful treatment and prevents complete eradication of the disease. Cancer is often diagnosed too late, when cancer cells have already invaded and metastasised into other parts of the body. At the time of clinical presentation, for example, more than 60 % of patients with breast, lung, colon, prostate and ovarian cancer have hidden or overt metastatic colonies.[31] Passive targeting with polymers should be very promising, because the EPR effect is much more pronounced in small, fast growing tumours. Conjugation of radiotracers such as technetium $^{99m}$Tc to polymers and their deliberate accumulation in tumour cells could greatly improve early cancer diagnosis. A major advantage of conjugates over small molecular tracers is that it drastically reduces the signal to noise ratio, making even small tumours visible, which is unprecedented so far.[16, 32]

Depending on which imaging modality is used, anatomical or molecular information can be obtained. Nuclear imaging techniques such as positron emission tomography (PET) or single photon emission computed tomography (SPECT) have excellent sensitivity and can provide biochemical information. In comparison, computed tomography (CT) and magnetic resonance imaging (MRI) have high spatial and temporal resolutions and can

provide superb anatomical information. Optical, fluorescent and confocal imaging on the other hand provide insight into molecular and cellular processes.[33, 34]

Metallic radionuclides are of particular interest for the development of radiopharmaceuticals due to their wider range of nuclear properties, such as type of radiation (gamma ray or beta particle energy), their half life, as well as their rich coordination chemistry. $^{99m}$Tc radiopharmaceuticals are the most widely used tracers for diagnostic nuclear medicine. The main reasons for the versatility of $^{99m}$Tc are not only its decay characteristics ($\tau_{1/2}$ = 6 h, $\gamma$-emission, 141 keV) but also its low price and availability using a $^{99}$Mo-$^{99m}$Tc generator. One such radiopharmaceutical, the complex cation $^{99m}$Tc-sestamibi (see Fig. 2.1) is widely used as a myocardial perfusion imaging agent, while neutral $^{99m}$Tc complexes such as $^{99m}$Tc-bicisate [$^{99m}$TcO(L,L-ethylenedicysteine diethyl ester)] are used to measure cerebral blood flow.[35, 36, 37]

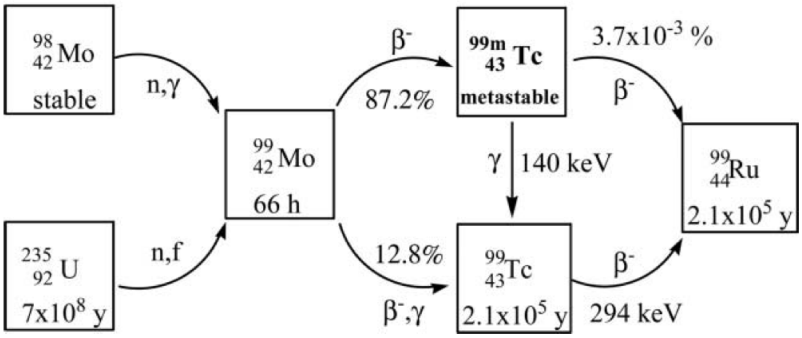


Figure 2.2.: Image shows the different isotopes and decay characteristics of the $^{99}$Mo-$^{99m}$Tc generator for the production of $^{99m}$Tc[36].

The higher homologue $^{188}$Re ($\tau_{1/2}$ = 17 h, high energy $\beta$-emission, 2.12 MeV, 85% abundance; $\gamma$-emission, 155 keV, 15% abundance) is interesting for radiotherapy, again, not only because of its decay characteristics, but because it is inexpensive and readily available using a $^{188}$W-$^{186}$Re generator.[36] For labelling purposes, the technetium and rhenium tricarbonyl cores $[M(CO)_3]^+$are extremely useful, since the metal centre is in the low oxidation state +I and therefore chemically very inert. The cores are very compact, with an almost spherical shape. Octahedral coordination with suitable ligands results in kinetically inert $d^6$ metal complexes that are efficiently protected against ligand exchange or re-oxidation.[38, 39] For rhenium as well as technetium, convenient preparation of the precursor $[M(CO)_3(H_2O)_3]^+$ is possible even at normal pressure in high yields.[40, 41, 42] This satisfies the requirement of being simple enough to be used in a kit formulation, because they need to be prepared within a routine clinical environment.

On top of the nuclear imaging properties of the radioactive isotopes, fluorescence can be introduced to the complexes by coordinating aromatic bisimine ligands. This way they are also detectable *in vitro* with confocal fluorescence microscopy. Fluorescence microscopy is a powerful, high resolution technique in biological imaging and specific fluorescent staining techniques make it especially useful for diagnostic investigations of

tissue samples. This technique has the potential to bridge the gap between clinical examination and invasive biopsy and thus facilitate the early detection and diagnosis of neoplastic changes. One of the challenges, however, is to differentiate the endogenous fluorescence of biological species (autofluorescence) from that derived from a dye which is applied to specifically stain a target organelle or cell component.[43, 44] Many of the endogenous fluorophores in tissue have been identified and are summarised in Table 1.1.[45]

| Fluorophores | Excitation maxima (nm) | Emission maxima (nm) |
|---|---|---|
| NADH | 290,340 | 440,450 |
| FAD | 450 | 515 |
| Collagen cross-links | 325 | 400 |
| Elastin cross-links | 325 | 400 |
| Collagen powder | 280,265,330,450 | 310,385,390,530 |
| Elastin powder | 350,410,450 | 420,500,520 |
| Tryptophan | 280 | 350 |
| Tyrosine | Not determined | 300 |
| Phenylalanine | Not determined | 280 |
| Pyridoxine | 332 | 400 |
| Lipofuscin | 340-395 | 430-460,540 |
| Eosinophils | 370,500 | 440,550 |

Figure 2.3.: Endogenous fluorophores, table as published in[45]

Autofluorescence may be filtered out from the desired signal when there is an appreciable difference in wavelength between the two modes of fluorescence and this is particularly likely if the dye has a large Stokes shift, as the typical Stokes shifts for the species involved in autofluorescence are comparatively small. Certain transition metal complexes offer Stokes shifts and lifetimes which allow differentiation from autofluorescence. In particular, there are ruthenium and rhenium complexes which have well understood fluorescence properties stemming from a triplet metal-to-ligand-charge-transfer ($^3$MLCT), which is characterised by large Stokes shifts (see fig. 2.4). The most studied system is ruthenium trisbipyridyl, however the excited state can be localised on any of the three bipyridine units. Conversely, *fac* rhenium tricarbonyl bipyridines and related species offer systems in which the excited state is localised on one single bipyridine unit, which leaves one coordination site available for further modification.[46, 47]

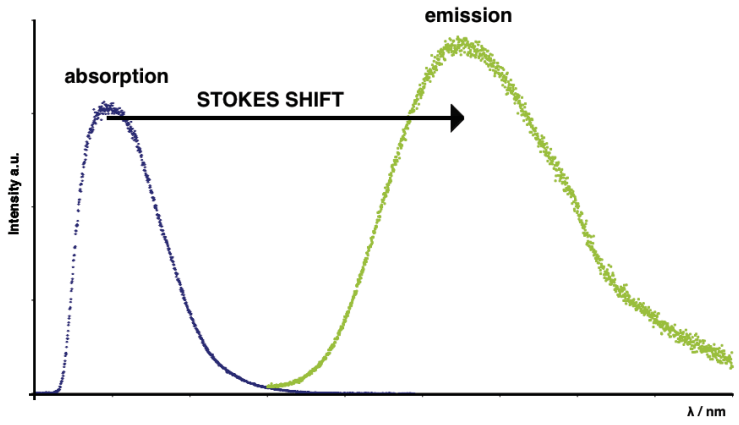


Figure 2.4.: Large Stokes shift, typical for $[Re(CO)_3(bisimine)]^+$ and $[Ru(bisimine)_3]^{2+}$ complexes.

Conjugation of rhenium tricarbonyl bisimines to a polymer carrier by using a monodentate ligand for attachment according to the [2+1] mixed ligand approach[48] could lead to interesting multimodal polymer-drug conjugates with fluorescence imaging and radiotherapy or -diagnostic properties.

# Part II.

# Main

# 3. Concepts for polymer metallodrug conjugates

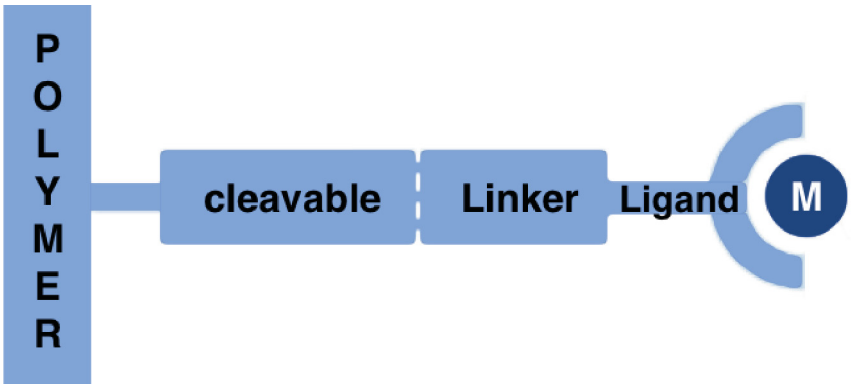


Figure 3.1.: General structure of a polymer-drug conjugate. M = metallodrug.

In light of the aforementioned requirements and considerations for polymer-drug conjugates and the research that has been done so far, a concept for the development of conjugates with cleavable side chains for the release of metallodrugs is presented. In general, a polymer backbone is needed as an attachment site for ligand functionalised side chains. This combines high molecular weight carrier systems, which are needed for tumour targeting, with high drug loading. In contrast, PEG polymers, which are also used as polymeric carriers can only carry two drug molecules per polymer, since the only site of derivatisation is the hydroxyl group on the chain end. The ligand functionalised polylactides proposed by Saatchi and Häfeli can even bind only one metallodrug per polymer. Increasing the drug loading capacity per carrier greatly increases the applied drug dose compared to the amount of intravenously applied polymer conjugate. The attached degradable side chains need to liberate the conjugated complex over a period of several hours, since it takes about an hour for a macromolecule to accumulate in the tumour tissue after injection into the blood stream[2]. The resulting degradation products have to be excretable, which means that the remaining backbone has to have a molecular weight of less than 50 kDa. The low molecular fragments of the side chain that are released during degradation must be non-toxic to prevent additional side effects. Furthermore, for successful coordination and transport of the drug to the target site, the side chains need to be functionalised with a ligand that forms inert complexes with the metallodrug.

With the aim of realising this concept, two different polymer-drug conjugates were developed over the course of this dissertation. The first conjugate **PC1** (shown in fig. 3.2) is capable of transporting and releasing M(I) (M = Tc, Re) tricarbonyl complexes for cancer imaging and therapy, respectively. The second conjugate **PC2** (shown in fig. 3.3) is capable of transporting and releasing Au(I) complexes for chrysotherapy.

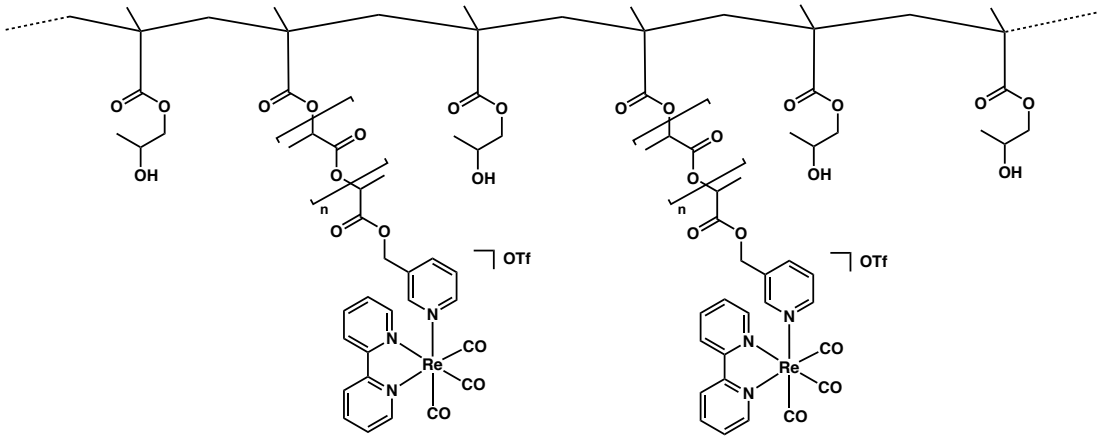


Figure 3.2.: Polymer-drug conjugate **PC1** with cleavable side chains for the release of fluorescent Re(I) metallodrugs.

Conjugate **PC1** is a statistical copolymer with a backbone consisting of methacrylate repeating units, some of which are derivatised with oligolactides. Methacrylates are a family of monomers for radical polymerisation with a variety of properties, depending on the functional groups of the specific methacrylate molecule. The side chains are made up of ligand functionalised oligolactides, which serve as hydrolytically cleavable linkers for release of the attached drug. The degradation of oligolactides releases lactic acid, which is naturally occurring in the body as it is produced during normal metabolism or as a result of muscular exercise. Useful anchor systems to attach $d^6$ metallodrugs to the linker are tridentate NNN- or NNO-ligands, such as tridentate bis(2-pyridylmethyl)amine or amino acid chelate ligands.[30, 33] The 4d and 5d Re(I) and Tc(I) tricarbonyls even form inert $d^6$ low spin complexes with monodentate ligands such as pyridines. The remaining two coordination sites can be used to introduce additional useful properties to the molecule. Conjugate **PC1** incorporates pyridyl ligands anchoring the rhenium tricarbonyl moiety to the polymeric carrier. 2,2'-bipyridine ligands introduce fluorescence properties to the metal complex for imaging purposes.

A similar polymer for the delivery of gold metallodrugs bears phosphinite ligands as anchoring units for the conjugation of gold(I) cores. The resulting conjugate **PC2** is presented in fig. 3.3. Again, the polymeric carrier system consists of a methacrylate backbone combined with cleavable lactide side chains, in this case functionalised with phosphinite ligands coordinating the gold(I) core.

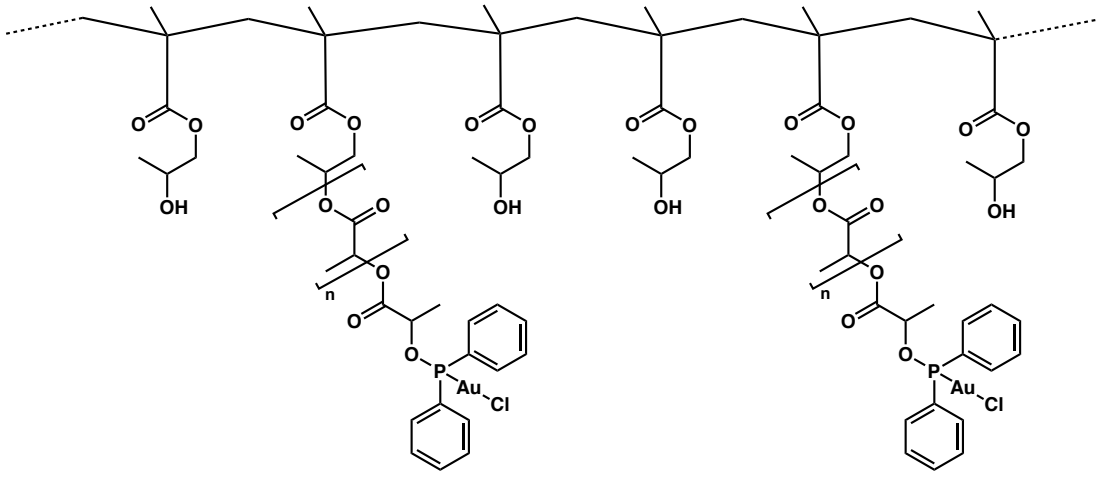


Figure 3.3.: Polymer-drug conjugate **PC2** with cleavable side chains for the release of Au(I) metallodrugs.

The main part of the dissertation thesis is divided into three sections. The first section presents the different steps involved in the preparation and analysis of the rhenium conjugate **PC1** (chapter 4) and the second section presents the steps involved in the preparation and analysis of the gold conjugate **PC2** (chapter 5). The third section covers application specific experiments and calculations that were undertaken to assess the properties of the developed conjugates. The latter encompasses pharmacokinetics, fluorescence properties and cell culture experiments (chapters 6, 7 and 8).

# 4. Development of the polymer-[Re(CO)$_3$] conjugate PC1

## 4.1. Rhenium precursors and complexes for [2+1]-coordination

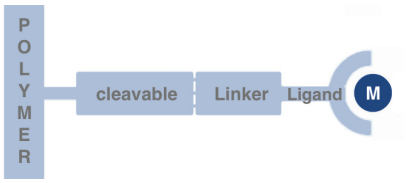


Bearing in mind that the active component in the polymer will most likely be radioactive rhenium or technetium tricarbonyl, a similar component must be integrated in the conjugate, serving as a model substance. The non-radioactive rhenium tricarbonyl cores are useful model components for radiopharmaceutical applications with radioactive technetium and rhenium isotopes, since rhenium is the higher homologue of technetium and their chemistry is quite similar. $Re(CO)_5Br$, and more importantly for *in vivo* applications $[Re(CO)_3(H_2O)_3]Br$, as well as $[Re(CO)_3(DMSO)_3]Br$ can be used as rhenium tricarbonyl precursors that are easily coordinated to carrier systems with tridentate ligands.[41, 49] For attachment of these cores to polymers via monodentate ligands, these precursors need to be reacted with the bidentate co-ligands first. This way, coordination of one metal tricarbonyl fragment to three ligand side chains can be avoided.

### 4.1.1. Coordination chemistry of [Re(CO)$_3$] complexes

The major advantage of $[Re(CO)_3(solvent)_3]Br$ as a precursor is the stability of the *fac* $[Re(CO)_3]^+$ moiety in water and air and the potential of exchanging the labile solvent ligands. The low oxidation state can be stabilised by pH independent ligands (such as phosphanes and aromatic amines), which can hardly be substituted by other ligands.[39] Furthermore, the M-C bonds are reasonably stable and prevent dissociative substitution. The LUMO is too high in energy to enable an interchange or associative reaction pathway - especially due to the sufficiently high ligand energy of carbonyl ligands. Apart from thermodynamic ligand exchange, the rhenium metal possesses a $d^6$ electronic configuration, which makes the resulting 18-electron complexes kinetically inert. Combining these two features, even monodentate ligands, providing low thermodynamic stability, form very inert complexes.

Studies by Alberto *et al.* showed that aromatic amines have a reasonably fast complexation rate and very high thermodynamic and/or kinetic stability, which leads to the conclusion that an aromatic amine is a suitable anchor group between the *fac* $[Re(CO)_3]^+$ moiety and a carrier system.[39, 37]

## 4.1.2. Synthesis of $[Re(CO)_3(bisimine)Br]$ complexes 1a-c

For functionalised polymers with monodentate ligands, two coordination sites are available for further derivatisation. With regard to diagnostic application, as previously discussed, aromatic bipyridine and related ligands coordinated to rhenium tricarbonyls create luminescent complexes with useful properties for fluorescence microscopy.

To this end, rhenium tricarbonyl complexes of 2,2'-bipyridine (bipy) **1a**, 1,10-phenanthroline (phen) **1b** as well as dipyrido[3,2-a:2',3'-c]phenazine (dppz) **1c** were prepared as published with minor modifications[50, 51] (see Fig.4.1).

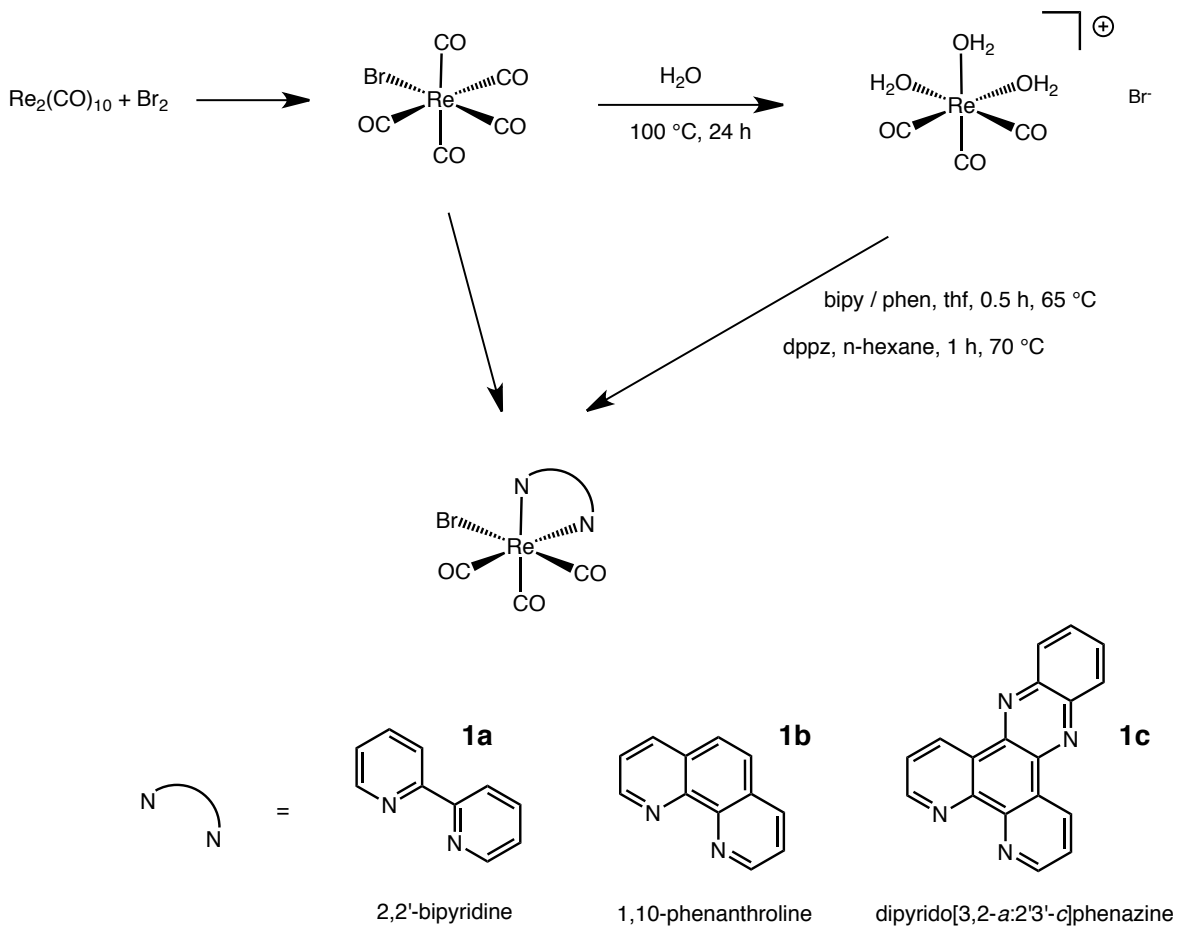


Figure 4.1.: Synthesis of rhenium precursor complexes and rhenium tricarbonyl bisimines.

Starting from rhenium decacarbonyl, $Re(CO)_5Br$ can be afforded after reaction with elemental bromine. Heating a suspension of $Re(CO)_5Br$ in water at 100 °C results in the formation of $[Re(CO)_3(H_2O)_3]Br$.[41] Both rhenium carbonyl precursors are readily reacted with the bisimine in a suitable solvent at temperatures of about 65 °C for up to an hour, whereupon the bright yellow complexes precipitate in yields of about 70 %. The resulting complexes were characterised by $^1H$ NMR and IR spectroscopy as well as ESI-MS.

Table 4.1.: Synthetic and analytical data of the complexes $Re(CO)_3$(bisimine)Br **(1a-c)**.

| **bisimine** | **yield** (%) | $\nu$**(C-O)** ($cm^{-1}$) | $^1$**H NMR** (ppm) |
|---|---|---|---|
| bipy[a] | 82 | 2012 | 9.06 (d, 2H) |
| | | 1905 | 8.80 (d, 2H) |
| | | | 8.37 (m, 2H) |
| | | | 7.79 (m, 2H) |
| phen[b] | 70 | 2017 | 9.48 (dd, 2H) |
| | | 1930 | 9.00 (dd, 2H) |
| | | | 8.36 (s, 2H) |
| | | | 8.14 (m, 2H) |
| dppz[b] | 86 | 2026 | 9.83 (m, 2H) |
| | | 1927 | 9.59 (m, 2H) |
| | | | 8.51 (m, 2H) |
| | | | 8.29 (m, 2H) |
| | | | 8.19 (m, 2H) |

[a] IR: KBr pellet, NMR: $CDCl_3$
[b] IR: KBr pellet, NMR: DMSO-$d_6$

### 4.1.3. Synthesis of $[Re(CO)_3$(bisimine)(3-HMP)]OTf complexes 2a, 2b

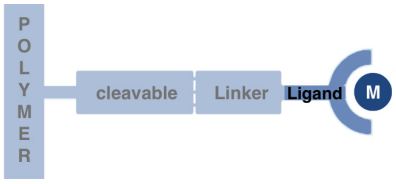


In order to study the properties of complexes resulting from a coordination of the rhenium bisimine complexes to a pyridyl functionalised polylactide, the corresponding complexes with 3-hydroxymethyl pyridine (3-HMP) as the monodentate ligand were prepared. Complex **2a** has been prepared according to literature procedures with minor modifications[44], complex **2b** was analogously prepared (see fig. 4.2).

In brief, the complexes **1a** or **1b** were dissolved in acetone under a nitrogen atmosphere and the halide abstracted with silver triflate. Silver bromide was filtered out after an hour of heating to reflux and the resulting yellow solution of $[Re(CO)_3$(bisimine)-(acetone)]OTf added to a solution of 3-HMP in acetone. The mixture was refluxed for

another hour, whereupon the solvent was removed. The product can be precipitated with diethyl ether from minimal acetone or recrystallised, e.g. from ethanol/diethyl ether with yields of about 80 %. The complexes were characterised by $^1$H NMR and IR spectroscopy as well as ESI-MS (**2a**) / MALDI-TOF (**2b**) spectrometry. Analytical data has been summarised in table 4.4.

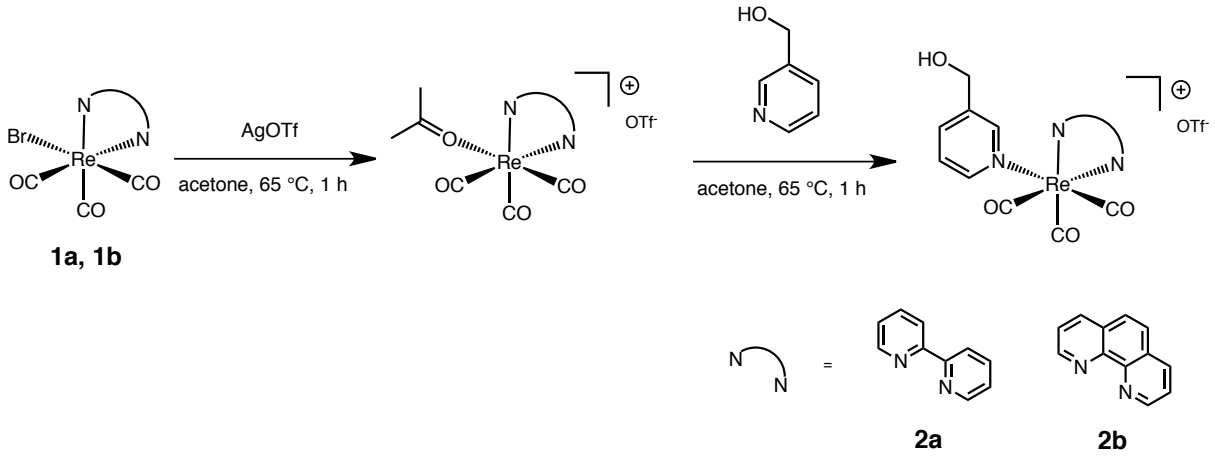


Figure 4.2.: Synthesis of [Re(CO)$_3$(bisimine)(3-HMP)]OTf.

The $^1$H NMR spectra of **2a** and **2b** show the signals of the bisimine as well as the pyridyl proton resonances. Figure 4.3 is a section of the NMR spectrum of **2a** showing the aromatic region of the spectrum. Most signals in the aromatic region of both complexes are baseline separated and can be attributed as illustrated in Fig 4.4. In the case of the 2,2'-bisimine ligand, the signals of the protons on C6 (and C6') are slightly downshifted, whereas the signals of the protons at C3 (and C3') are slightly shifted towards higher field after coordination of the pyridyl ligand. In the case of 1,10-phenanthroline, the signals of the protons at C2/C9 and C5/C6 are slightly downshifted after coordination of the pyridyl ligand. The mass spectra of **2a** and **2b** show the molecular ions as the base peak at 536 and 560 m/z, respectively.

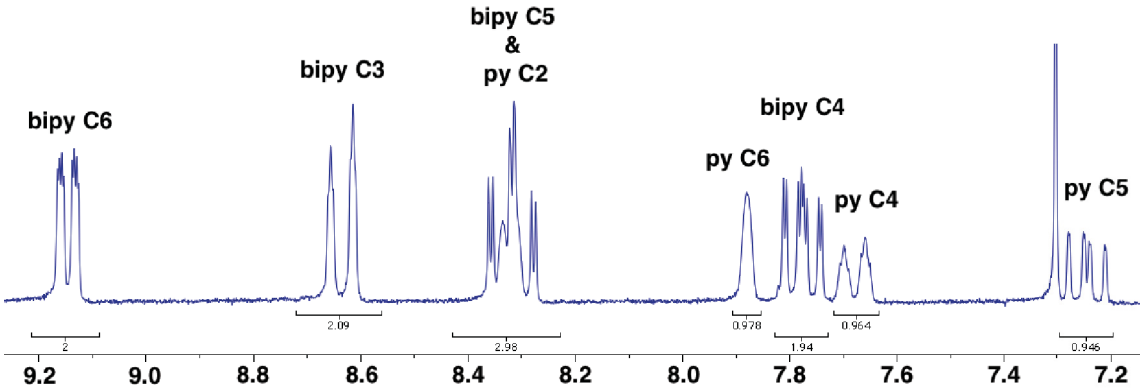


Figure 4.3.: Aromatic proton NMR shifts of [Re(CO)$_3$(bipy)(3-HMP)]OTf in $CDCl_3$. Signal of $CHCl_3$ at 7.26 ppm truncated.


Figure 4.4.: $^1$H NMR shifts of [Re(CO)$_3$(bisimine)(3-HMP)]OTf.

Application specific experiments were undertaken, which are presented and discussed in chapters 6, 7 and 8. In short, cytotoxicity was evaluated towards the human ovarian carcinoma cell line A2780 using a standard MTT assay. This was done to investigate the toxicity of the free complexes upon release from the polymer. To determine cellular localisation, **2b** was incubated for two hours on living A2780 cells and confocal microscopy images were taken. To ascertain the inertness of such complexes under physiological conditions, ligand-challenge experiments with histidine methyl ester as well as cystein methyl ester were carried out and the complex degradation monitored by $^1$H NMR spectroscopy.

Table 4.2.: Synthetic and analytical data of the complexes Re(CO)$_3$(bisimine)(3-HMP)OTf **(2a, 2b)**.

| **bisimine** | **yield** (%) | $\nu$**(C-O)** (cm$^{-1}$) | $^1$**H NMR** (ppm) **(3-HMP)** | | **(bisimine)** | |
|---|---|---|---|---|---|---|
| bipy[a] | 67 | 2031 | 8.34 | (m, 1H) | 9.15 | (m, 2H) |
| | | 1917 | 7.89 | (s,1H) | 8.63 | (d, 2H) |
| | | | 7.68 | (d, 1H) | 8.32 | (m, 2H) |
| | | | 7.24 | (m, 1H) | 7.78 | (m, 2H) |
| | | | 4.53 | (s, 2H) | | |
| phen[b] | 82 | 2031 | 8.38 | (m, 1H) | 9.80 | (m, 2H) |
| | | 1916 | 8.34-8.24 | (m, 1H) | 9.07 | (m, 2H) |
| | | | 7.78 | (m, 1H) | 8.34-8.24 | (m, 4H) |
| | | | 7.30 | (m,1H) | | |
| | | | 4.34 | (s, 2H) | | |

[a] IR: KBr pellet, NMR: $CDCl_3$
[b] IR: KBr pellet, NMR: DMSO-$d_6$

## 4.2. N-Ligand functionalised polylactides

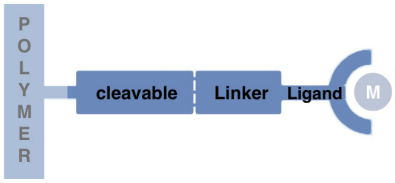


Choosing a polyester, specifically polylactide, as a cleavable side chain is a favourable choice for several reasons. Polyesters are commonly produced by polycondensation reactions from a diol and a diacid or by ring-opening polymerisation (ROP) of cyclic esters. Although the application of condensation polymerisation techniques certainly allows access to a broader range of polymer structures than ROP through a higher accessibility of the monomers involved, the most convenient and efficient method to obtain aliphatic polyesters is the ROP of cyclic esters. In contrast to polyesterification, ROP of cyclic monomers uses mild reaction conditions and avoids the formation of small molecule byproducts. The thermodynamic driving force for ROP processes is the relief of ring strain, which enables the entropy, unfavourable in all polymerisations, to be overcome.[52] Particularly interesting is the use of cyclic dilactides as they are a starting material from a natural, renewable source and the corresponding polylactides are biodegradable as they are hydrolytically and enzymatically cleavable. Metabolisation *in vivo* results in the release of non-toxic lactic acid molecules, which occur naturally in the body.

The synthesis of the ligand functionalised polylactides (PLAs) was carried out using ring-opening polymerisation of the cyclic dilactide L-lactide. Adapting Saatchi and Häfeli's approach of opening lactides with hydroxyl functionalised tridentate ligands, the monodentate 3-hydroxymethyl pyridine (3-HMP) was used as the initiator for the polymerisation.[30, 53] For comparison to the monodentate coordination mode, tridentate tris(pyrazolyl)methane functionalised polylactides were also prepared, which were initiated using 3,3,3-tris(3'-pyrazol-1-yl)propanol (tppa).

### 4.2.1. Mechanism of the ring-opening polymerisation of lactides

Among the various ROP processes, including anionic, cationic, organocatalytic and coordination-insertion, the latter has gained increasing attention. It is now commonly accepted that the most efficient method for the production of well-controlled polyesters in terms of molecular weight, composition and microstructure is the ROP with metal-coordination catalysts, such as tin(II) octoate or zinc(II) lactate. The coordination-insertion mechanism of lactide polymerisation proceeds via coordination of the cyclic dimer to the metal center, followed by insertion into the metal-alkoxide species through the acyl-oxygen bond with retention of the configuration. This results in a new metal-alkoxide species capable of further insertion (see Fig.4.5).

The side reactions of ROP are usually reversible chain transfers with chain scission (via transesterification), which can be either unimolecular (backbiting) or bimolecular

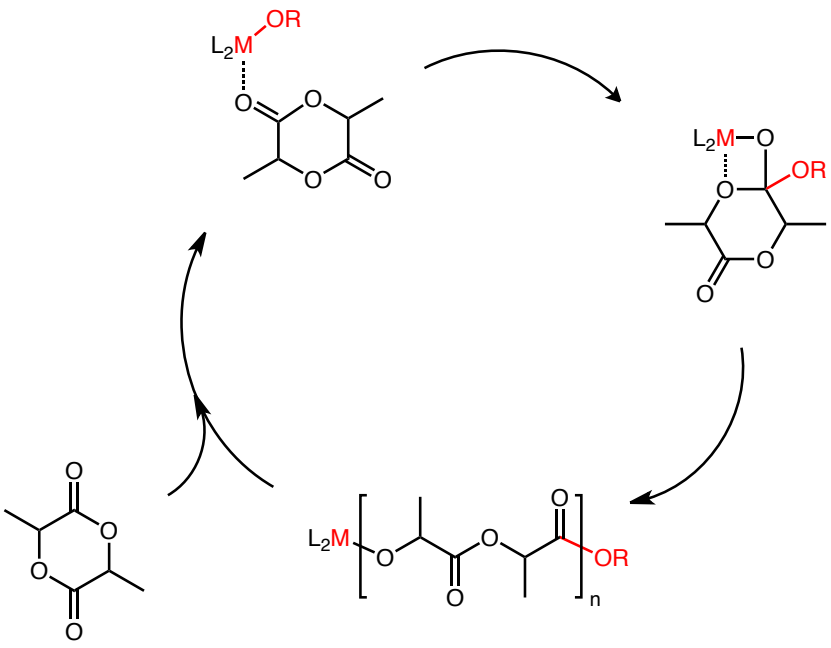


Figure 4.5.: Coordination-insertion mechanism of lactide polymerisation using metal-alkoxide catalysts adapted from [52].

(chain transfer with chain rupture - reshuffling). In polymerisations with covalent metal alkoxides as active centers, backbiting is kinetically suppressed, whereas reshuffling is not depriving polymerisation processes from their living character. For bulk polymerisations, mostly done in the melt, the metal catalyst is added to the lactide dimers in very small amounts, resulting in polylactides of high molecular masses - easily 100 kDa and more can be achieved. End-functionalised polylactides are achieved by adding initiators such as primary alcohols or amines that start the chain propagation.

The number of chains started does not change throughout the whole polymerisation process (since the chains remain active for living polymerisation, even with chain reshuffling reactions).[54] It amounts to one growing chain per alkoxide substituent of the catalyst, plus one growing chain for every hydroxyl or amine group on any co-initiators (such as primary alcohols) used. By changing the initiator/monomer ratio, the average polymer chain lengths and number of repeating units can be adjusted.

### 4.2.2. Monodentate pyridyl functionalised polylactide L1

To synthesise the monodentate pyridyl functionalised polylactide, 3-hydroxymethyl pyridine (3-HMP) was used to initiate the ring-opening polymerisation of L-lactide using the FDA approved $Sn(oct)_2$[55] as the catalyst. The average molecular weight can be varied by choosing the appropriate monomer/initiator ratio. In a typical experiment

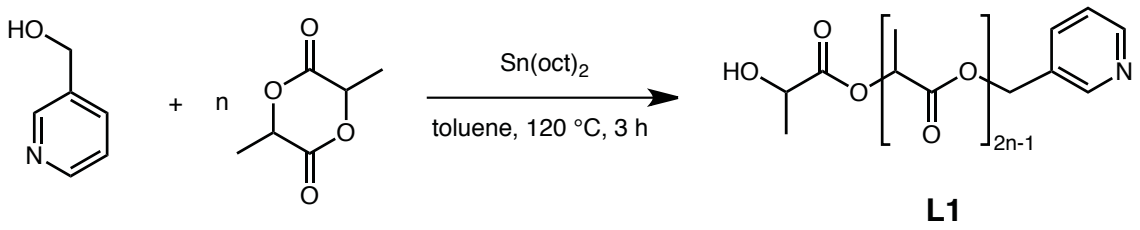


Figure 4.6.: Ring-opening polymerisation of L-lactide initiated by 3-hydroxymethyl pyridine in the presence of stannous octoate yields PLA-HMP.

either ten, five or two equivalents of L-lactide were used, resulting in polylactides with an average of twenty, ten and four repeating units, respectively. The reaction is carried out under inert conditions in refluxing toluene over the course of three hours. After removal of the solvent, the crude polymer is redissolved in dichloromethane and washed with 0.1 M hydrochloric acid, brine and water. The organic phase is dried over sodium sulfate, the solvent removed and the product dried under high vacuum. The polymers are obtained as oils or waxes, depending on their chain lengths. Polylactides with chain lengths of about twenty or more repeating units can easily be purified by precipitation from dichloromethane with diethyl ether. After precipitation, yields of about 65 % are achieved. Simple removal of the solvent after extraction leads to higher yields, but obviously slightly less pure products. The polymers were characterised by $^1$H NMR and IR spectroscopy as well as MALDI-TOF mass spectrometry.

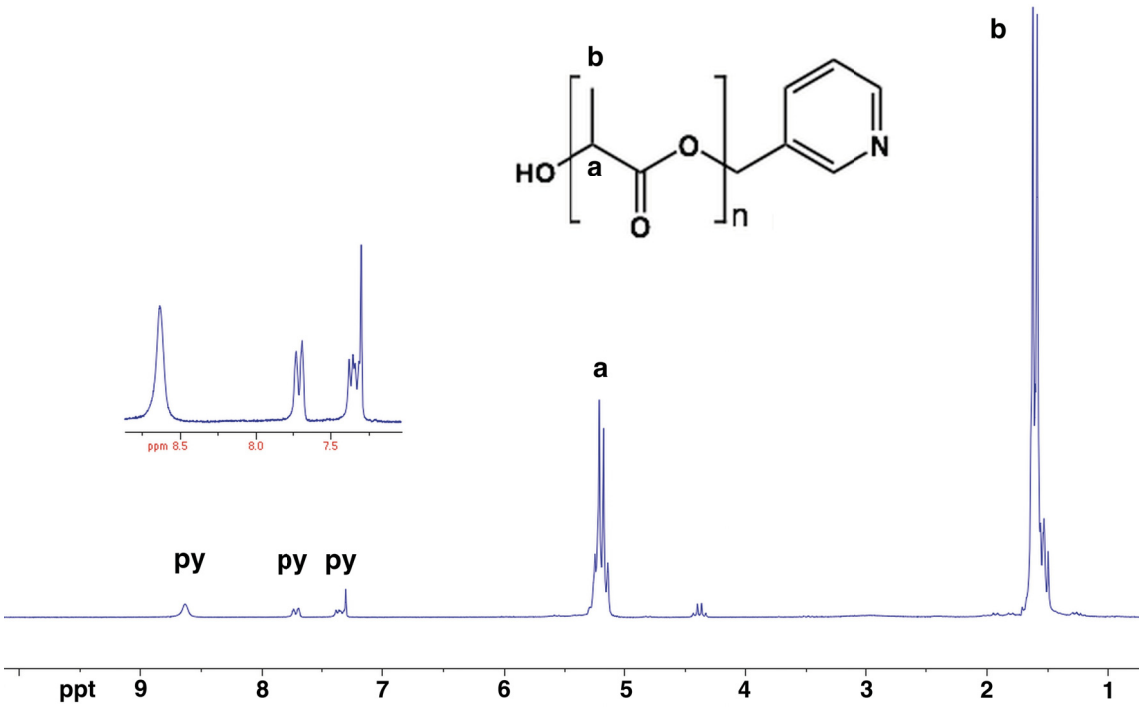


Figure 4.7.: $^1$H NMR-spectrum of PLA-HMP in $CDCl_3$, average n = 20

It is important to note that low molecular weight polylactides remain in solution when the product is precipitated from dichloromethane/ether. $^1$H NMR and MALDI-TOF analyses of the precipitate will therefore not reflect the actual average molecular mass of the polymer if a low monomer/initiator ratio ($\sim 5$) is used.

$^1$H NMR signals of the polylactide as well as the signals for the pyridyl ligand appear in the spectrum as well resolved signals. The singlet at 8.65 ppm, the doublet at 7.73 ppm as well as the multiplet at 7.37 ppm, with integrals of 2:1:1, can be attributed to the proton resonances of the aromatic pyridyl ring. Proton resonances of the methine and methyl groups of the lactide repeating units appear as a quartet at 5.20 ppm and as a doublet at 1.6 ppm, respectively, with integrals of 1n:3n, where n is the number of repeating units.

The integration ratios of the methine signal of the repeating unit to the pyridyl ligand signals can be used to estimate the number of repeating units. This estimation can be verified by mass spectrometry. The average polymer chain length calculated by $^1$H NMR is in good agreement with the polymer chain length associated with the signal at $m/z_{max}$ of the corresponding MALDI-TOF mass spectrum (see Table 4.3).

Table 4.3.: Summary of monomer/initiator ratios and average number of repeating units (n) of **L1** calculated by $^1$H NMR and MALDI-TOF.

| $\mathbf{n}_{eq}$ **L-lactide** | $\mathbf{n}_{eq}$ **initiator (3-HMP)** | $\mathbf{n}_{(NMR)}$ | $\mathbf{n}_{(MALDI-TOF)}$ |
|---|---|---|---|
| 2 | 1 | $5^a$ | $4^a$ |
| 5 | 1 | $10^a$ | $10^a$ |
| 5 | 1 | $18^b$ | $18^b$ |
| 10 | 1 | $20^b$ | $20^b$ |
| 18 | 1 | $27^b$ | $26^b$ |
| 29 | 1 | $42^b$ | $40^b$ |

[a] oil
[b] precipitate

The IR spectrum of **L1** shows a broad -OH vibrational band at about 3507 cm$^{-1}$, probably from residual water, maybe from hydrogen bonding of the terminal hydroxyl group. The aliphatic valence vibration bands are found at 2998 and 2948 cm$^{-1}$. The sharp C=O stretching vibration is found at 1759 cm$^{-1}$, which is expected from the average C=O bond strength of about 720 kJ mol$^{-1}$ in ester groups[56]. The C=C valence vibration bands from the aromatic system are found at 1457, 1386 and 1360 cm$^{-1}$ and the bands associated with monosubstituted aromatic rings are at 756 and 694 cm$^{-1}$.

The obtained polylactides are soluble in dichloromethane, acetone, ethylacetate, DMSO, acetonitrile, slightly soluble in THF and insoluble in ether, cyclohexane, methanol and water.

## 4.3. Polylactide rhenium bisimine conjugates L1a-c

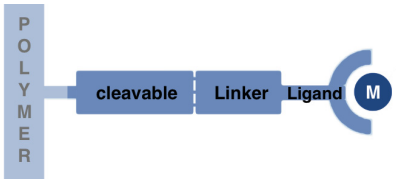


The prepared pyridyl lactide **L1** was then used to coordinate the rhenium complex. Bidentate bisimine ligands were coordinated to the complex in advance (**1a-c**) to avoid coordination of three pyridyl lactides to the rhenium carbonyl moiety. This concept, the so called [2+1]-mixed ligand approach has already been successfully applied for medical purposes.[37, 39, 48] Here, it is applied to create additional fluorescence properties for *in vitro* imaging. The distal hydroxyl group of the polylactide can later be used for further derivatisation, e.g. for attachment to biomolecules or other macromolecular vectors.

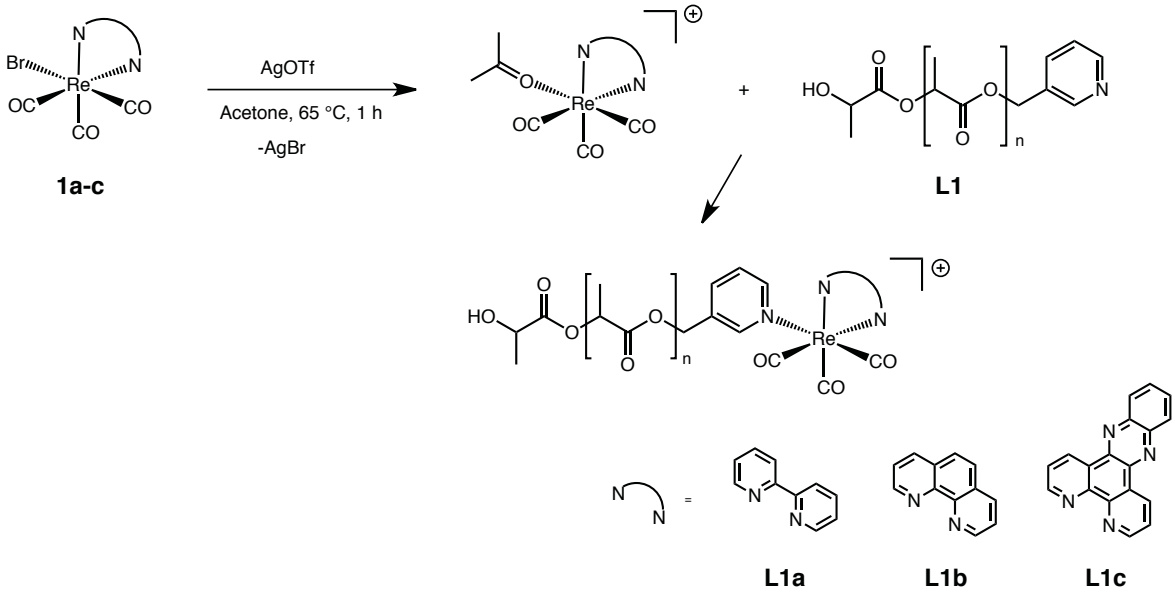


Figure 4.8.: Synthesis of PLA-HMP-Re(CO)$_3$(bisimine) conjugates **LC1a-c**

The synthesised fluorochromes **1a-c** were bound to the polymer via the pyridyl function after halide abstraction (see Fig. 4.8). To this end, the rhenium complexes are refluxed in acetone for an hour with silver triflate under inert conditions. Precipitated silver bromide is filtered out and the filtrate added to a solution of the polylactide. The solution is refluxed for two more hours and then stirred at room temperature for 72 hours. After reduction of the solvent volume to a few milliliters, the product can be precipitated and washed with diethyl ether. The polymers were characterised by $^1$H NMR and IR spectroscopy as well as MALDI-TOF mass spectrometry.

In the case of **LC1a** as well as **LC1b**, lactide methine and methane protons of the repeating unit appear as a quartet at 5.20 ppm and as a doublet at 1.60 ppm with integrals of 1n:3n, where n is the number of the repeating units. The signals attributed to aromatic pyridyl protons are the singlet at 8.4 ppm, the doublet at 7.7 ppm as well

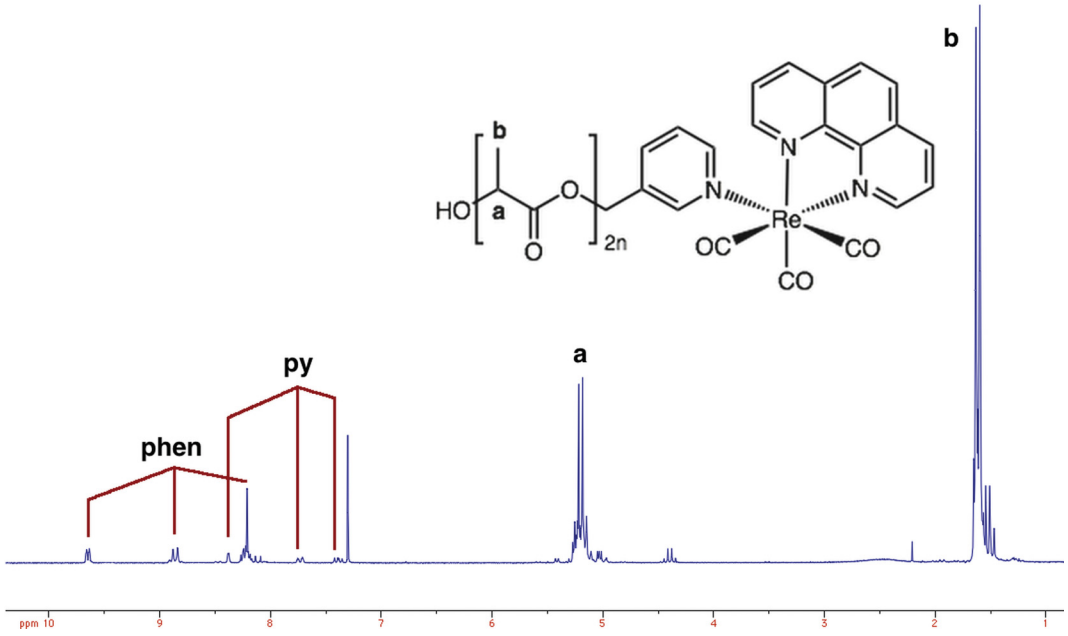


Figure 4.9.: $^{1}$H NMR-spectrum of PLA-HMP-Re(CO)$_3$(phen)OTf **LC1b** in $CDCl_3$, average 2n = 20

as the multiplet at 7.3 ppm, with integrals of 2:1:1 (the chemical shifts of the pyridyl protons vary slightly depending on the bisimine ligand, therefore only one decimal place is given here). The proton resonances of the coordinated 2,2'-bipyridyl ligand are a multiplet at 9.15 ppm, a doublet at 8.63 ppm, a multiplet at 8.32 ppm and a multiplet at 7.78 ppm with intensities of 2:2:2:2. In case of the coordinated 1,10-phenanthroline ligand, proton resonances are multiplets at 9.80 ppm, 9.07 ppm and from 8.34-8.24 ppm with intensities of 2:2:4, as expected.

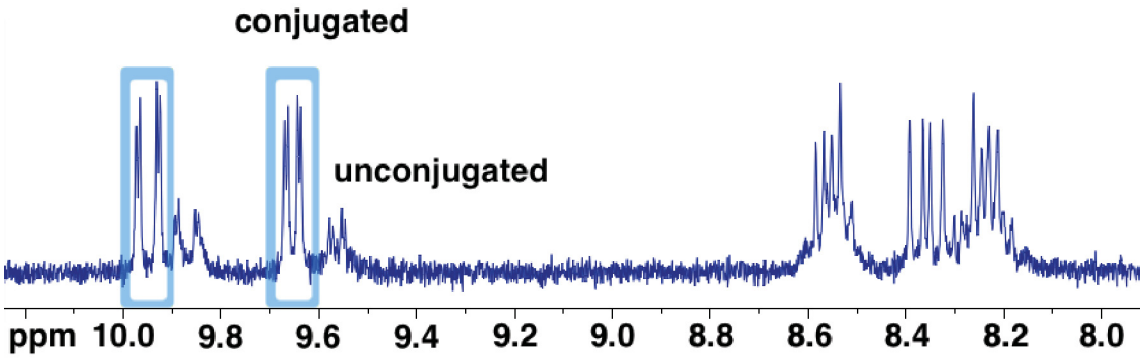


Figure 4.10.: Aromatic region of $^{1}$H NMR-spectrum of **LC1c**, the signals between 10.0 and 9.6 ppm are baseline separated. The signals between 8.6 and 8.2 ppm are overlapping. Framed signals can be assigned to the conjugate **LC1c**, shifted slightly downfield. Corresponding signals upfield can be assigned to the unconjugated complex **1c**.

Coordinating the dppz-complex **1c** to the lactide, however, does not result in a complete conversion. This may be a result of the low solubility of $[Re(CO)_3(dppz)]Br$ in acetone. For bromide abstraction, $[Re(CO)_3(dppz)]Br$ and silver triflate were stirred in methanol for three hours instead of one hour. Precipitated silver bromide was filtered out and the methanol solution added to PLA-HMP **L1** in acetone. A mixture of the two solvents was necessary, as the lactides are sparingly soluble in methanol. The $^1H$ NMR shows an overlap of coordinated and uncoordinated dppz and pyridyl signals in the aromatic region (see fig. 4.10).

In the MALDI-TOF spectra, the peaks correspond to the masses of the **L1** polylactides with increasing repeating units (n) plus the molecular weight of the $Re(CO)_3$(bisimine)-fragment. The intensity of even-numbered peaks is generally higher, representing one lactide monomer for every 2n. The signals in the spectrum of **LC1b** shown in fig. 4.11 are associated to lactide conjugates with chain lengths of 2n = 12 (1424 m/z) to 2n = 32 (2864 m/z). The absence of peaks corresponding to the ligand lactide **L1** confirms complete conversion to the lactide conjugate.

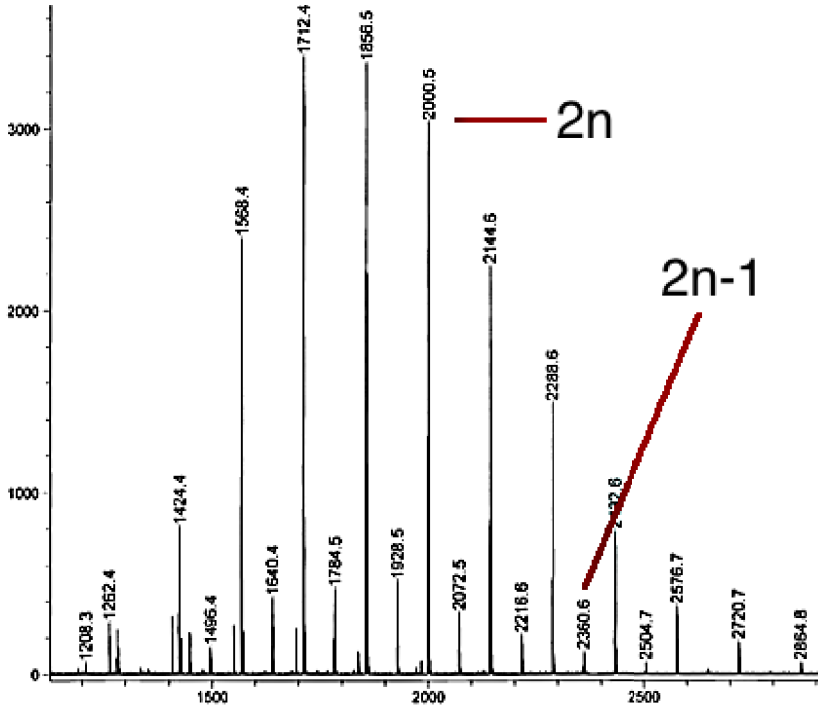


Figure 4.11.: MALDI spectrum of PLA-HMP-$Re(CO)_3$(phen)OTf **LC1b**, signals of 2n corresponding to 2n = 12 to 2n = 32

Incomplete conversion of the lactide results in two intermeshed curves of peaks, one for the unreacted lactide, which is shifted to lower masses and the other for the coordinated polymer. MALDI-TOF confirmed successful coordination of **1a** and **1b** to the ligand functionalised polymer **L1**, but it also confirmed unsuccessful coordination of **1c** to **L1**, showing peaks of both polymer conjugate **LC1c** and uncoordinated polymer **L1**.

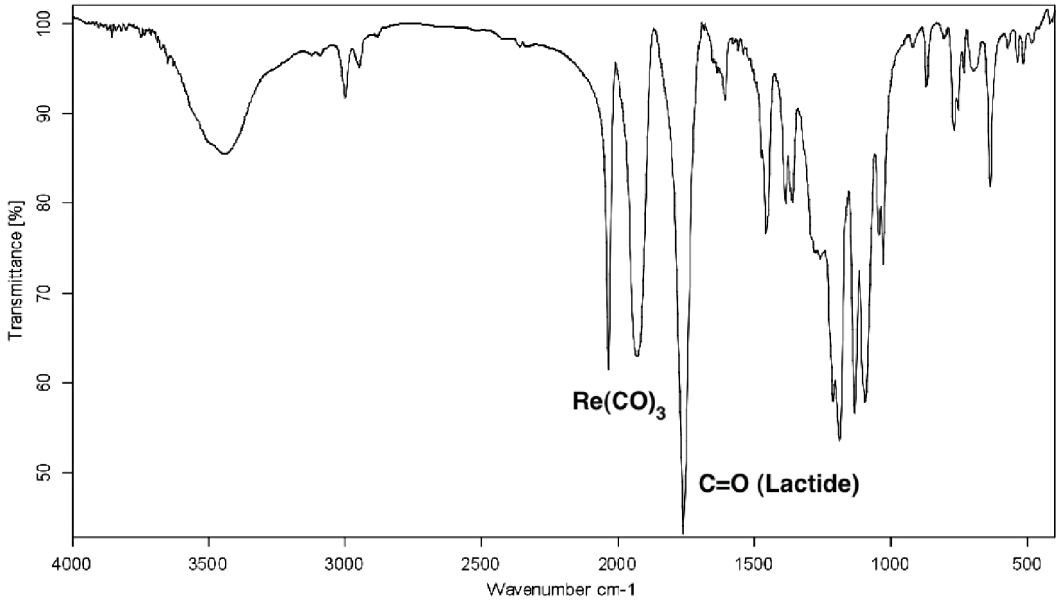


Figure 4.12.: IR spectrum of PLA-HMP-Re(CO)$_3$(bipy)OTf **LC1a**

The IR spectra of the rhenium bisimine coordinated polymers show the lactide signals (as described in chapter 4.2.2), as well as the prominent C=O vibrational bands of the facially coordinated carbonyls of the rhenium complex. Two bands are observed for the C=O vibrations (A1 and E band) at 2035 and 1929 cm$^{-1}$ which indicate a local $C_{3v}$-like symmetry at the Re(CO)$_3$ core.

Table 4.4.: Synthetic and analytical data of conjugates PLA-Re(CO)$_3$(bisimine)OTf **(L1a, L1b)**.

| **bisimine** | **yield** (%) | $\nu$**(C-O)** (cm$^{-1}$) | $^1$**H NMR** (ppm) **(py)** | | **(bisimine)** | |
|---|---|---|---|---|---|---|
| bipy[a] | 72 | 2035 | 8.26 | (m, 1H) | 9.13 | (m, 2H) |
| | | 1929 | 8.08 | (s,1H) | 8.78 | (d, 2H) |
| | | 1759 | 7.78 | (d, 1H) | 8.34 | (m, 2H) |
| | | | 7.41 | (m, 1H) | 7.78 | (m, 2H) |
| phen[a] | 40 | 2035 | 8.38 | (m, 1H) | 9.64 | (m, 2H) |
| | | 1926 | 8.27-8.18 | (m, 1H) | 8.86 | (m, 2H) |
| | | 1759 | 7.73 | (m, 1H) | 8.27-8.18 | (m, 4H) |

[a] IR: KBr pellet, NMR: $CDCl_3$

The fluorescence properties of the Re(CO)$_3$(bisimine) conjugates (**LC1a, LC1b**) were determined with fluorescence spectroscopy and the results compared to those of the corresponding free complexes [Re(CO)$_3$(bisimine)(3-HMP)]OTf (**2a, 2b**), investigating their usefulness as targeted dyes for fluorescence imaging. The toxicity of **LC1b** was evaluated using an MTT cytotoxicity assay on the human ovarian carcinoma cell line A2780. In order to gain some understanding of basic pharmacokinetic parameters, espe-

cially distribution and interaction of the polylactides with tissue and cells, localisation on living cells was investigated by incubating **LC1b** on A2780 for two hours and subsequent confocal microscopy. To determine, whether the polylactides affect cell membrane integrity, a trypan blue test was performed with **LC1b**, again on A2780 cells. The trypan blue test was done in conjunction with an eosin staining to assert membrane coherence and cell viability. These experiments and their findings are discussed in chapters 6, 7 and 8.

### 4.3.1. Tridentate trispyrazolylmethyl functionalised polylactide L2

Tris(pyrazolyl)methane (tpm) is a ligand often used to model nature's tris-histidin-metal conjugation, found in the active centers of many enzymes and it is known to readily form $Re(CO)_3$ complexes.[53] Tpm was thus chosen as the ligand for the tridentate coordination mode to be compared with the monodentate mode of **L1**.

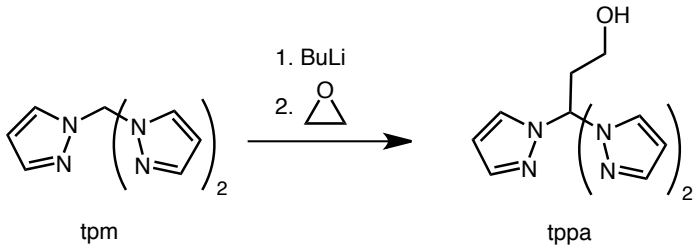


Figure 4.13.: Synthesis of 3,3,3-tris(3'pyrazol-1-yl)propanol.

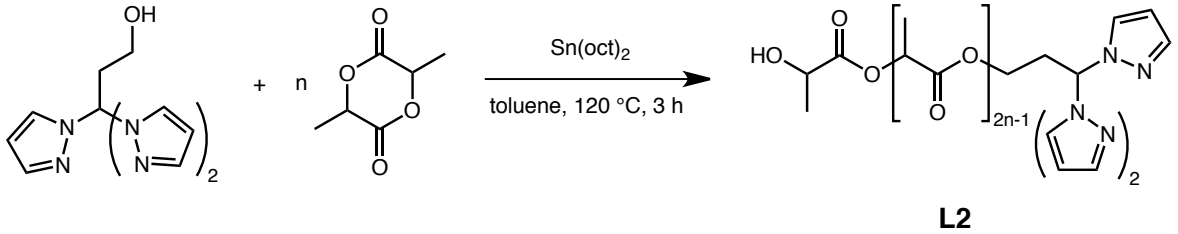


Figure 4.14.: Ring opening polymerisation of L-lactide initiated by 3,3,3-tris(3'pyrazol-1-yl)propanol.

In order to prepare tris(pyrazolyl)methane functionalised polylactide **L2**, the hydroxyl functionalised 3,3,3-tris(3'-pyrazol-1-yl)propanol (tppa) was used to initiate the polymerisation. It was synthesised by deprotonation of the parent tris(pyrazolyl)methane and subsequent reaction of the carbanion with ethylene oxide, as published by our workgroup (see fig. 4.13).[53] After a polymerisation time of three hours in refluxing toluene with stannous octoate as catalyst and subsequent work up, the functionalised PLA-tppa

was received as a white powder in yields about of 75 %. The polymers were characterised by $^1$H NMR spectroscopy and MALDI-TOF mass spectrometry. The $^1$H NMR chemical shifts are summarised in figure 4.15.

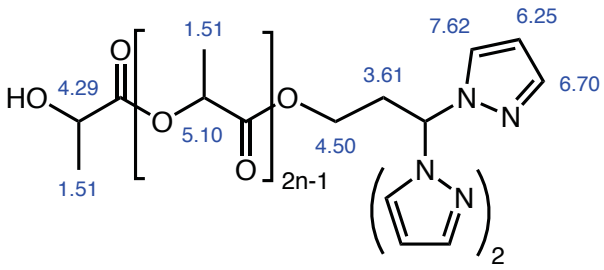


Figure 4.15.: $^1$H NMR shifts of PLA-tppa.

However, for unknown reasons, almost no coordination to $Re(CO)_3$ could be achieved when reacting in acetone for several hours under refluxing conditions with the precursors $[Re(CO)_3(H_2O)_3]Br$ or $(NEt_3)_2[Re(CO)_3Br_3]$. In contrast to the ligand functionalised polymer, the complex $[Re(CO)_3(tppa)]Br$ can be readily prepared with the free ligand tppa according to literature procedures.[53]

## 4.4. Methacrylate functionalised pyridyl lactide ML1

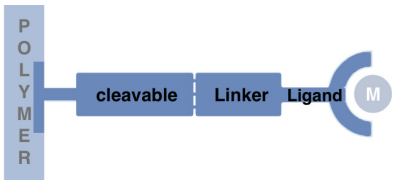


The next step in preparing the conjugate is to bind the lactide side chains to the backbone of the polymeric carrier system. This can be achieved by turning them into macromonomers, introducing polymerisable end-groups. Methacrylate groups open up the possibility of polymerising the lactide with a library of comonomers via radical polymerisation. This way, the lactide side chains can be incorporated into large carrier systems with additional functionalities and properties.

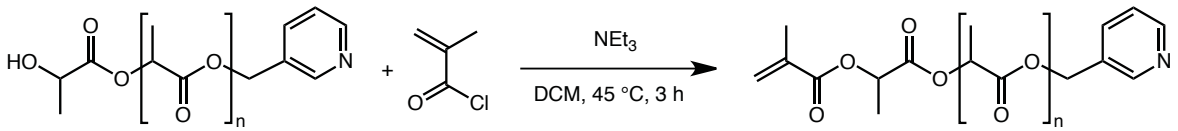


Figure 4.16.: Introducing methacrylate endgroups by esterification with methacryloyl chloride.

Synthesis of MA-PLA-HMP **ML1** was done by esterification of the hydroxyl endgroup with methacryloyl chloride under basic conditions. To this end, the pyridyl lactide and triethylamine were dissolved in dichloromethane and a slight excess of methacryloyl

chloride in dichloromethane was added drop wise at 45 °C over the course of an hour. The solution was heated for three more hours and then worked up by successively washing with 0.1 M HCl, saturated brine and water and drying over sodium sulfate. Following reduction of the solvent volume until the solution turned slightly viscous, the product was precipitated with diethyl ether in yields of close to 90 %.

It is important to note, that complete conversion to the methacrylated lactides could only be achieved with short chain lengths of ten or less repeating units. Otherwise NMR as well as MALDI-TOF analyses show that about 35 to 50% of the lactides remain unfunctionalised, even when more than a two fold excess of methacryloyl chloride and triethylamine is used in the reaction. This problem could probably be solved by using an even higher excesses or longer reaction durations, but for the use of these lactides as the cleavable linker of a larger carrier system, oligomers already fulfill the requirements. **ML1** was characterised by $^{1}$H NMR and IR spectroscopy as well as MALDI-TOF mass spectrometry.

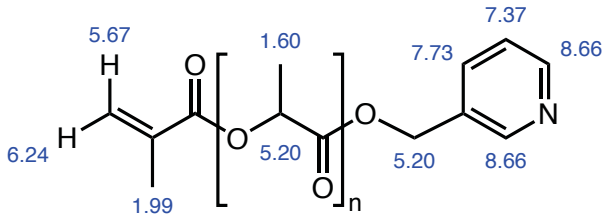


Figure 4.17.: $^{1}$H NMR chemical shifts of MA-PLA-HMP.

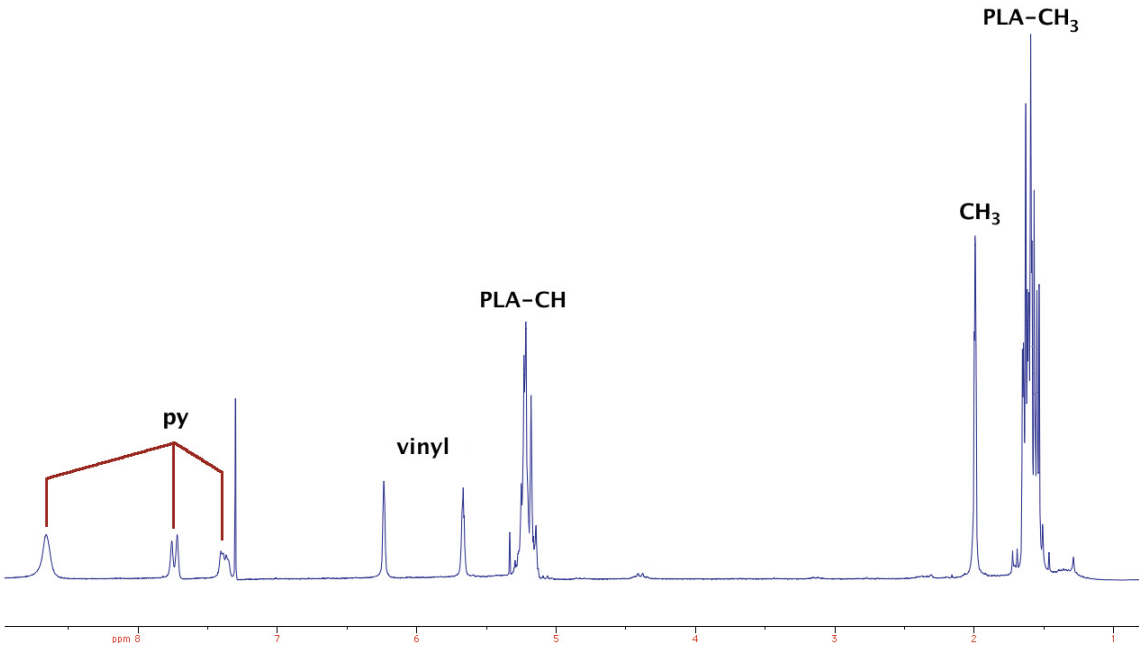


Figure 4.18.: $^{1}$H NMR spectrum of MA-PLA-HMP in $CDCl_3$, average n = 5

$^1$H NMR signals for the pyridyl group appear in the spectrum as a singlet at 8.66 ppm, a doublet at 7.73 ppm as well as a multiplet at 7.37 ppm, with integrals of 2:1:1. The vinyl protons are found at 6.24 and 5.67 ppm, the methyl proton resonance of the methacrylate is found at 1.99 ppm, respective integrals are 1:1:3. Proton resonances of the methine and methyl groups of the lactide repeating units appear as a multiplet at 5.2 ppm and as a multiplet at 1.6 ppm, with integrals of 1n:3n, where n is the number of repeating units. Usually, the protons in the repeating units of polymers have the exact same chemical shift, because their chemical and electronic vicinity is exactly the same. Very close to the chain ends, however, the chemical shifts of the protons differ slightly, as their chemical and electronic vicinity changes. In case of oligolactides, as can be seen in Fig. 4.18, the proton signals of the methine and methyl groups in the repeating units are no longer one well resolved quartet and doublet, but overlapping quartets and doublets with similar chemical shifts.

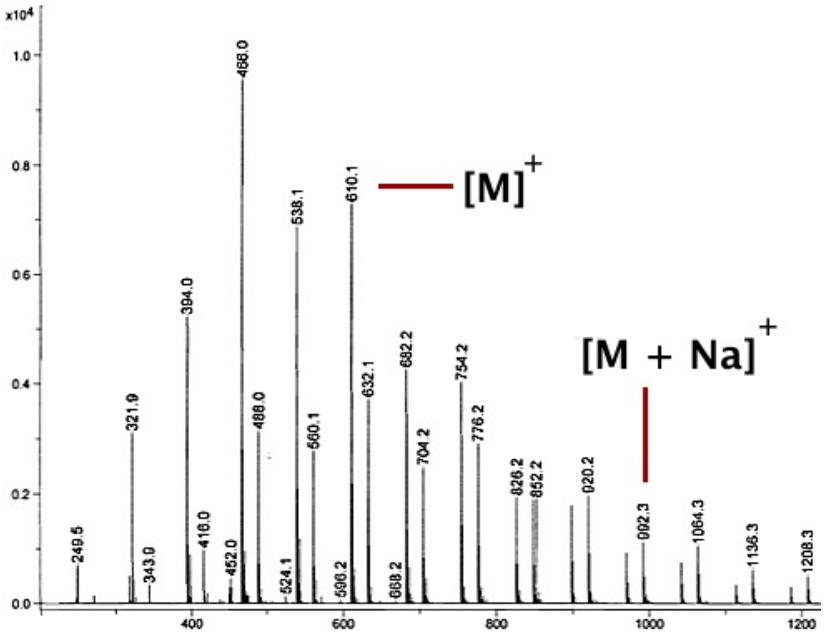


Figure 4.19.: MALDI-TOF spectrum of methacrylated polylactide **ML1** and their corresponding sodium ion adducts.

The MALDI-TOF spectrum of **ML1** shows the distribution pattern of the masses corresponding to the polymers with increasing chain lengths, confirming successful esterification of all lactide chains. Signals for the sodium ion adducts are often observed in the MALDI-TOF spectra, as well (see Fig.4.19).

The IR vibrations associated with the functional groups of MA-PLA-HMP are the aliphatic vibrational bands at 2997 and 2957 $cm^{-1}$ and the sharp C=O stretching vibration at 1751 $cm^{-1}$. The C=C valence vibration bands from the aromatic system are found at 1457, 1385 and 1360 $cm^{-1}$ and the bands associated with monosubstituted aromatic rings are at 756 and 713 $cm^{-1}$.

## 4.5. The polymeric carrier system

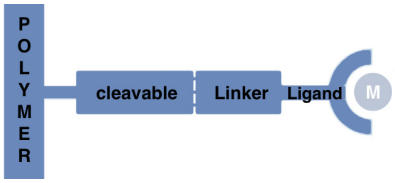


To incorporate the prepared methacrylated macromonomers into larger carrier systems, the monomers have to be copolymerised with other methacrylic or vinylic monomers. Often these monomers have very different polymersation rates, which poses a challenge for conventional radical polymerisation. Moreover, the importance of low polydispersities for polymeric carrier systems makes reversible addition-fragmentation chain transfer (RAFT) polymerisation the method of choice.[57] RAFT is a radical polymerisation that confers the attributes of a living polymerisation, first introduced by Thang *et al.*[58]

### 4.5.1. RAFT polymerisation

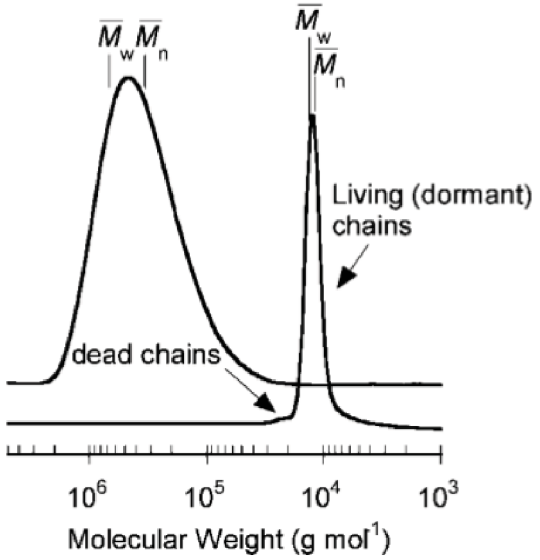


Figure 4.20.: Typical molecular-weight distributions for a conventional (left) and RAFT polymerisation (right) under similar experimental conditions.[59]

Radical polymerisation is a well established and widely used method for the commercial production of high-molecular weight polymers. This is mainly because a wide variety of monomers, even those with unprotected functional groups, can be polymerised. The method shows a wide tolerance of reaction conditions and solvents and is simple to implement as well as inexpensive in comparison to alternative polymerisations.[59]
Conventional radical polymerisation has several drawbacks with respect to the degree of control that can be asserted over molecular-weight distribution, copolymer composition and macromolecular architecture. Polydispersity for example is typically >2.0 if the chains are terminated by disproportionation or chain transfer, or >1.5 if termination is by chain recombination.

In RAFT polymerisations, these shortcomings are addressed by introducing attributes of living polymerisation using chain transfer agents (CTAs). CTAs are capable of reversibly deactivating propagating radicals, so that the majority of chains are maintained in a dormant form. The equilibrium of dormant and active chains is rapid with respect to propagation. Consequently, all chains grow simultaneously on average, which in turn leads to very low polydispersities of about 1.1.[60]

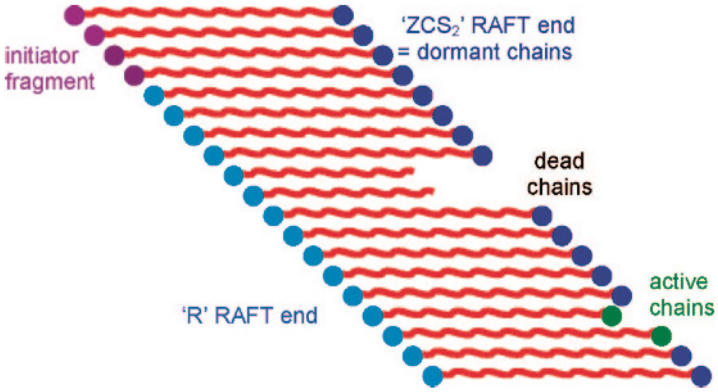


Figure 4.21.: RAFT polymerisation schematic. The fraction of active chains is in reality much smaller than shown. Image as published in[59].

The mechanism of chain activation and deactivation in RAFT is shown in Fig. 4.22. These reactions occur in addition to the initiation, propagation and termination reactions of conventional radical polymerisations. Central to these reactions is the chain transfer agent, usually a dithiobenzoate or other aromatic dithioester. Depending on the monomers and reaction conditions, CTAs with different substituents R and Z must be selected.

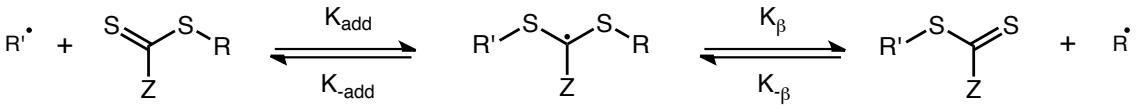


Figure 4.22.: Mechanism of chain activation and deactivation by CTAs.

Methyl methacrylates (MMAs) are the most demanding monomers with regard to the CTA because the polymeric growing chain is a tertiary radical. R must thus be an excellent leaving group and also a good reinitiating radical. The group Z also plays an important role in MMA polymerisation because it influences the stability of the intermediate radicals and modifies the reactivity of the C=S double bond toward radical addition, which alters the addition and fragmentation rates.[61]
2-Cyanoisopropyl dithiobenzoate is reportedly one of the CTAs best suited for methyl methacrylate polymerisation and was chosen for the RAFT polymerisation of the polymeric carrier systems in this work.[57] Guidelines and an overview for the selection of RAFT agents for various monomers can be found in the review of Moad *et al.*[59]

### 4.5.2. CTA: Synthesis of 2-cyanoisopropyl dithiobenzoate

There are several routes to synthesise dithiobenzoyldisulfide, from which the RAFT chain transfer agent 2-cyanoisopropyl dithiobenzoate is prepared. The best yield and purity was achieved using the method published by Mitsukami *et al.*[62] with minor modifications.

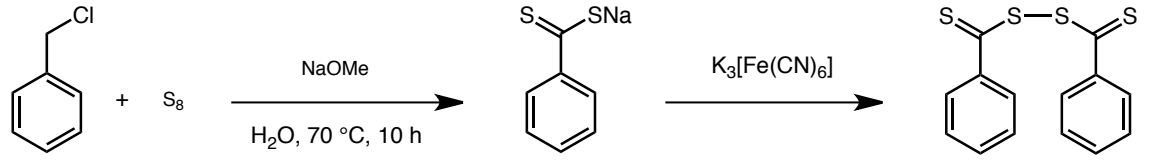


Figure 4.23.: Synthesis of dithiobenzoyldisulfide.

Under inert conditions, sulfur is added to an aqueous solution of sodium methoxide. Benzoylchloride is then added slowly over a period of 1 h. After stirring at 70 °C for ten hours, the reaction mixture was cooled to 0 °C and precipitated salts were filtered out. The crude dithiobenzoate solution is washed several times with diethyl ether. It is then extracted into diethyl ether by protonating the dithiobenzoate using hydrochloric acid and then back into the aqueous phase using sodium hydroxide solution. This is repeated three times. The resulting aqueous solution of sodium dithiobenzoate is transferred into a round bottom flask with dropping funnel. Potassium ferricyanide(III) solution was then added dropwise under vigorous stirring until no further precipitation of dithiobenzoyldisulfide occured. The product can be filtered out, washed with water and dried at room temperature under high vacuum.

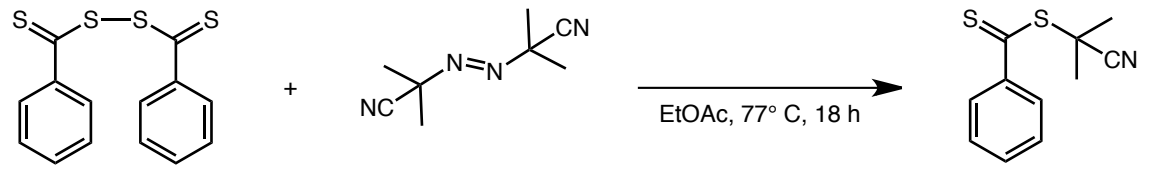


Figure 4.24.: Synthesis of 2-cyanoisopropyl dithiobenzoate.

Dithiobenzoyldisulfide is reacted with 1.5 equivalents of AIBN in refluxing ethyl acetate over a period of 18 hours. The solvent is removed in vacuo and the product purified by column chromatography (silicagel 60, ethyl acetate/n-hexane 1:9). 2-Cyanoisopropyl dithiobenzoate is afforded as a red oil, which turns solid upon keeping in the freezer.

### 4.5.3. Copolymer HPMA-co-MA-PLA-HMP P1

Integration of the pyridyl functionalised macromonomer into a larger carrier system was realised using N-(2-hydroxypropyl)methacrylate as a comonomer. A monomer ratio (HPMA to MA-PLA-HMP, **ML1**) of 5:1 was used in the experiments, the macromonomers had an average number of four repeating units.

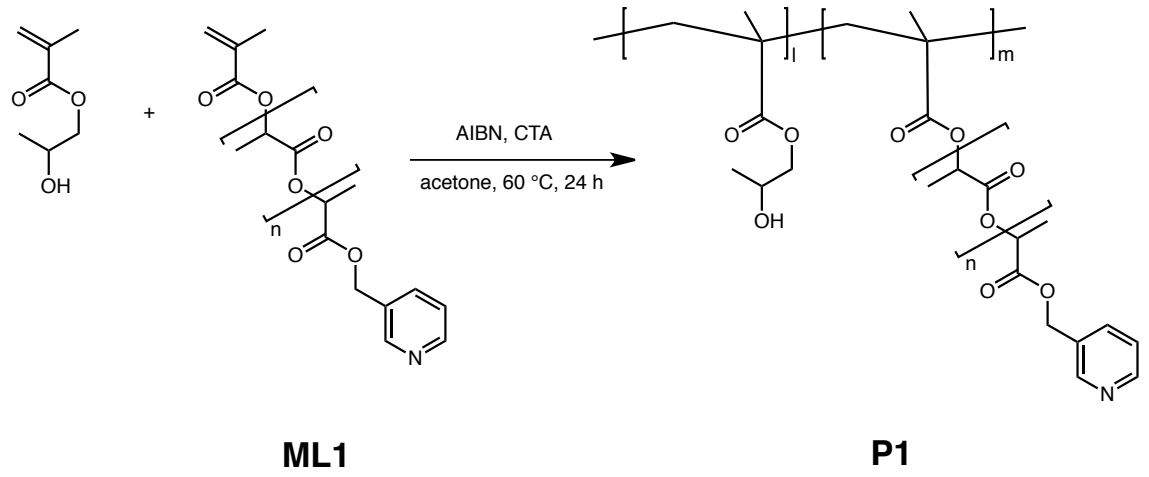


Figure 4.25.: RAFT polymerisation of HPMA and MA-PLA-HMP to afford **P1**.

The monomers were put in a Schlenk tube under inert conditions and dissolved in dry toluene. The radical starter AIBN as well as the chain transfer agent 2-cyanoisopropyl dithiobenzoate were added and the reaction mixture heated to 60 °C. It was stirred at this temperature for 24 hours. The solvent was then evaporated at the rotary evaporator until the solution turned viscous. The polymeric solution was dripped into acetone/diethyl ether (25/75, v/v), whereupon the polymer precipitates. It was filtered out, washed with diethyl ether and dried under high vacuum. Yields of about 73 % are achieved. **P1** was characterised using $^1$H NMR and IR analysis.

Unfortunately polymethacrylates cannot be analysed using MALDI-TOF mass spectrometry. An estimation of the molecular weight of such methacrylates using GPC analysis, as well as an estimation of their hydrodynamic volume using DLS was done analysing the similar polymeric carrier **P2** (see chapter 5.5) and is discussed there. In brief, methacrylate copolymers with molecular weights of more than 50 kDa are easily obtained by RAFT polymerisation using this procedure. The corresponding hydrodynamic diameter was measured to be about 10 nm.

The $^1$H NMR spectrum confirms the successful copolymerisation of the two monomers, as signals from both monomers appear in the spectrum of the precipitated polymer. The typical broadening of the proton signals in polymers can be observed, as well. Also important to note is the fact that no vinyl proton resonances are to be seen in the spectrum and thus no residual monomers are retained in the polymer.

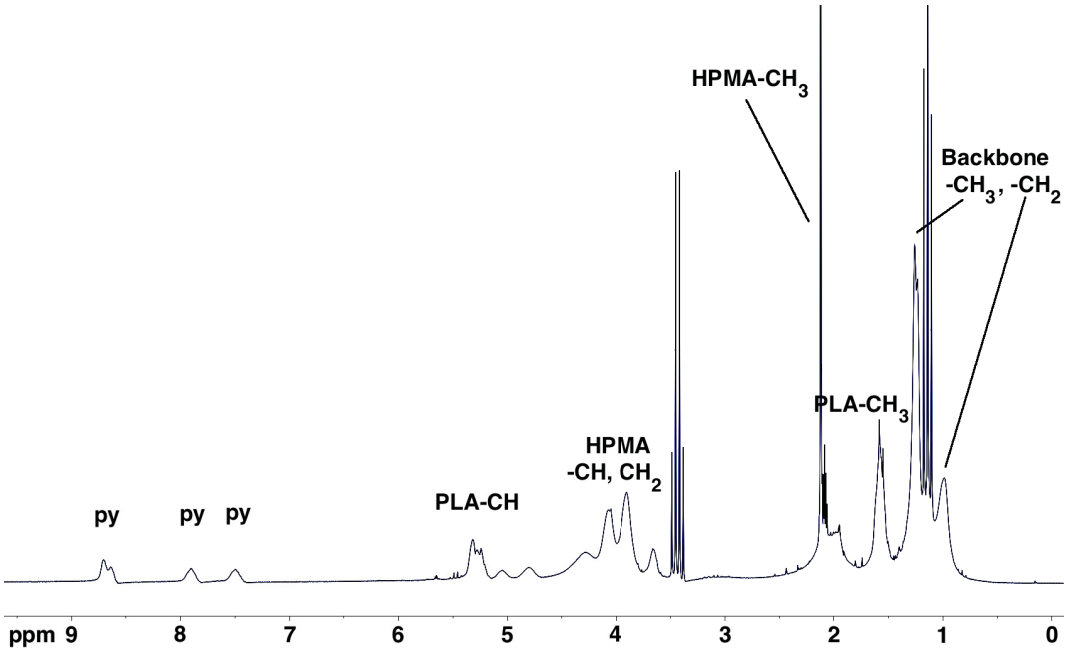


Figure 4.26.: $^1$H NMR spectrum of HPMA-co-MA-PLA-HMP (**P1**) in acetone-$d_6$.

Pyridyl proton resonances are a multiplet at 8.66 ppm and two singlets at 7.90 and 7.49 ppm with integral ratios of 2:1:1. Protons resonances from the lactide repeating units are multiplets at 5.20 ppm in case of the methine proton and at 1.60 ppm in case of the methyl protons. Their integral ratios are as expected 1:3. HPMA-$CH_2$ and HPMA-CH resonances result in a multiplet between 4.5-3.6 ppm, the HPMA-$CH_3$ resonance of the methyl group located in the side chain is shifted to 2.13 ppm, integral ratios are (2+1):3. The -$CH_2$ and -$CH_3$ protons of the polymer backbone form broad multiplets between 1.4 and 0.8 ppm.

The integral ratios of specific HPMA to lactide proton resonances in the NMR spectrum can be used to estimate the ratio of HPMA to the lactide side chains in the copolymer. The baseline separated signals of the pyridyl ring are useful analytical probes for the lactide, whereas the HPMA methyl group is the best analytical probe for the HPMA fragment.

$$\frac{n_{HPMA}}{n_{MA-PLA-HMP}} = \frac{\int(\mathrm{HPMA} - \mathrm{CH_3})/3}{\int(\mathrm{py})/4} \tag{4.1}$$

A different way to estimate the copolymer composition is to compare the amount of backbone protons to the amount of HPMA side chain protons. In a HPMA homopolymer, the ratio of backbone to HPMA side chain protons is 5/6. In a copolymer, this ratio increases with increasing amount of lactide side chains. In a copolymer consisting of one lactide macromonomer per five HPMA monomers, the ratio would e.g. be (5+1)/6,

in a copolymer with two lactide macromonomers per five HPMA monomers (5+2)/6. etc. Both methods should indicate the same copolymer composition. The spectrum of the **P1** polymer shown in fig. 4.26 for example, has integral ratios of 6/1 for the two monomer components (HPMA/MA-PLA-HMP) and the ratio of backbone protons to HPMA is roughly 6/6. The latter value is an estimate, since the signal of the protons from residual diethyl ether is within the range of the backbone signals and has to be subtracted from the integral. 6/6 indicates a monomer ratio of five HPMA units per lactide monomer. 6.2/6 would point to six HPMA monomers per lactide. Factoring in the read-off accuracy, a copolymer consisting of about six HPMA monomers per lactide macromonomer can be deduced.

The ratio of lactide methine protons to pyridyl protons gives information on the average lactide chain length of the compound. The chain length should not change during copolymerisation. Unless degradation occurred during the polymerisation reaction or subsequent work up, chain length of macromonomer and side chain length of the copolymer are the same.

$$(-C_3H_4O_2-)_n = \frac{\int(\text{PLA} - \text{CH})}{\int(\text{py})/4} \tag{4.2}$$

In summary, analysis of the spectrum of **P1** (fig. 4.26) indicates an average amount of six HPMA side chains per lactide side chain, with lactide chains consisting of four repeating units on average. The estimated chemical formula is therefore $HPMA_6$-co-$(MA\text{-}PLA_4\text{-}HMP)_1$. The HPMA content of this specific copolymer is therefore about 20 % higher than the monomer ratio used in the polymerisation reaction. Lactide chain lengths remain unchanged.

The IR spectra of HPMA-co-MA-PLA-HMP show the broad -OH vibrational band at 3446 $cm^{-1}$, the aliphatic C-H valence vibration bands at 2983 and 2943 $cm^{-1}$, the sharp C=O stretching vibration at 1730 $cm^{-1}$ as well as the bands associated with monosubstituted aromatic ring at 756 and 694 $cm^{-1}$.

The precipitated copolymers are soluble in acetone, DMF, dichloromethane and DMSO. They are air and light stable and can be stored for months without degradation.

## 4.6. The polymer-[$Re(CO)_3$] conjugate PC1

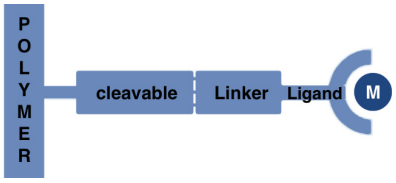


The final step in synthesising the polymer-metallodrug conjugate is the coordination of the rhenium tricarbonyl moiety [$Re(CO)_3$(bisimine)]Br to the prepared polymeric carrier system **P1**.

To this end, $Re(CO)_3(bipy)Br$ was reacted with silver triflate in acetone for halide abstraction. Precipitated silver bromide was filtered off and the resulting solution of $[Re(CO)_3(bipy)(acetone)]OTf$ added to a solution of the pyridyl functionalised copolymer in acetone. It was stirred for one hour under refluxing conditions and then stirred for five days at room temperature. The solvent volume was subsequently reduced until the solution turned slightly viscous. The conjugate was precipitated by adding the polymeric solution dropwise to a solution of acetone/diethyl ether (25/75, v/v). The polymer was washed with diethyl ether and dried under high vacuum. Yields of about 70 % are achieved. **PC1** was characterised using $^1H$ NMR and IR analysis.

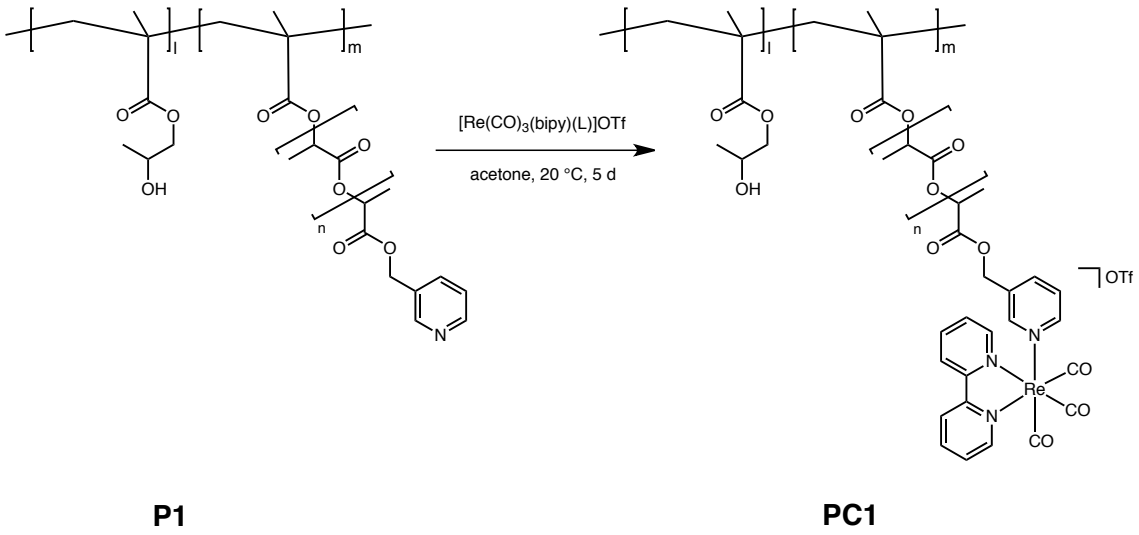


Figure 4.27.: Coordination of $[Re(CO)_3(bipy)(L)]OTf$ to the polymeric carrier system.

The $^1H$ NMR spectrum consists of the signals of the polymeric carrier system (see chapter 4.5.3), as well as the aromatic proton resonances of 2,2'-bipyridine at the rhenium core. Most importantly, the integrals of the pyridine and bipyridine signals are as expected, amounting to 4 pyridyl protons and 8 bipyridine protons, which indicates full coordination of rhenium bipyridine to the ligand polymer (see insert of Fig. 4.28).

IR spectroscopy is the second important analytical tool to ascertain whether the coordination of the rhenium bisimine moiety to the polymer was successful. The IR spectrum shows the polymer signals, consisting of the broad -OH vibrational band at 3450 $cm^{-1}$, the aliphatic C-H valence vibration bands at 2983 and 2943 $cm^{-1}$, as well as the sharp C=O stretching vibration at 1728 $cm^{-1}$. Moreover, two prominent C=O vibrational bands are observed at 2035 and 1937 $cm^{-1}$ (A1 and E band) stemming from the local $C_{3v}$-like symmetry at the $Re(CO)_3$ core. Comparison of the IR data of the synthesised 2,2'-bipyridine complexes shows that especially the asymmetric stretching vibration remains the same (at about 2035 $cm^{-1}$) whenever the co-ligand 3-hydroxymethyl pyridine is coordinated. The corresponding neutral complex with a bromo ligand has slightly weakened carbonyl bonds. Asymmetric stretching vibrations of the trisaquo tricarbonyl are also a bit lower in energy than the NNN-coordinated complexes (see table 4.5).

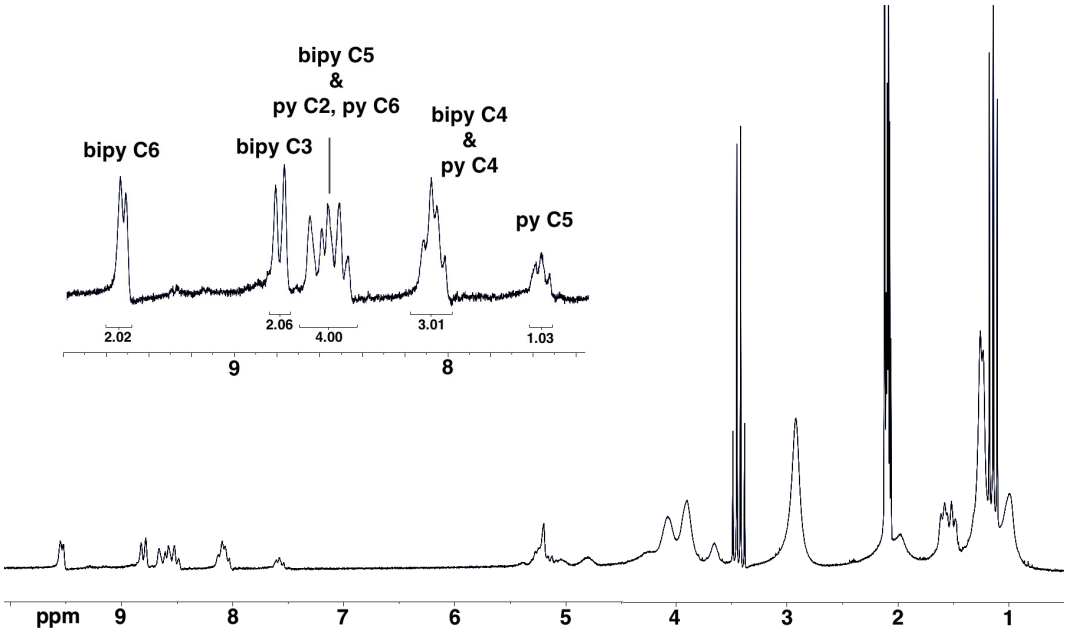


Figure 4.28.: $^{1}$H NMR spectrum of the polymer-drug conjugate **PC1** in acetone-$d_6$.

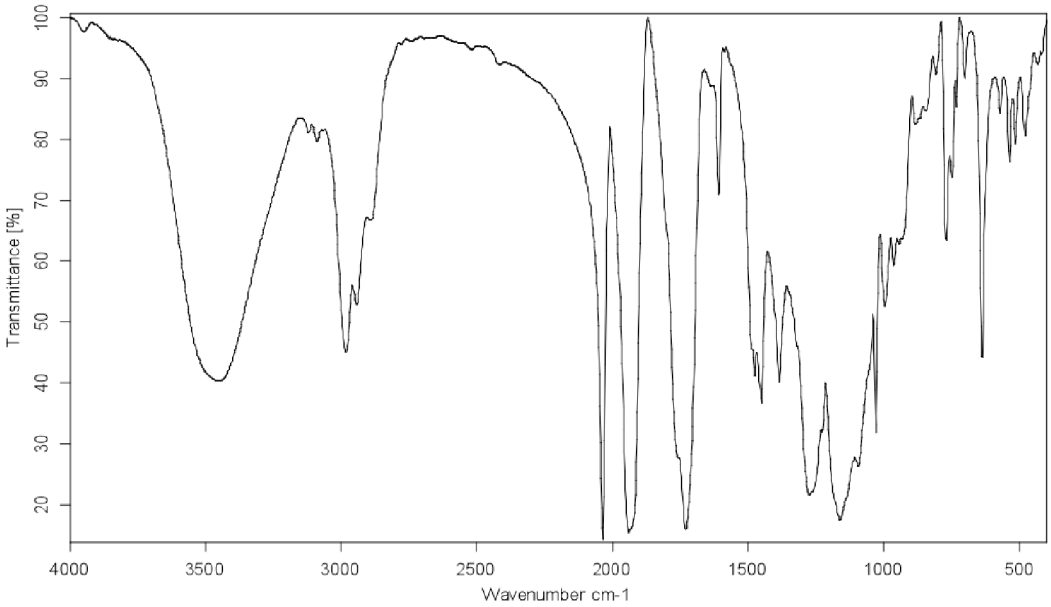


Figure 4.29.: IR spectrum of the polymer-drug conjugate **PC1** carrying the fluorescent rhenium tricarbonyl cores.

In conclusion, a polymeric system composed of backbone, cleavable side chain and conjugated $Re(CO)_3$(bisimine) was successfully prepared, which could prove useful in the early detection of cancer through fluorescence and nuclear imaging, when selecting the radioactive technetium isotope $^{99m}$Tc and the option of therapeutic use when selecting

the radioactive rhenium isotope $^{186/188}$Re. The distribution properties, degradation of the cleavable side chain and drug release kinetics of the carrier system are evaluated and discussed in chapter 6.

Table 4.5.: Compiled IR data for comparison of the carbonyl bond strength of rhenium tricarbonyl complexes and conjugates.

| | $\nu$(**C=O**) (**cm**$^{-1}$) |
|---|---|
| $Re(CO)_3(H_2O)_3Br$[a] | 2026, 1942 |
| $Re(CO)_3$(bipy)Br **1a** | 2012, 1905 |
| $Re(CO)_3$(bipy)(3-HMP)OTf **2a** | 2031, 1917 |
| PLA-HMP-$Re(CO)_3$(bipy)OTf **LC1** | 2035, 1929 |
| HPMA-co-MA-PLA-HMP-$Re(CO)_3$(bipy)OTf **PC1** | 2035, 1937 |

[a] published by Lazarova *et al.*[41]

# 5. Development of the polymer-Au(I) conjugate PC2

## 5.1. Why gold?

Many gold compounds were proven to have anti-inflammatory potential,[63, 64] which led to the general term chrysotherapeutics. In the 1980's a number of systematic investigations into the anticancer potential of gold compounds were done. Two prominent examples are gold thiolates such as sodium aurothiomalate, myochrysin,[65] and the triethylphosphane gold thioglucose species, auranofin.[66] A systematic evaluation of these types of chrysotherapeutics was done by Mirabelli *et al*, concluding that structures with the linear P-Au-S arrangement such as auranofin are most promising for antitumour activity.[67] It is very likely, that gold-based drugs undergo substitution reactions with sulphur-containing biomolecules such as albumin and glutathione, which is already a means of passive targeting to inflammation sites with defective endothelial structures.[68, 69] Ligand exchange speed of Au(I) complexes in aqueous media increases in the order $R_3P < RS^- < Hal^-$.[70]

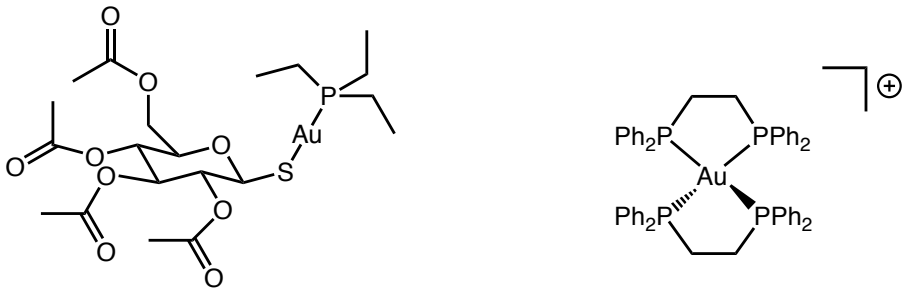


Figure 5.1.: Chrysotherapy agents: auranofin and $(dppe)_2AuCl$

The phosphane based gold complex $[(dppe)_2Au]Cl$ (dppe = bis(diphenylphosphino)-ethane) (see Fig.5.1) was the first gold based phosphane complex to show *in vivo* antitumour activity.[3] Preclinical studies showed that the limiting factor of $[(dppe)_2Au]Cl$ is the drug-related cardio- and hepatotoxicity.[71] These toxicities result from the lipophilic nature of such complexes, which is why a lot of research is being done to improve tumour specificity and thereby reducing the side effects. The potential targets of gold therapeu-

tics are cysteine and selenocysteine proteins, because coordination of the Au(I)-drug to the thiole or selenole groups at the active site results in inhibition of the enzyme. Cathepsins, for example, are a family of highly homologous cysteine proteases, playing a role in inflammation processes, as they are part of the neoangiogenesis pathway.[72] They have been associated with diseases such as cancer (and are even used as a prognosis marker for the occurrence of new metastases),[73] as well as stroke,[74] rheumatoid arthritis, Alzheimer's disease and glaucoma. Cathepsins are localised in the lysosomes, where gold is known to accumulate. It was demonstrated by Gunatilleke *et al.* that cathepsin B is reversibly and competitively inhibited by Au(I) phosphane complexes.[70, 75] A crystal structure of the gold therapeutic myochrysin could be obtained while it was bound to the active site of the protein cathepsin K (see fig. 5.2).

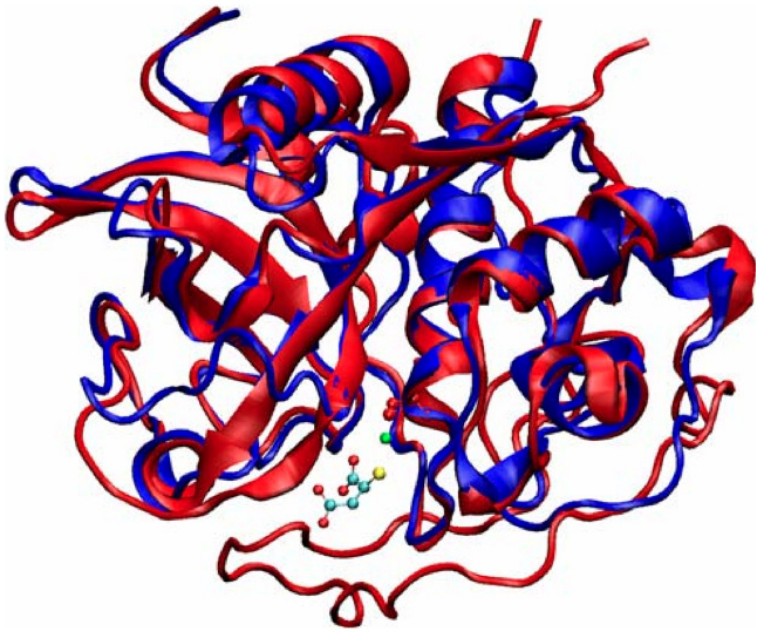

Figure 5.2.: The blue ribbon structure is the covalent complex formed between the cathepsin K and myochrysin. The myochrysin is shown in a ball-and-stick representation where cyan represents carbon, red represents carbon, yellow represents sulfur and green represents gold ion. The red ribbon structure is cathepsin B. The red ball-and-stick representation is the overlay of the active-site cysteine residue in both enzymes.[45]

The ability to transport chrysotherapeutics to centres of inflammation by passive macromolecular targeting has hardly been investigated and could prove quite useful for the improvement of therapeutic success. Inflammation causes leakage in endothelial vessels in a fashion similar to tumours, which can be analogously exploited by passive targeting. Gold-based therapeutics of interest are, as previously discussed, gold complexes with phosphane ligands that are e.g. known to reversibly inhibit cathepsin enzymes. It would therefore make sense to develop carrier systems with phosphane ligands for the transport of Au(I).

## 5.2. P-Ligand functionalised polactides

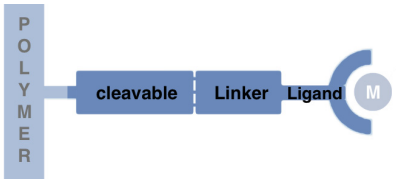


Two ligand funtionalised polylactides were developed for the coordination of Au(I) cores. One bearing a diphenylphosphane, the other a diphenylphosphinite ligand. Both form linear complexes with gold, a chloro ligand opposite of the phosphorus donor atom completes the coordination sphere.

### 5.2.1. Diphenylphosphinite functionalised polylactide L3

In a two step reaction, a polylactide bearing a diphenylphosphinite moiety for the coordination of gold(I) centres was prepared as shown in Fig 5.3.

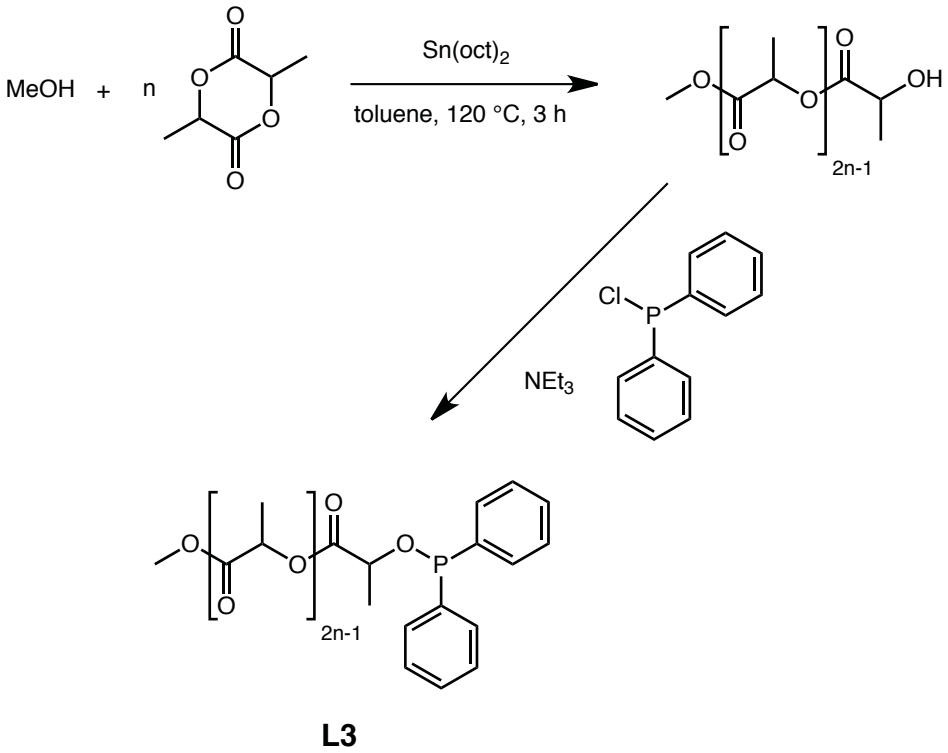


Figure 5.3.: Ring-opening polymerisation of L-lactide initiated by methanol to MeO-PLA and subsequent reaction with chlorodiphenylphosphane to MeO-PLA-$PPh_2$ (**L3**)

First, methanol was used to initiate the ring-opening polymerisation to yield a lactide with a methyl ester and a hydroxyl endgroup. After a polymerisation time of three hours, the lactide can be worked up as usual and precipitated as a white powder in yields of about 65 %. The lactide was then reacted under inert conditions with

chlorodiphenylphosphane in dichloromethane using triethylamine as base, both added in slight excess. Stirring at room temperature for eight hours resulted in phosphinite functionalised polylactides, which can either be worked up under inert conditions and the resulting white powder stored under a nitrogen atmosphere or reacted *in situ* with (tht)AuCl to afford the polymer-gold conjugate in yields of about 85 % (discussed in detail in chapter 5.3.1). The phosphinite functionalised lactides **L3** were characterised by $^{1}$H NMR, $^{31}$P{$^{1}$H} NMR and IR spectroscopy as well as MALDI-TOF mass spectrometry.

$^{1}$H NMR signals of the polylactide as well as the phenyl proton signals appear in the spectrum as well resolved signals. The signals attributed to the lactide are a quartet at 5.20 ppm and a doublet at 1.61 ppm for the methine and methyl protons of the repeating units, in ratios of 1:3. The signals attributed to the phenyl proton are a multiplet between 8.0 and 7.4 ppm and the singlet resulting from the protons of the methoxy group is found at 3.78 ppm.

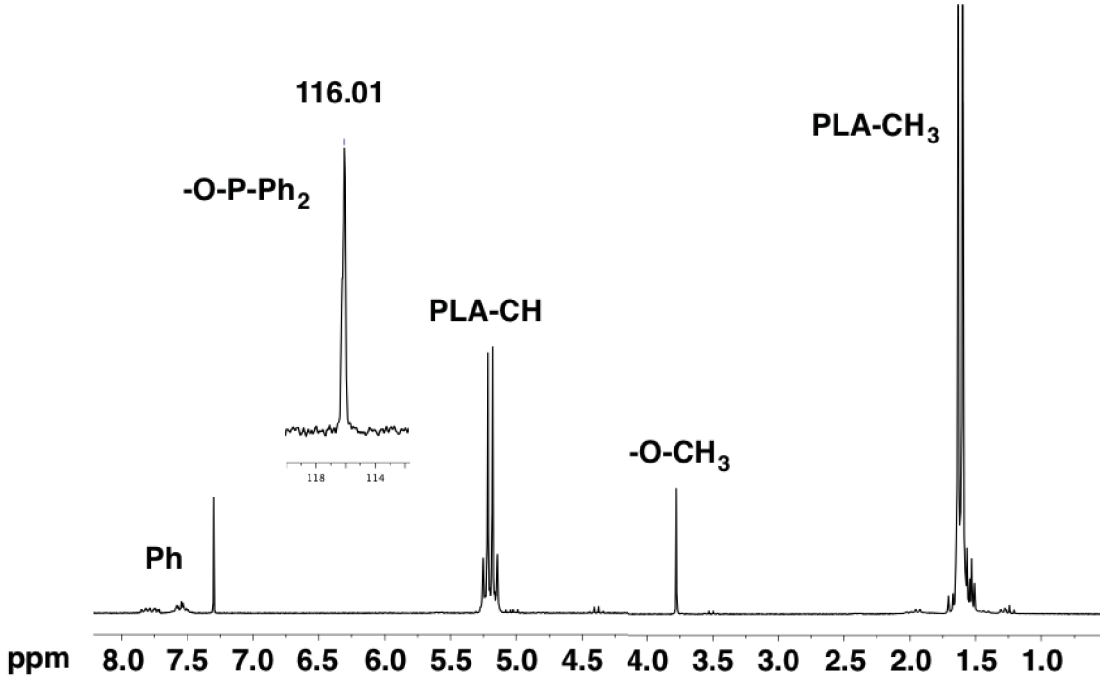


Figure 5.4.: $^{1}$H NMR and $^{31}$P{$^{1}$H} NMR data of MeO-PLA-PPh$_2$ (**L3**) in $CDCl_3$; signal at 1.61 ppm truncated.

$^{31}$P{$^{1}$H} NMR signals are found at 116 ppm attributed to the resonance of the phosphorus atoms in the phosphinite ($Ph_2$-P-O-PLA) as well as at 34 ppm in the phosphonate ($Ph_2$-P(O)-O-PLA) functional group, as the samples were exposed to atmospheric oxygen before and during measurement.

The MALDI-TOF spectrum shows the peaks corresponding to the masses of the oxidised phosphorus(V) species $Me(C_3H_4O_2)_nP(O)Ph_2^+$ and their respective sodium ion adducts

$Me(C_3H_4O_2)_nP(O)Ph_2+Na^+$. MALDI-TOF is especially useful to confirm the complete conversion to the ligand functionalised polymer, as the unreacted polylactides would be observable as another distribution curve of peaks in the spectrum.

The IR spectrum of MeO-PLA-$PPh_2$ shows the aliphatic C-H valence vibration bands at 2997 and 2947 $cm^{-1}$, the sharp C=O stretching vibration at 1759 $cm^{-1}$ as well as the C=C valence vibration bands from the aromatic system are found at 1456, 1385 and 1360 $cm^{-1}$ and the band associated with monosubstituted aromatic rings at 755 $cm^{-1}$.

## 5.2.2. Phosphane functionalised polylactide L4

In order to prepare a phosphane functionalised polylactide, a triphenylphosphane derivative was chosen as the initiator. The reason for choosing this particular phosphane is that Gunatilleke *et al.* have discovered that the ability to inhibit cathepsins increases with the number of phenyl rings on the phosphane ($Et_2PPh < EtPPh_2 < PPh_3$).[75] To this end, *o*-diphenylphosphinophenol was synthesised as published by Bianchi et al.[76]. In short, phenol was reacted with sodium hydride and chloromethyl methyl ether, to obtain methoxymethyl phenyl ether. This in turn was ortholithiated and reacted with chlorodiphenylphosphane to yield methoxymethyl *o*-diphenylphosphinophenyl ether. Subsequent acid hydrolysis leads to the hydroxy functionalised triphenylphosphane.

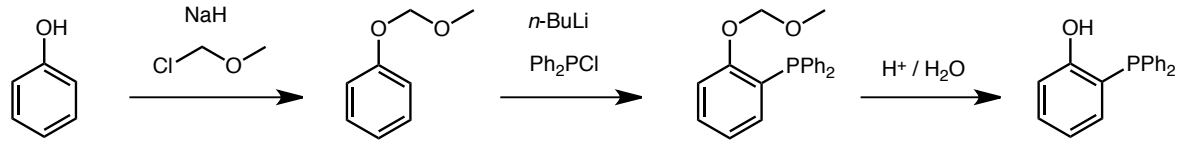


Figure 5.5.: Synthesis of *o*-diphenylphosphinophenol.[76]

Reaction of *o*-diphenylphosphinophenol with L-lactide was unsuccessful. Analysis confirmed only the synthesis of polylactides with octoyl endgroups, initiated by the catalyst stannous octoate. No phosphane functionalised lactides were obtained using this initiator. In this nucleophilic substitution reaction, the hydroxyl group of the phosphane needs to attack the electrophilic carbonyl group of the lactide ring to form tetrahedral intermediates ($S_N2t$). A possible explanation could be that the high steric demand of *o*-diphenylphosphinophenol hinders nucleophilic attack of the HOMO lone pair to the $\pi^*$ LUMO of the carbonyl or the subsequent formation of the tetrahedral intermediate. Looking at the literature, Kricheldorf *et al.* found that potassium phenoxide was unable to initiate the ring opening polymersation of L-lactide, concluding that the phenoxide ion ($pK_s \approx 9.5$) was either not basic or not nucleophilic enough to initiate the polymerisation.[77]

As an alternative approach, a phosphane functionalised polylactide can be afforded when using (diphenylphosphino)ethanol as the initiator. (Diphenylphosphino)ethanol can be prepared according to literature procedures by lithiation of diphenyl phosphane, subsequent reaction with oxirane and hydrolytic work-up (see Fig. 5.6).[78] This leads to polylactides with diphenylphosphane ligands with a distal hydroxyl endgroup for further derivatisation.

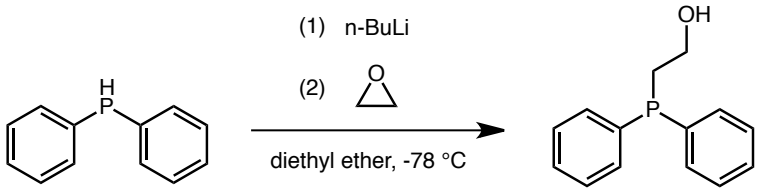


Figure 5.6.: Synthesis of (diphenylphosphino)ethanol.[78]

Ring-opening polymerisation of L-lactide with (diphenylphosphino)ethanol under inert conditions results in polylactides with diphenylphosphane endfunctionalisation for later coordination of gold(I). Yields of 29 % were achieved. The polymers have to be handled and stored under inert conditions to avoid oxidation to phosphorus(V) due to atmospheric oxygen. Alternatively, the ROP can be directly initialised by the corresponding gold(I) complex (discussed in detail in chapter 5.3.2). **L4** was characterised by $^{1}$H NMR, $^{31}$P{$^{1}$H} NMR and IR spectroscopy as well as MALDI-TOF mass spectrometry.

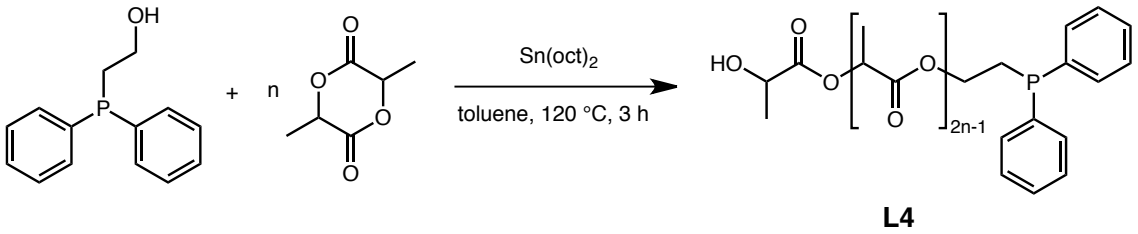


Figure 5.7.: Ring-opening polymerisation of L-lactide initiated by (diphenylphosphino)ethanol to yield PLA-$(CH_2)_2PPh_2$ (**L4**).

The $^{1}$H NMR spectrum of **L4** is quite similar to the spectrum of **L3**, since the signals of the ethyl protons (3.6 ppm for O-$CH_2$- and 2.7 ppm for -$CH_2$-P) are very weak compared to the intense signals of the protons in the repeating units, especially with increasing chain lengths. In comparison: the corresponding resonances of (diphenylphosphino)ethanol are at 3.8 ppm (O-$CH_2$-) and at 2.4 ppm (-$CH_2$-P). The signals attributed to the lactide are a quartet at 5.20 ppm and a doublet at 1.61 ppm for the methine and methyl protons of the repeating units, in ratios of 1n:3n with respect to the number of repeating units. The signals attributed to the phenyl proton signals result in a multiplet between 7.8 and 7.3 ppm.

$^{31}P\{^{1}H\}$ NMR signals are found at 29.5 ppm resulting from the oxidised polylactide $R_2P(O)$-$(CH_2)_2$PLA as well as at -21.6 ppm resulting from the phosphane resonance of **L4**.

In an NMR experiment, (tht)AuCl was added to the crude solution of **L3**, the sample taken directly after polymerisation. The $^{31}P\{^{1}H\}$ NMR was measured after one hour, displaying the signal for the oxidised polylactide at 29.5 ppm and a signal at 23.8 ppm, which can be attributed to the gold coordinated phosphine. The coordination shift amounts to 45.4 ppm; from -21.6 ppm of the free ligand to 23.8 ppm after coordination (see Fig. 5.8).

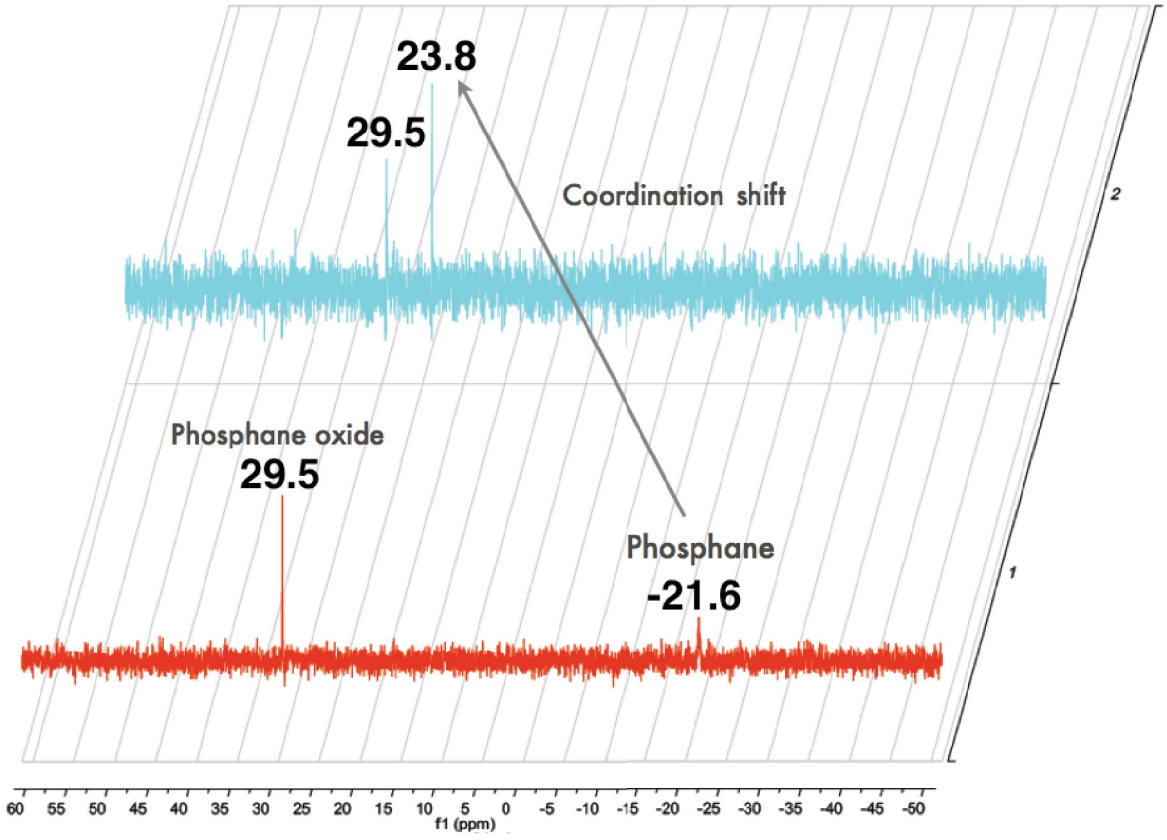


Figure 5.8.: Chemical shift of the phosphorus resonance before (below) and after (above) coordination to gold(I).

In comparison, the previously prepared (diphenylphosphino)ethanol has a similar $^{31}P$ chemical shift of -22.7 ppm, which is in accordance with the value of -23.0 ppm published by Muller *et al.*[79] The prepared the corresponding complex $[Ph_2P(CH_2)_2OH)AuCl]$ has a chemical shift of 24.1 ppm, amounting to a coordination shift of 46.8 ppm. Unfortunately, no value for the $^{31}P$ chemical shift of this compound could be found in the literature for comparison. Comparing the values for the lactide bound phosphane **L3** and the lactide gold conjugate **LC3** shows that the chemical shifts differ only slightly

from those of (diphenylphosphino)ethanol and [$Ph_2P(CH_2)_2OH$)AuCl]. Instead of the ethanol phosphane, the values for the ethyl phosphane $EtPPh_2$ and the corresponding gold(I) complex can be found in the literature. Their $^{31}P$ chemical shifts are 12 and 33.7 ppm[80, 70], respectively, resulting in a coordination shift of about 22 ppm. While the coordination shift is smaller, the tendency to shift towards lower field strength remains the same.

The MALDI-TOF spectrum shows the peaks corresponding to the oxidised polylactide $R_2P(O)$-$(CH_2)_2$PLA as well as their respective sodium ion adducts, as the samples are exposed to atmospheric oxygen during measurement.

The IR spectrum of PLA-$(CH_2)_2PPh_2$ **L4** shows the hydroxyl vibration at 3432 $cm^{-1}$, the aliphatic C-H valence vibration bands at 2997 and 2947 $cm^{-1}$ and the sharp C=O stretching vibration at 1759 $cm^{-1}$. The C=C valence vibration bands from the aromatic system are found at 1456, 1385 and 1360 $cm^{-1}$ and the bands associated with monosubstituted aromatic rings at 755 and 697 $cm^{-1}$.

## 5.3. Polylactide gold conjugates

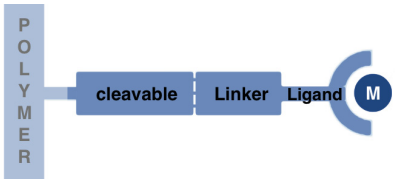


Coordinating gold complexes to carrier systems with phosphane or phosphinite ligands is best done directly after preparation of the polymer, since the phorphorus(III) atoms are sensitive to oxidation and the polymers would have to be handled and stored under a nitrogen atmosphere otherwise.

### 5.3.1. Phosphininte conjugate MeO-PLA-$PPh_2$-AuCl LC3

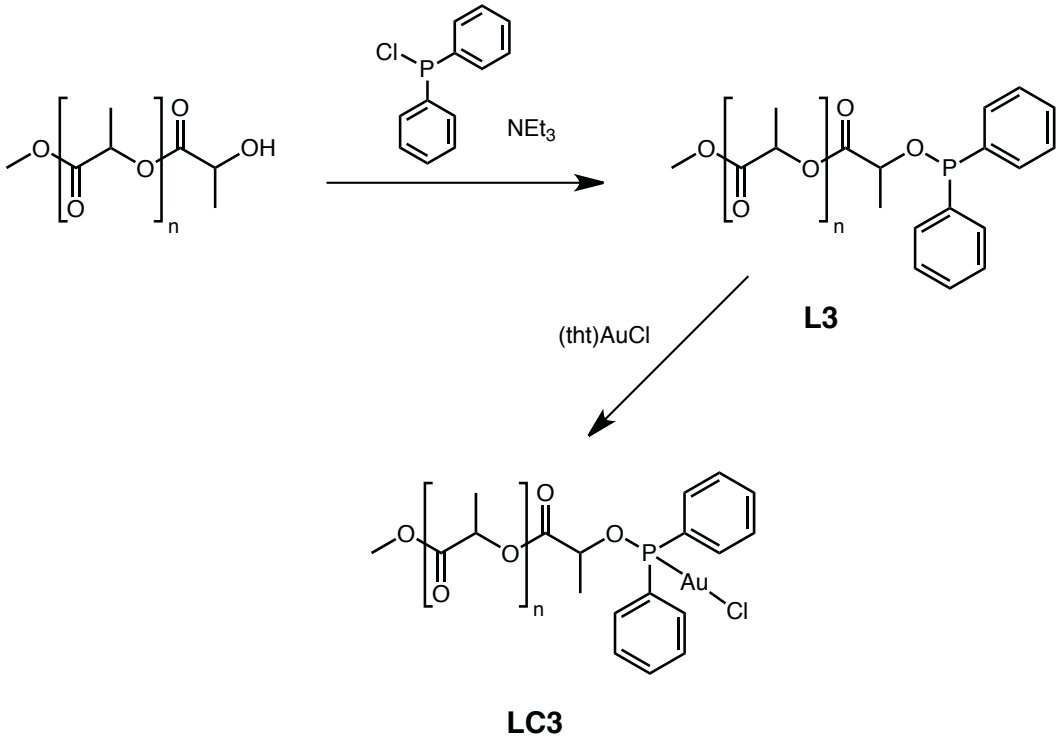


Figure 5.9.: Esterification of MeO-PLA with chlorodiphenylphosphane to **L3** and subsequent gold(I) coordination to **LC3**.

The prepared MeO-PLA (see chapter 5.2.1) was dissolved in dichloromethane and triethylamine was added in slight excess as the base. The reaction was carried out under a nitrogen atmosphere. Chlorodiphenylphosphane, also added in slight excess, was dissolved in dichloromethane and added drop wise to the solution using a syringe. The solution was stirred for three more hours at room temperature, whereupon (tht)AuCl was added stoichiometrically and the solution stirred for another hour. After the standard workup of washing with 0.1M HCl, brine and water, drying over $Na_2SO_4$ and solvent

removal in vacuo, the product was precipitated as a white powder from dichloromethane with diethyl ether. Yields of 86 % could be achieved. **C3** was characterised by $^{1}$H NMR and $^{31}$P{$^{1}$H} NMR spectroscopy as well as MALDI-TOF mass spectrometry.

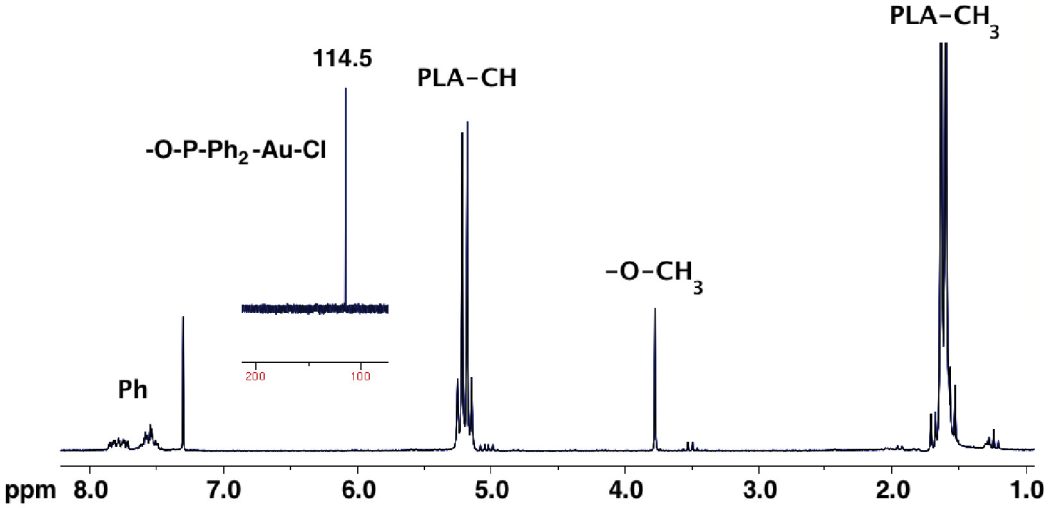


Figure 5.10.: $^{1}$H NMR and $^{31}$P{$^{1}$H} NMR data of **LC3** in $CDCl_3$; signal at 1.61 ppm truncated.

The $^{1}$H NMR spectrum of **LC3** corresponds to the spectrum of **L3** (see chapter 5.2.1), showing the signals of lactide and phenyl protons. The $^{31}$P{$^{1}$H} NMR signal of the phosphinite resonance on the other hand is slightly shifted downfield to 114.5 ppm upon coordination to gold(I). Since this coordination shift of 2 ppm is rather small, MALDI-TOF can be used to confirm the preparation of the conjugate.

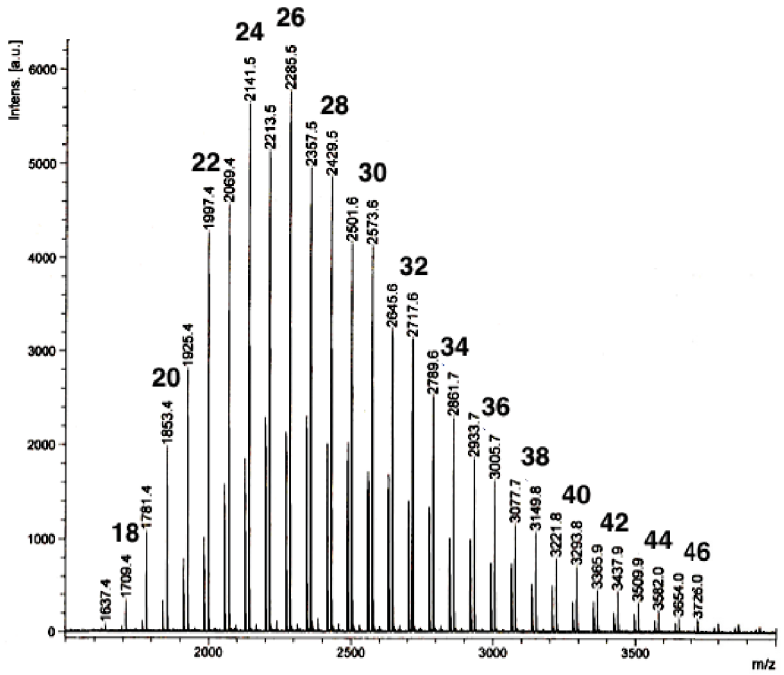


Figure 5.11.: MALDI-TOF spectrum of MeO-PLA-$PPh_2$-AuCl **LC3**

The MALDI-TOF spectrum confirms complete conversion to the gold-lactide conjugates. The only peaks in the spectrum are those resulting from the sodium ion adducts of the conjugates (high intensity peaks) as well as those of the conjugate cations themselves (lower intensity peaks, see Fig 5.11). The number of repeating units is marked on every even numbered peak from the sodium ion adducts.

### 5.3.2. Phosphane conjugate PLA-$(CH_2)_2PPh_2$-AuCl LC4

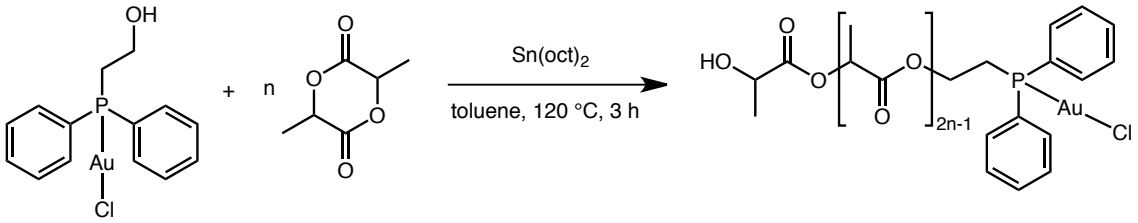


Figure 5.12.: ROP of L-lactide with $[Ph_2P(CH_2)_2OH\text{-}AuCl]$ to **LC4**.

Starting with $[Ph_2P(CH_2)_2OH\text{-}AuCl]$ instead of (diphenylphosphino)ethanol to initiate the ring-opening polymerisation of L-lactide leads to polylactide-gold conjugates in a single step. This is elegant, since it guarantees drug loading of each polylactide chain. In contrast, coordinating the gold(I) core to the preformed ligand polymer requires inert conditions for workup and storage of the polymer ligand, since it is otherwise rendered inactive by oxidation to the phosphine oxide. Furthermore, subsequent drug loading does not necessarily result in complete conversion to lactide-gold conjugates. Uncoordinated ligand polymers precipitate alongside the conjugates and are easily identifiable in the MALDI-TOF spectra. The reaction is carried out as usual, polymerising in refluxing toluene for three hours with stannous octoate as the catalyst. After workup and subsequent precipitation from dichloromethane with diethyl ether, the polymer is received as a white powder in yields of close to 50 %. **LC4** was characterised by $^1$H NMR, $^{31}P\{^1H\}$ NMR and IR spectroscopy as well as MALDI-TOF mass spectrometry.

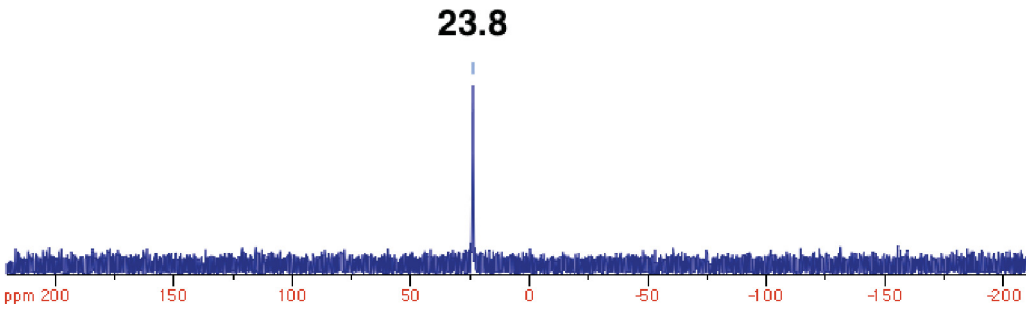


Figure 5.13.: $^{31}P\{^1H\}$ NMR of PLA-$(CH_2)_2PPh_2$-AuCl (**LC4**) in $CDCl_3$

The $^{1}$H NMR spectrum of **LC4** is equivalent to the spectrum for the unconjugated lactide **L4**. The signals attributed to the phenyl proton signals result in a multiplet between 7.8 and 7.3 ppm, methine and methyl protons of the repeating units result in a quartet at 5.20 ppm and a doublet at 1.61 ppm respectively, in ratios of 1n:3n, where n is the number of repeating units. More importantly, the $^{31}$P{$^{1}$H} NMR shows only one signal, at 23.8 ppm. This signal stems from the gold coordinated phosphane. No signals of free phosphane or phosphine oxide are be observed in the spectrum (see Fig. 5.13).

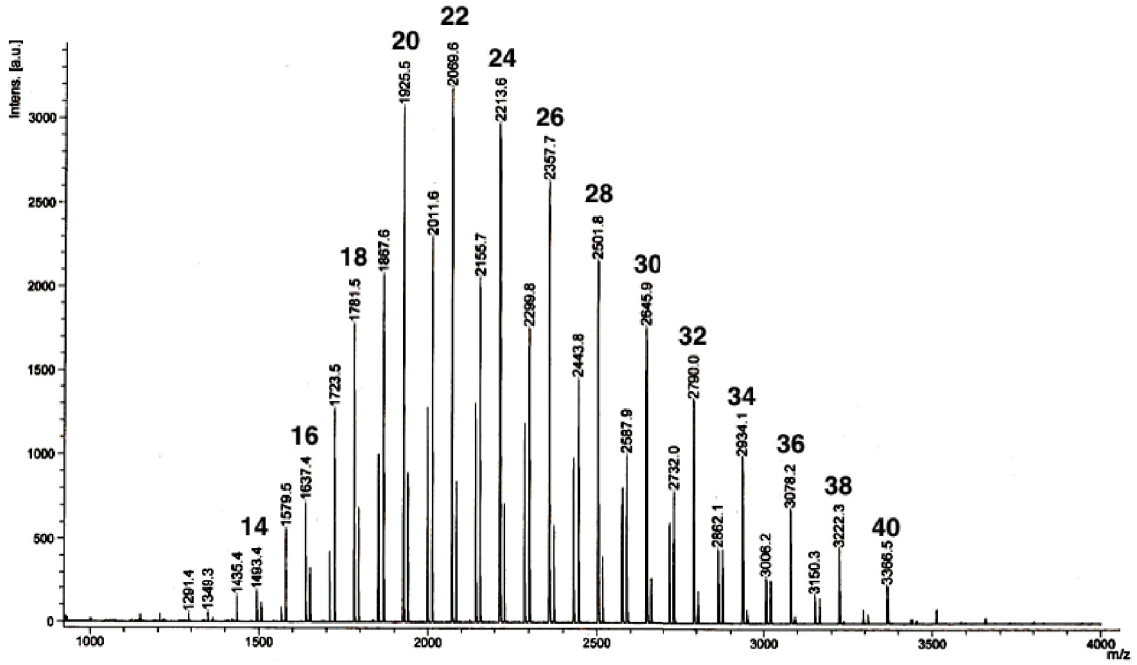


Figure 5.14.: MALDI-TOF spectrum of conjugate **LC4** with n = 14 to 40 repeating units.

The MALDI-TOF mass spectrum shows two intermeshed distribution curves of peaks (see Fig. 5.14) with alternating high and low intensities spaced in intervals of 72 m/z, which represents the mass of one repeating unit. Marked in the spectrum are the sodium ion adducts with even numbered repeating units. Usually, intermeshed curves of peaks mean incomplete conversion of the lactide, but in this case the gold was already coordinated to the ligand. Looking closer at the individual masses (see Fig. 5.15), the peaks of the sodium ion adducts of the gold-lactide conjugates as well as peaks of conjugates where a chlorido ligand was abstracted are discernible. Again, the MALDI-TOF spectra confirm the formation of the intended gold-phosphane polylactides.

The polylactide-gold conjugates **LC3** and **LC4** are quite air and light stable, as no degradation was observed during workup, analysis and further experiments, but they were nonetheless stored in Schlenk tubes under a nitrogen atmosphere at -20 °C as a precautionary measure. Their stability, especially regarding their possible application in medicine is very convenient, as they can be handled without knowledge of inert gas

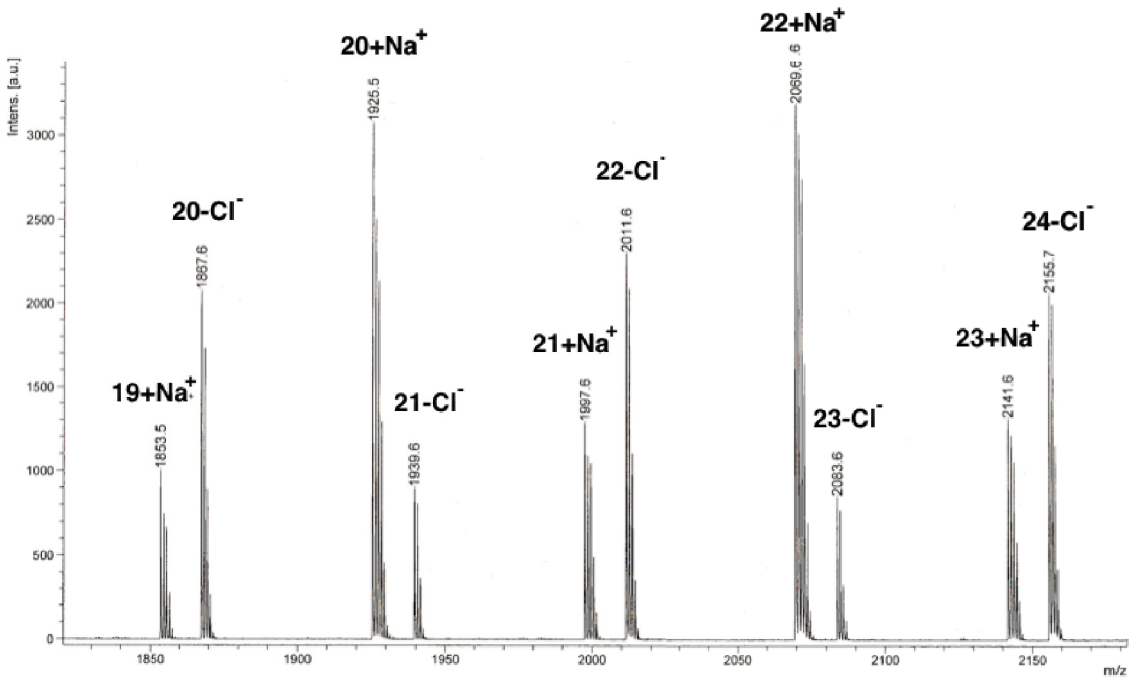


Figure 5.15.: Excerpt of MALDI-TOF spectrum of PLA-$(CH_2)_2PPh_2$-AuCl (**LC4**), signals attributed to polymer conjugates with n = 19 to 24 repeating units.

techniques etc. in a hospital context. The stability of such conjugates is not self-evident, as it is known that e.g. gold complexes with phosphinite ligands are very light sensitive which makes handling them quite arduous. Phosphinite gold complexes are particularly difficult to prepare and usually obtained in low yields as they are very soluble in most solvents and have the tendency to form oils when subjected to recrystallisation procedures.[81]

## 5.4. Methacrylate functionalised lactides and their gold conjugates

### 5.4.1. HPMA-PLA

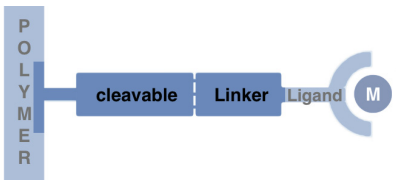


Devising macromonomers for gold coordination, HPMA monomers (N-(2-hydroxypropyl)-methacrylamide or N-(2-hydroxypropyl)methacrylate) can be chosen to initiate the ROP of L-Lactide, resulting in a methacryl functionalised lactide with a hydroxyl group on the other end. The two monomers differ in their polarity - the acrylamide is quite hydrophilic and soluble in polar solvents, whereas the methacrylate is quite lipophilic and soluble in organic solvents. Increased hydrophilicity is interesting in light of the *in vivo* application, but at the same time often poses a problem for synthesis with lipophilic reactants such as L-lactide etc. Both macromonomers were prepared. RAFT polymerisation with the resulting methacrylated polylactides can lead to quite versatile copolymers, since the hydroxyl group allows many ways of functionalisation and conjugation with ligands, complexes, as well as established chemotherapeutics. To create gold conjugates, it can be esterified with chlorodiphenylphosphane, forming a phosphane functionalised polymer.

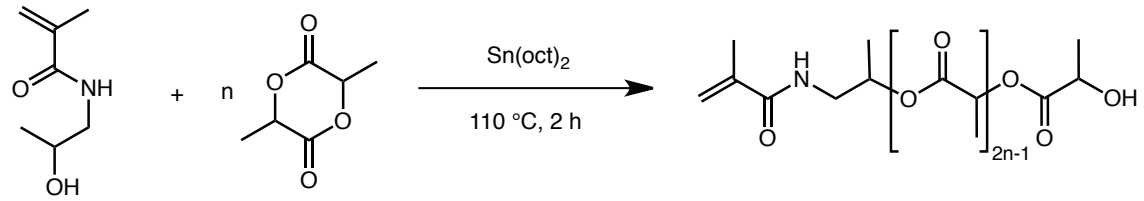


Figure 5.16.: Synthesis of HPMAn-PLA, ROP initiated by N-(2-hydroxypropyl)methacrylamide.

Synthesis using the methacrylate initiator was done analogously to the reactions using the equally lipophilic ligand initiators: L-lactide, initiator and catalyst were dissolved in toluene and refluxed at 115 °C for three hours. Yields of 87 % were achieved. The synthesis for the ROP with N-(2-hydroxypropyl)methacrylamide was modified from Neradovic *et al.*[82] The monomers were molten at 110 °C under a nitrogen atmosphere and stannous octoate in 0.5 mL dry toluene was added. The mixture was allowed to polymerise for two hours. After subsequent workup and drying under high vacuum, yields of about 80 % were achieved.

The methacrylated polylactides were characterised by $^{1}$H NMR and IR spectroscopy as well as MALDI-TOF mass spectrometry. The spectra of both compounds are obvi-

ously very similar. The analysis of the polylactide initiated with the methacrylamide is presented here, while the analytical data for both compounds can be found in the experimental part, chapter 12.2.

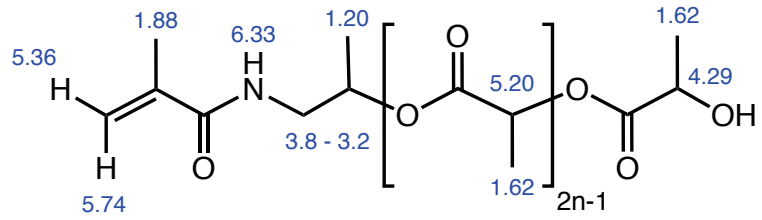


Figure 5.17.: $^{1}$H NMR chemical shifts of HPMAn-PLA

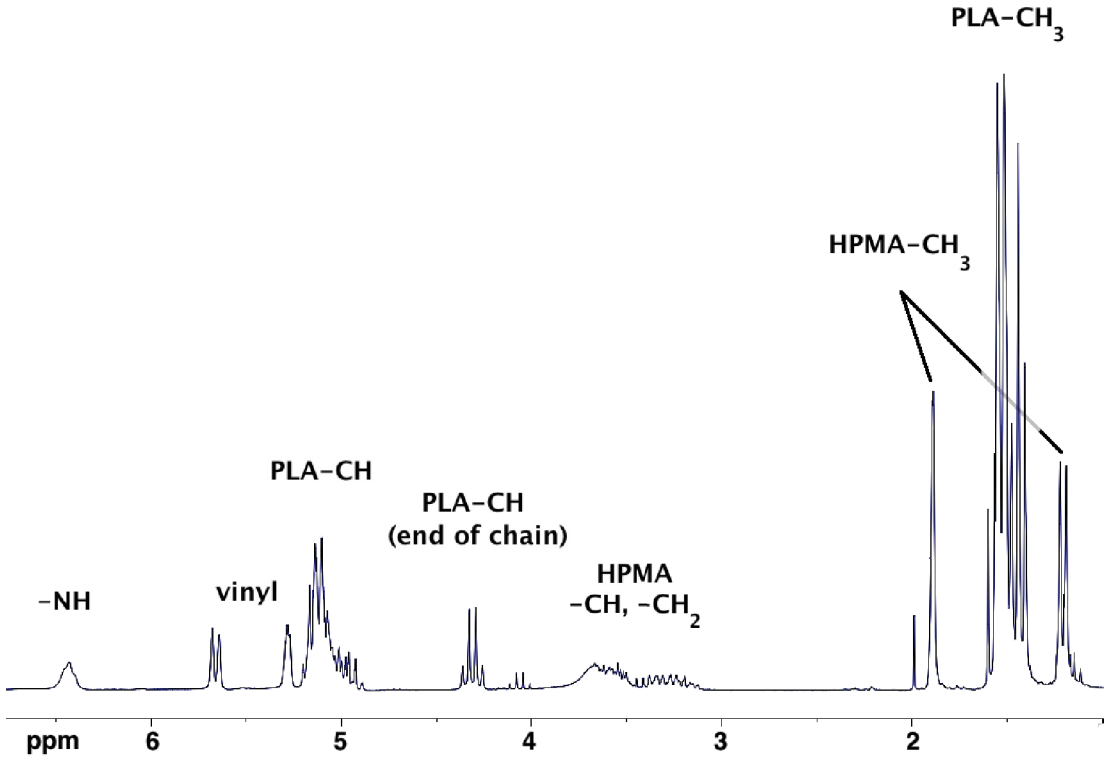


Figure 5.18.: $^{1}$H NMR spectrum of HPMAn-PLA in $CDCl_3$; oligolactide with an average of 4 lactide repeating units.

As represented in Fig 5.17, the proton resonances of the polylactide as well as those of the HPMA fragment can be assigned in the $^{1}$H NMR spectrum. The amide proton resonance appears at 6.33 ppm, the vinyl proton resonances are found at 5.74 and 5.36 ppm. HPMA-CH and -$CH_2$ protons appear as a multiplet between 3.8 and 3.2 ppm, resonances of the HPMA-$CH_3$ protons next to the vinyl group are at 1.88 ppm, the resonances of HPMA-$CH_3$ protons next to the ester group at 1.20 ppm. Resonances of the lactide repeating unit appear at 5.20 ppm in case of the methine and 1.62 ppm in case of the methyl protons. Usually, the signals are a quartet and a doublet. However, when

oligomers are measured, the resonances of methine and methyl groups in the repeating units close to the chainend are shifted towards the higher fieldstrengths, resulting in overlapping quartets and doublets (see Fig.5.18). The resonance of the terminal methine proton is shifted to 4.29 ppm.

The MALDI-TOF spectra show the distribution pattern of the masses corresponding to the sodium ion adducts of HPMA-PLA polymers with respect to the number of repeating units. Typical IR vibrations appear at 3453 $cm^{-1}$, associated with the hydroxyl valence vibration, the bands at 2991 and 2943 $cm^{-1}$ result from the aliphatic C-H valence vibrations and at 1754 $cm^{-1}$ resulting from the sharp C=O stretching vibration.

## 5.4.2. Methacrylated lactide-gold conjugate MLC3

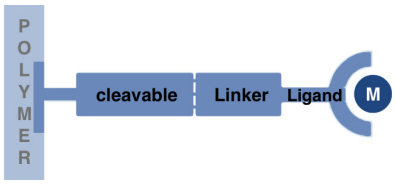


Conjugates of the phosphinite macromonomers were prepared as well, to test whether the vinyl group would interfere with the synthesis. This also opens up the possibility of copolymerising preformed conjugates. Starting from methacrylated polylactides, the hydroxy function was esterified with chlorodiphenylphospane to attain macromonomers for gold coordination.

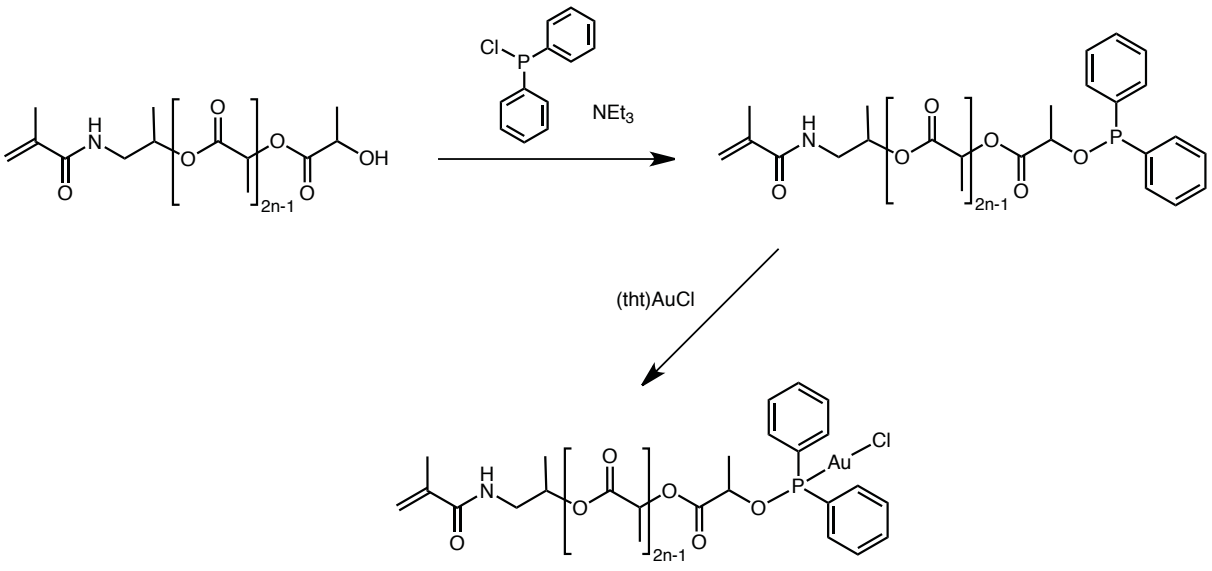


Figure 5.19.: Esterification of HPMA-PLA with chlorodiphenylphosphane and coordination to gold(I).

HPMA-PLA was dissolved in dry dichloromethane under inert conditions and a slight excess of triethylamine was added. Chlorodiphenylphosphane, also in slight excess, was dissolved in dry dichloromethane then added drop wise to the solution. After stirring for three hours, (tht)AuCl, equimolar to chlorodiphenylphosphane was added and it was stirred for another hour. The solution volume was reduced to a few mL at the rotary evaporator and the product precipitated and washed with diethyl ether. After drying under high vacuum, the product is received as a white powder in yields of about 85 %. **MLC3** was characterised by $^{1}$H NMR, $^{31}$P{$^{1}$H} NMR and IR spectroscopy as well as MALDI-TOF mass spectrometry.

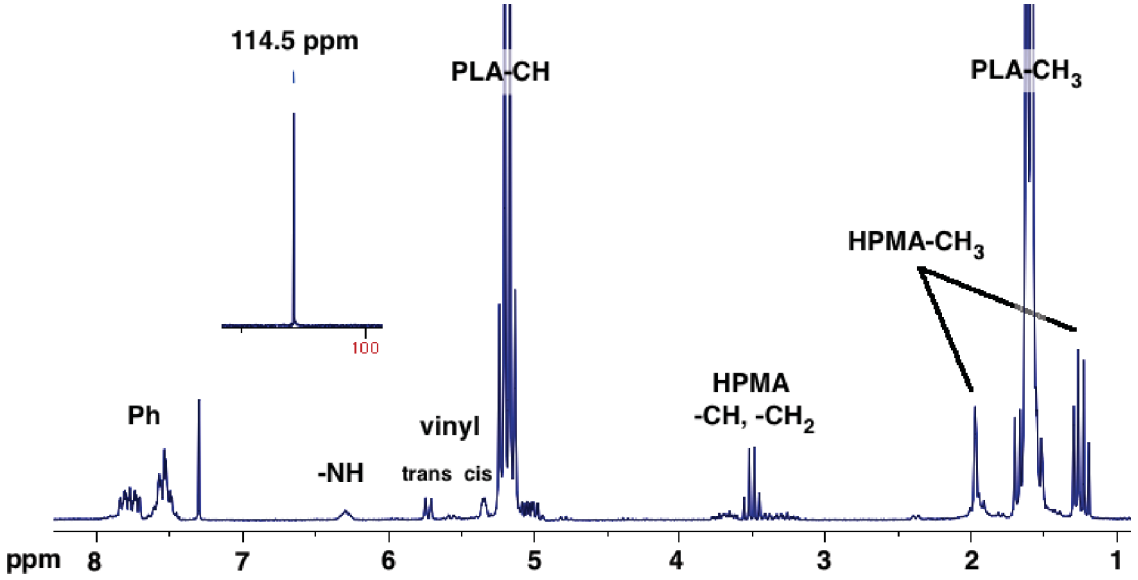


Figure 5.20.: $^{1}$H NMR spectrum of **MLC3** in $CDCl_3$, PLA signals truncated. Insert: $^{31}$P{$^{1}$H} NMR signal.

The proton resonances of the phosphane ligand, the polylactide and those of the HPMA fragment can be assigned in the $^{1}$H NMR spectrum (see Fig. 5.20). The phenyl proton resonances appear as a multiplet between 7.84-7.48 ppm, the amide proton resonance appears as a singlet at 6.33 ppm, vinyl-trans and vinyl-cis proton resonances at 5.74 ppm and 5.36 ppm respectively. HPMA-CH and -$CH_2$ protons appear as a multiplet between 3.8 and 3.2 ppm, resonances of the HPMA-$CH_3$ protons next to the vinyl group are 1.88 ppm, the resonances of HPMA-$CH_3$ protons next to the ester group at 1.20 ppm. Resonances of the lactide repeating unit appear at 5.20 ppm in case of the methine and 1.62 ppm in case of the methyl protons.

The $^{31}$P{$^{1}$H} NMR signal of the gold(I) coordinated phosphinite is found at a chemical shift of 114.5 ppm.

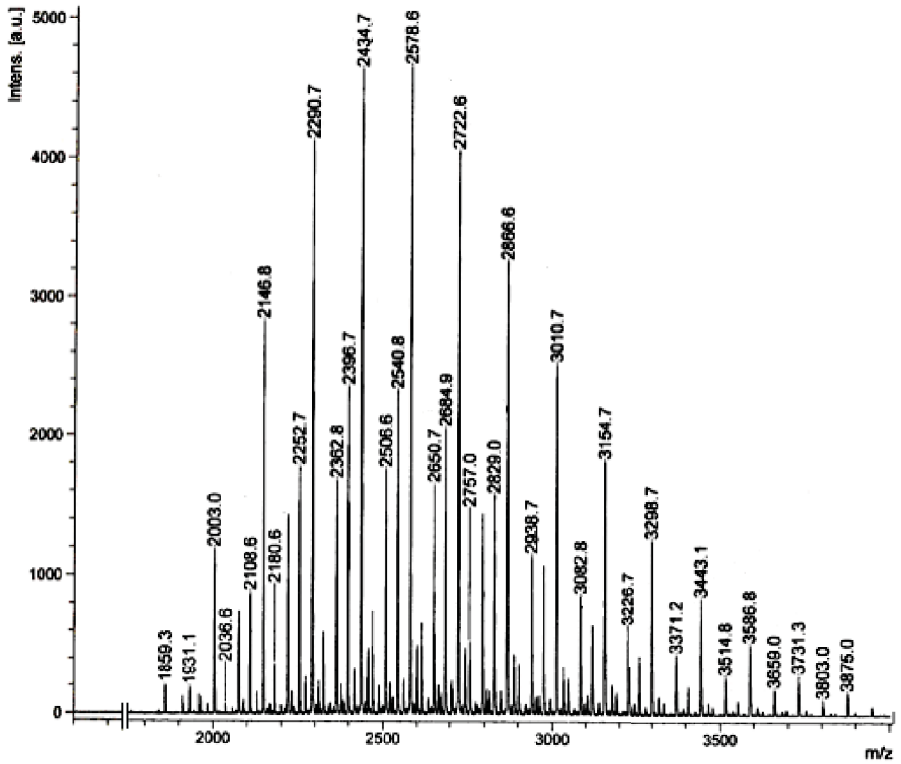


Figure 5.21.: MALDI-TOF spectrum of HPMA-PLA-$PPh_2$-AuCl.

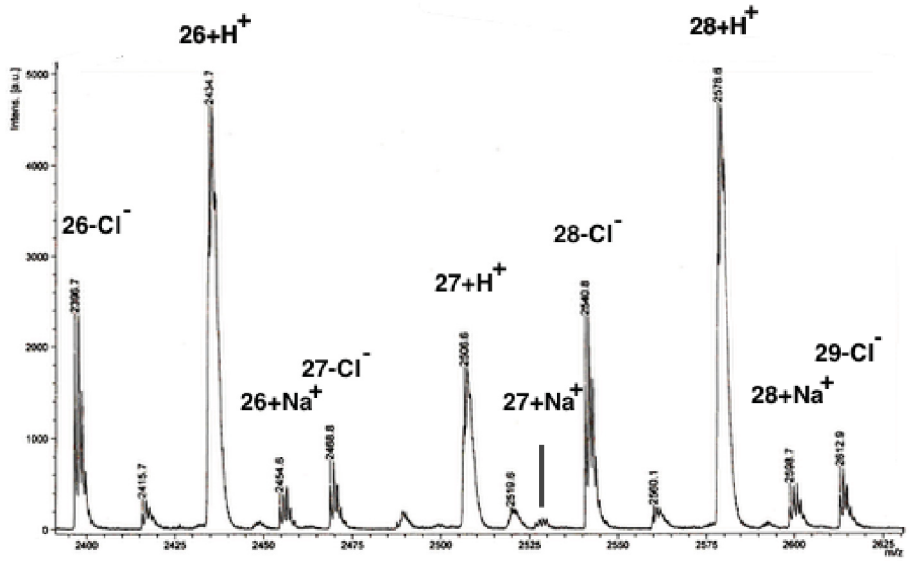


Figure 5.22.: Excerpt of the MALDI-TOF spectrum of **MLC3**, n = 26 to 29 repeating units.

The MALDI-TOF mass spectrum confirms derivatisation of the lactide to the phosphinite as well as the coordination of the gold fragment. The spectrum primarily shows two distribution curves of mass signals that can be attributed to the protonated polylactide-gold conjugate and those of the conjugates where the chlorido ligand has been cleaved off. Looking closer at the individual signals, a third pattern of signals of low intensity can

be attributed to the sodium ion adducts. There is one more pattern of signals, spaced according to the mass of the repeating unit, which still remains unassigned. No signals attributed to unreacted HPMA-PLA or uncoordinated HPMA-PLA-P(O)$Ph_2$ appear in the spectrum, however (see Fig. 5.22).

The IR spectrum of **MLC3** shows the aliphatic C-H valence vibration bands at 2998 and 2947 $cm^{-1}$ and the C=O stretching vibration at 1759 $cm^{-1}$. The phenyl C=C vibrations appear at 1457 and 1384 $cm^{-1}$ and the bands associated with monosubstituted aromatic rings at 754 and 697 $cm^{-1}$.

## 5.5. The polymeric carrier system P2

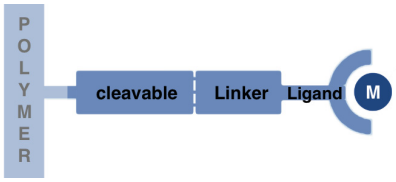


The previously prepared hydroxy functionalised HPMA-PLA was copolymerised with N-(2-hydroxypropyl)methacrylate). As with **P1**, a monomer ratio (HPMA to HPLA-PLA) of 5:1 was chosen for the preparation of the polymeric carrier-system **P2**.

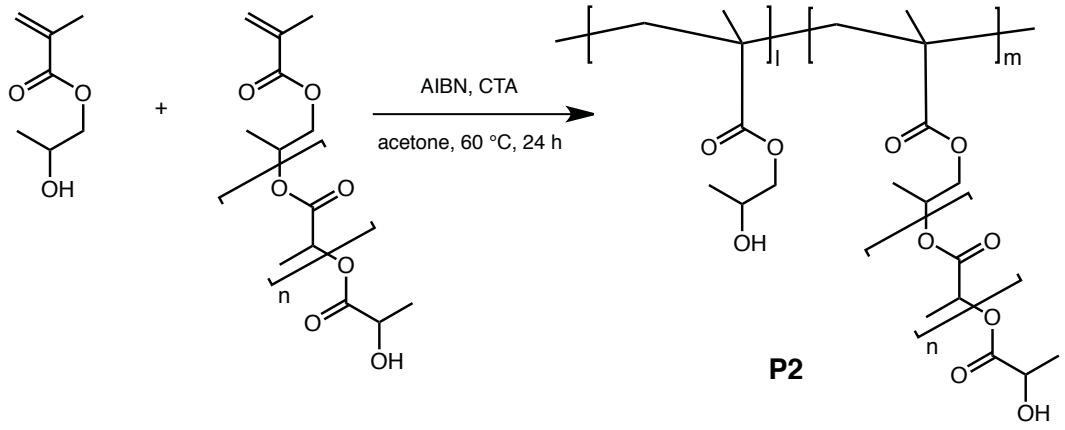


Figure 5.23.: RAFT polymerisation of HPMA and HPMA-PLA to synthesise **P2**.

The monomers, the radical starter AIBN as well as the chain transfer agent 2-cyano-isopropyl dithiobenzoate were put in a Schlenk tube under inert conditions and dissolved in dry toluene. The reaction mixture was stirred at 60 °C for 24 hours. The solvent was then evaporated at the rotary evaporator until the solution turned viscous. The polymeric solution was dripped into acetone/diethyl ether (25/75, v/v), whereupon the product precipitated. It was washed with diethyl ether and dried under high vacuum. The polymer is received in yields of about 45 %. HPMA-co-HPMA-PLA was characterised using $^1$H NMR and IR spectroscopy. To determine the average molecular weight

distribution of the polymer, a GPC analysis was carried out. The hydrodynamic volume of the carrier-system was investigated by DLS analysis. The findings of the GPC and DLS analyses are discussed in light of the applicability of **P2** as a carrier system in chapter 6.

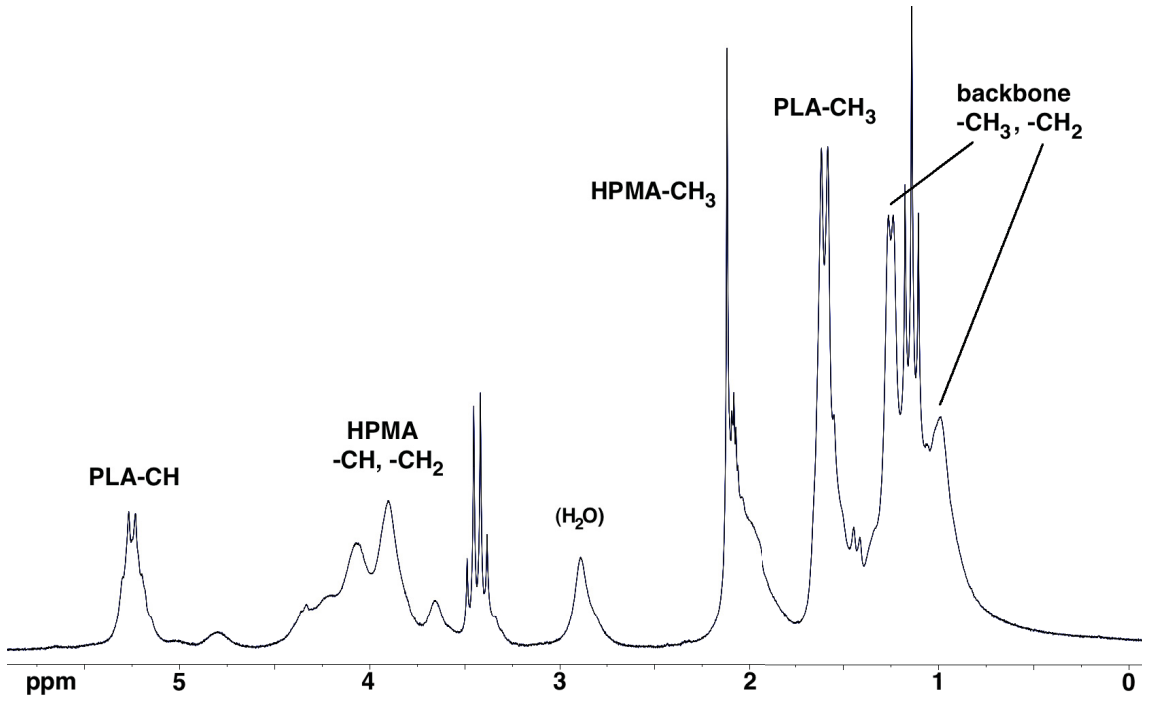


Figure 5.24.: $^{1}$H NMR spectrum in acetone-$d_6$ of HPMA-co-HPMA-PLA **P2**.

The $^{1}$H NMR signals of the lactide side chain are the two multiplets at 5.20 and 1.60 ppm from the methine and methyl protons with integral ratios of 1:3. HPMA proton resonances are the broad signals forming a multiplet between 4.4 and 3.6 ppm associated to the -$CH_2$ and -CH protons as well as the signal at 2.1 ppm associated to the methyl protons located in the side chain. The integral ratios are (2+1):3. The resonances from the -$CH_2$- and -$CH_3$ protons in the backbone of the polymer are resulting in a multiplet between 1.4 and 0.8 ppm. Factoring in the associated integrals of the fragments in the example of **P2**, depicted in fig. 5.24, shows a composition of ten HPMA monomers per lactide side chain. The lactide side chain has an average number of ten repeating units. This means that the final copolymer carries only about half the amount of lactide side chains then is expected from the monomer ratio before the polymerisation. The reason for this might be the chain length of the macromonomers. Longer chains could curl up on themselves, for example, and thus slow down their accessibility for the radical polymerisation.

The IR spectrum of **P2** shows the O-H valence vibration at 3453 $cm^{-1}$, the aliphatic C-H valence vibration bands at 2991 and 2945 $cm^{-1}$ and the C=O stretching vibrations at 1761 and 1729 $cm^{-1}$.

Determination of the chain length and molecular mass distribution by gel permeation chromatography revealed a number average molecular weight ($M_n$) of 52.5 kDa, a weight average molecular weight ($M_w$) of 67.7 kDa and a polydispersity of 1.29. Dynamic light scattering in acetone showed a number size distribution of 6.07 nm and a z-average diameter of 9.60 nm[1].

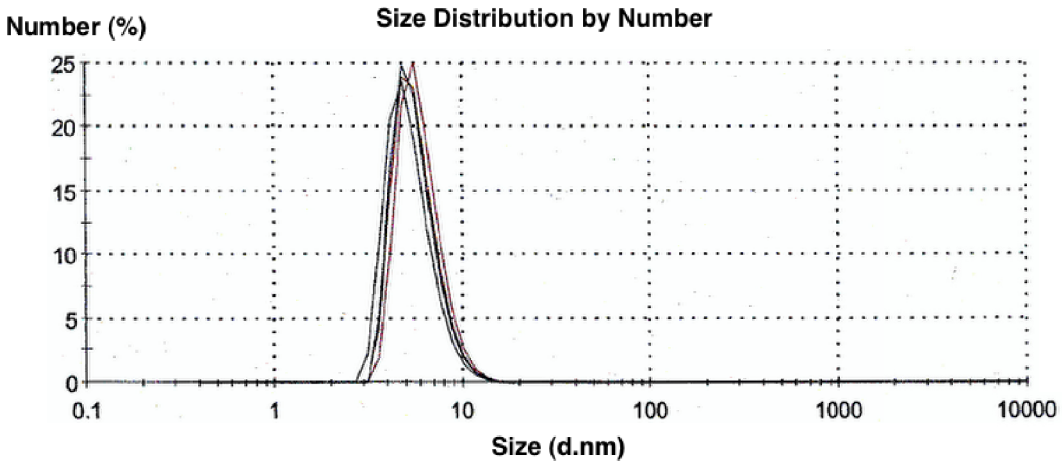


Figure 5.25.: Number size distribution data of **P2** after five repetitions of the DLS measurement in acetone at 25 °C.

## 5.6. The polymer-Au(I) conjugate PC2

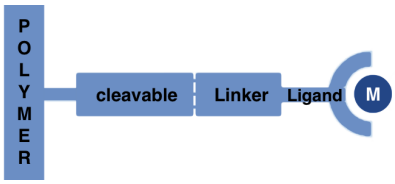


Finally, the prepared polymeric carrier system HPMA-co-HPMA-PLA **P2** was functionalised with chlorodiphenylphosphane and subsequently coordinated to the gold(I) fragment, affording the polymer-gold conjugate **PC2**.

The synthesis of the polymer-gold conjugate was done in two steps. First, HPMA-co-HPMA-PLA was dissolved in dry dichloromethane under a nitrogen atmosphere. Then the base, triethylamine was added and a solution of chlorodiphenylphosphane in dry dichloromethane was added drop wise to the reaction mixture and it was allowed to stir at room temperature for three hours. Secondly, (tht)AuCl was added and the solution stirred for another hour. The solvent volume was reduced in the rotary evaporator until the solution turned slightly viscous, whereupon it was added drop wise into a solution of acetone/diethyl ether (25/75, v/v). The polymer precipitated, was washed with diethyl ether and dried under high vacuum. The product is obtained in yields of close to 65 %. HPMA-co-HPMA-PLA-$PPh_2$-AuCl was characterised using $^1$H NMR, $^{31}$P{$^1$H} NMR and IR spectroscopy. The average molecular weight distribution of the polymer was

[1]The z-average diameter is the mean diameter based on the intensity of the scattered light.

determined by GPC analysis. Furthermore, an AAS was done to ascertain the gold content of the polymer and determine the degree of drug loading.

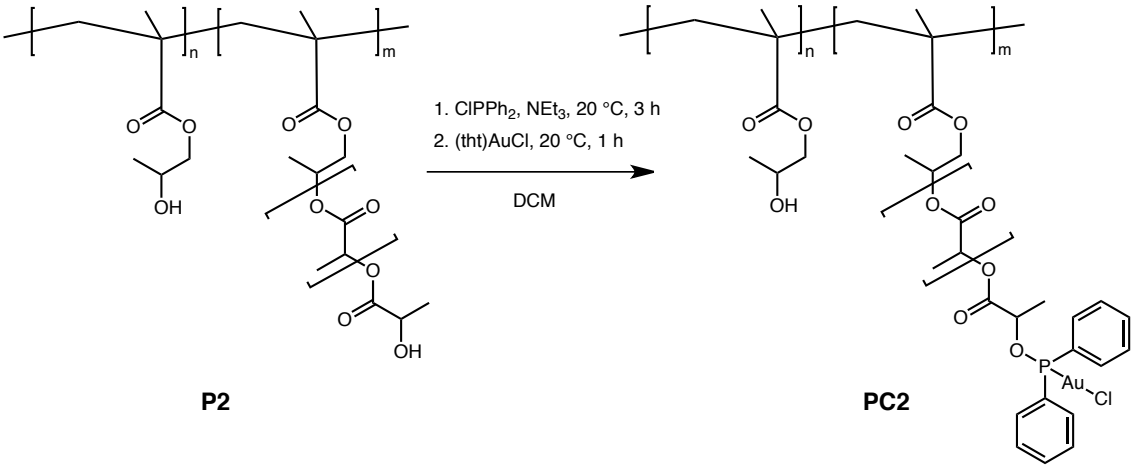


Figure 5.26.: Esterification of **P2** with chlorodiphenylphosphane and subsequent coordination of Au(I).

It is important to note that Fig. 5.26 does not reflect the actual structure of the polymer, as esterification can also occur on the HPMA hydroxyl group. To avoid this problem, it should be possible to polymerise the phosphinite functionalised macromonomer. In this case, great care has to be taken, since the monomer must be handled under an inert gas atmosphere at all times to avoid oxidation of the phosphinite ligand. Coordinating the gold core to the macromonomer before polymerisation could also be considered.

The proton resonances from the polymeric carrier system **P2** are found in the $^{1}$H NMR spectrum as described in chapter 5.5. Additionally, the resonances of the aromatic phenyl protons appear in the spectrum as a multiplet between 7.84-7.48 ppm. The $^{31}$P{$^{1}$H} NMR shows the singlet of the gold(I) coordinated phosphinite with a chemical shift of 114.5 ppm. Also in the spectrum are a small, but broad signal at 114.2 ppm as well as a small singlet at 92.4 ppm with as of yet undetermined origin.

The IR spectrum of **PC2** shows the O-H valence vibration at 3440 cm$^{-1}$, the aliphatic C-H valence vibration bands at 2998 and 2947 cm$^{-1}$ and the C=O stretching vibration at 1759 cm$^{-1}$. The phenyl C=C vibrations appear at 1457 and 1384 cm$^{-1}$ and the bands associated with monosubstituted aromatic rings at 749 and 692 cm$^{-1}$.

Gel permeation chromatography determined the number average molecular weight ($M_n$) as 64.6 kDa, the weight average molecular weight ($M_w$) as 71.4 kDa and the polydispersity as 1.10.

For AAS analysis, 14 mg polymer-gold conjugate were put in a conical flask and the organic material decomposed by refluxing in 4 mL concentrated nitric acid until complete

evaporation of the acid. This was repeated three times. The residue was dissolved in 2 mL refluxing aqua regia and diluted with 18 mL of distilled water. The solution was measured with AAS at a wavelength of $\lambda$=242.8 nm. As an external standard, gold(I) solutions of 1, 5, 15 and 45 mg/L were prepared and measured using the same parameters. The resulting linear equation (Fig. 5.27) was used to calculate the gold concentration of unknown samples.

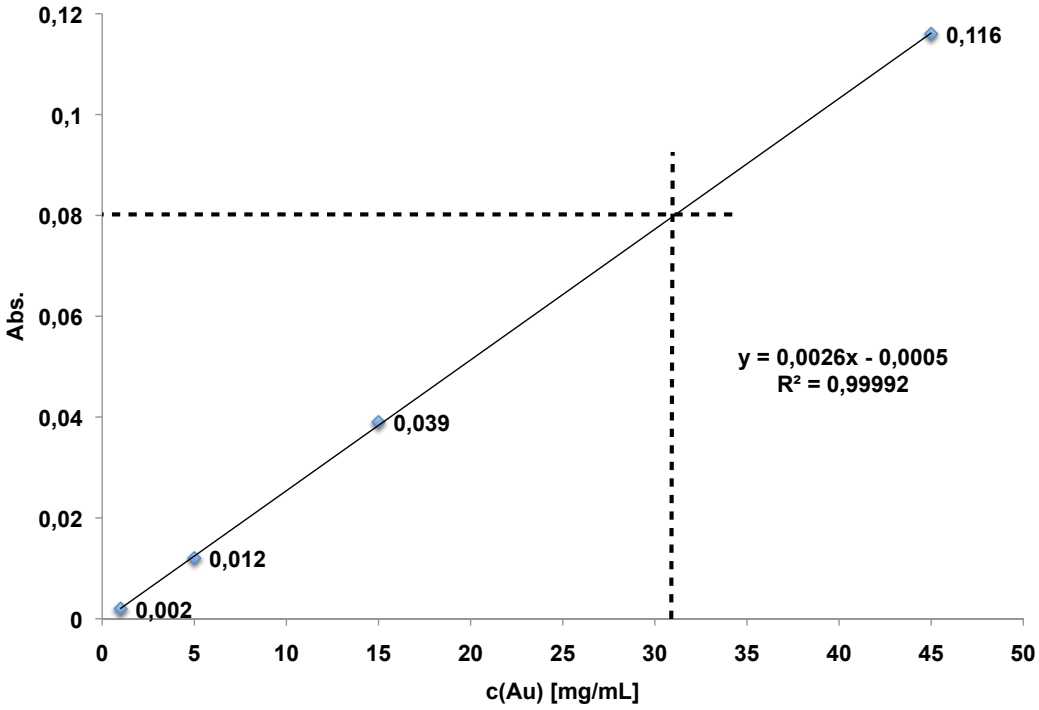


Figure 5.27.: Absorption vs. gold concentration, atomic absorption measured at $\lambda$=242.8 nm. Discontinuous line indicates absorption of polymer-gold sample.

The absorption of the sample from the polymer-gold conjugate was 0.161, which exceeds the range of the external standard. Consequently, the sample concentration was halved and the measurement repeated, resulting in an absorption value of 0.080 (indicated as a discontinuous line in fig. 5.27). Plugging the value in the linear equation of the external standard, this translates to a gold concentration of 62.5 mg/L for the undiluted sample, or 1.25 mg gold in 14 mg of the polymer conjugate. The polymer-drug conjugate thus contains 8.9 weight-% of gold(I).

Hopefully, this carrier system can improve current chrysotherapeutics by releasing the gold complexes in inflammation sites and tumour tissue. The distribution properties, degradation and drug release kinetics are evaluated and discussed in chapter 6. Experiments to reflect their ability to inhibit cathepsin B were done as well, using a cathepsin B activity assay[70], but without any definitive results. In short, lactide gold conjugates were added to a mixture of the enzyme cathepsin B and a substrate, which releases a

dye upon being cleaved by cathepsin B. The amount of dye released was compared to a standard amount of dye, measured with UV-Vis spectroscopy. [$PPh_3AuCl$] was used as an external standard for the inhibition of cathepsin B. Measurements were taken after 90 minutes of incubation with increasing concentrations ($10^{-6}$, $10^{-8}$, $10^{-10}$ and $10^{-12}$) of the conjugates **LC3** and **LC4**. Unfortunately, no decrease in cathepsin B activity was measured. This might be because of their inability to inhibit cathepsins - more probable, however, is the fact that the concentrations of **LC3** and **LC4** were too low (due to the low water solubility of the lactide conjuagtes), since the external standard also showed no notable inhibition at these concentrations (see fig. 5.28). Furthermore, inhibition could be hindered by residual undegraded oligolactide. A way of adressing this problem could be to use the corresponding gold complexes instead of the conjugates in a similar cathepsin B activity assay. Unfortunately, [$EtOPPh_2AuCl$] could not be prepared in sufficient purity, so far. As mentioned, phosphinite gold complexes are very light sensitive, very soluble in almost all solvents and tend to form oils when subjected to recrystallisation procedures.[81]

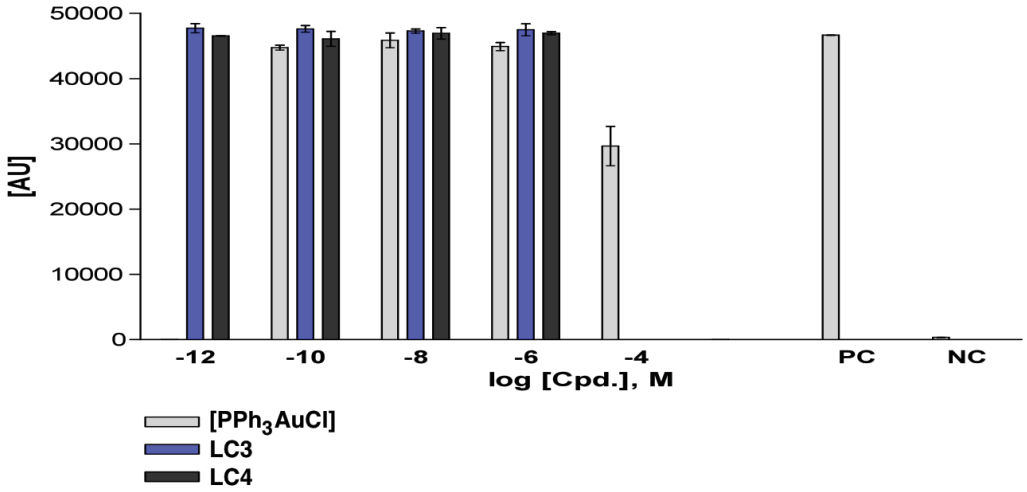


Figure 5.28.: Inhibition of cathepsin B by **LC3**, **LC4** and [$PPh_3AuCl$].

# 6. Pharmacokinetics

Now that routes to the successful preparation of macromolecules with conjugated rhenium tricarbonyl and gold metallodrugs have been found, it is necessary to take a closer look at their properties and how they could be useful in medicinal application.

## 6.1. Tissue distribution and tumour uptake

One of the basic requirements of targeted polymer-drug conjugates is that the molecular weight must be high enough for the polymers to accumulate specifically in tumour tissue due to EPR effect. Maeda et al. described that the key mechanism for the EPR of large molecules was the retention, whereas small molecules were simply not retained in the tumour but were returned to the circulation blood by diffusion.[83]

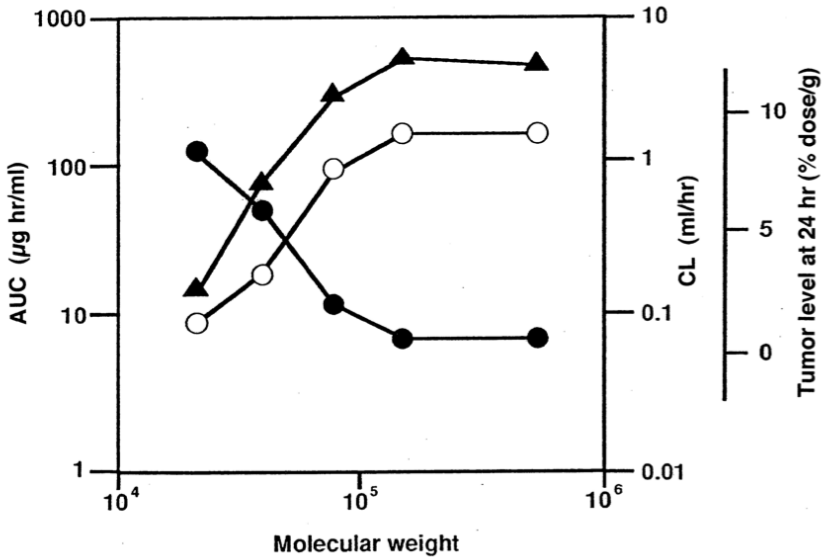


Figure 6.1.: Relationships for molecular weight, tumour uptake and clearance of $^{125}$I-Tyr-HPMA-polymer drugs. Mice bearing S-180 solid tumours received about 1.8 x $10^6$ cpm per injection i.v. Chart as published in [2].

It was discovered that macromolecules of more that 40 kDa remain at high levels in circulating blood because they have a much lower clearance rate than small molecular drugs. The findings of the study are summarised in Fig. 6.1. The values for the area under the concentration curve and tumour uptake increase in parallel, whereas the rate of urinary clearance is inversely related to the tumour uptake.[2]

At the same time, it is important to know the interaction and possible accumulation of such carrier systems in various organs. Studies have been done by Noguchi *et al.*[2] as well as Takakura and Hashida[84], regarding detailed organ biodistribution of macromolecles and clearance kinetics. An overview is presented in Fig. 6.2.

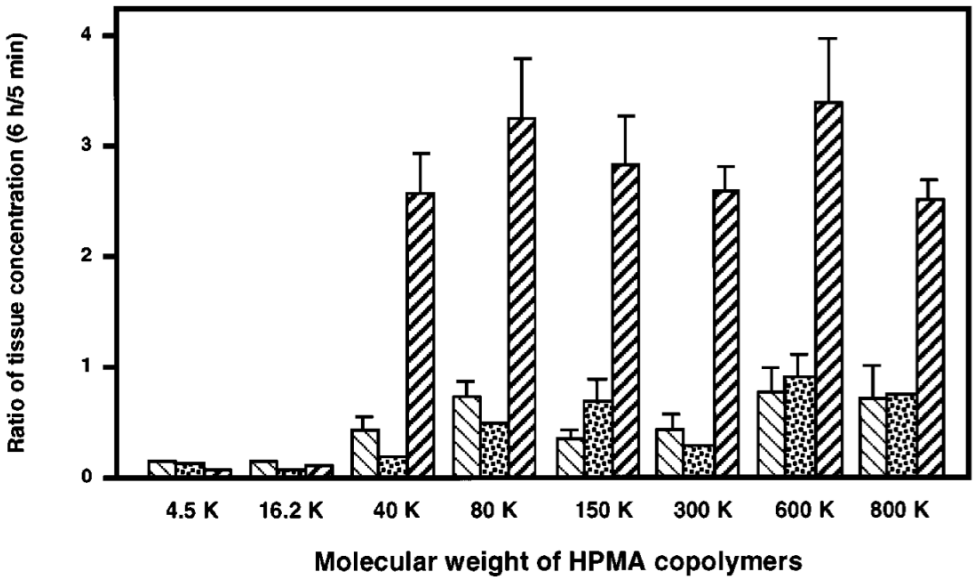


Figure 6.2.: Molecular weight-dependent accumulation in tumor and normal tissues following i.v. administration to tumor bearing (S-180) mice. Left column: liver; middle column: kidney; right column: tumour.[2]

The data clearly shows that a molecular mass threshold between 16 and 40 kDa exists, above which the polymers accumulate in tumours. Organ uptake increases as well, but to a much lesser extent. It is also interesting to note that once the weight threshold is exceeded, the ratio of HPMA copolymer concentration in the tumour tissue (to the applied dosage) remains the same. There is no increase in accumulation with further increase of molecular weight.

The molecular weight of HPMA polymers can be adjusted simply by varying the ratio of radical initiator to monomer used in the polymerisation reaction. A higher initiator concentration leads to lower molecular weights, lowering the initiator concentration will accordingly lead to higher molecular weight polymers.[85]

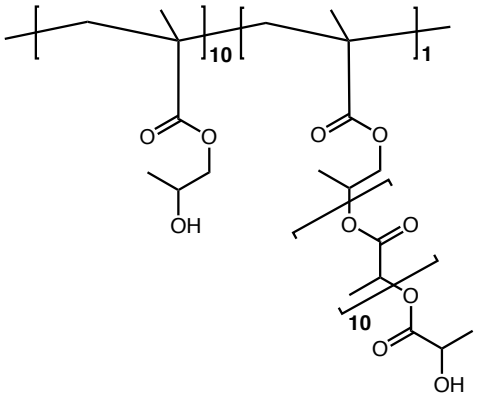


Figure 6.3.: HPMA based carrier with hydroxy functionalised oligolactide side chains.

The hydroxy functionalised polymeric carrier system depicted in fig. 6.3 was initiated by 0.55 mol-% AIBN and 1.10 mol-% 2-cyanoisopropyl dithiobenzoate (based on the total amount of monomers). GPC analysis determined a number average molecular weight ($M_n$) of 52.5 kDa and a weight average molecular weight ($M_w$) of 67.7 kDa, putting the molecular weight considerably above the threshold needed for passive targeting.

Altering initiator/monomer ratio can change the resulting average molecular weight as described. Derivatisation and drug loading of the carrier further increases the molecular weight. It should be kept in mind, however, that the non-degradable backbone must not exceed a weight of roughly 50 kDa to still be excreted by the kidneys.[86, 87]

Polymers are eliminated in the kidney by filtration through pores with a size of 5 nm, which is usually comparable to the hydrodynamic diameter of the polymer. In contrast, the openings in the defective vascular system of tumours are an order of magnitude greater than the hydrodynamic diameter of the polymers, sometimes even two. Thus, everything that influences the polymer structure, such as molecular conformation, chain flexibility, branching and location of the attached drug can greatly impact elimination of the polymer from the kidney, but has a much smaller effect on the extravasation of the tumour. Linear polymers with a hydrodynamic diameter of a little over 5 nm for example are flexible and might readily pass through the kidney glomerulus pores, whereas spherical, mostly inflexible dendrimers might not. A investigation into how polymer architectural features impact the renal filtration, as well as tumour penetration and accumulation was done by Frechet *et al*[4]. For size comparison see fig. 6.4. Depicted are (a) poly(vinyl alcohol) PVA (13.5 kDa), (b) PVA (580 kDa), (c) kidney glomerulus pore, (d) very large interendothelial junction in healthy tissue, (e) typical range of tumour pore diameters, (f) very large interendothelial junction in cancerous tissue.

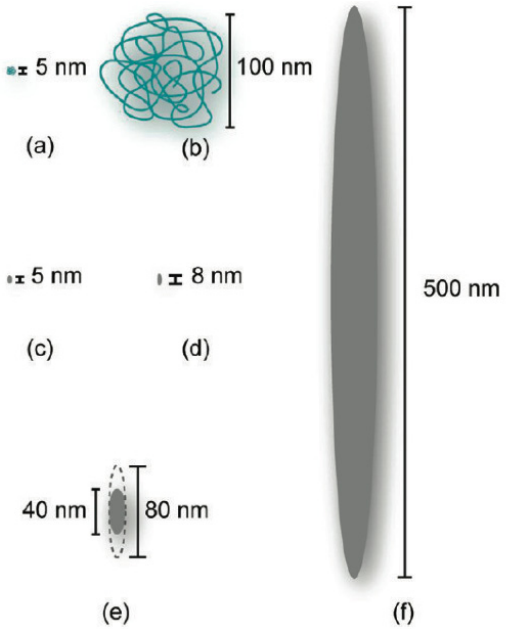


Figure 6.4.: Relative sizes of polymers of different molecular weights and various pores in the body.[4]

The prepared polymeric carrier systems are linear polymers, albeit with rather long side chains, making them more sterically demanding and less flexible than simple linear polymers without side chains. The prepared carrier system **P2** for example, with a number average molecular weight of 52.5 kDa has a z-average diameter of 9.6 nm as determined by DLS. This puts it above the the renal glomerular cut-off, which hinders fast renal elimination and increases the circulation time of the conjugate in the blood system, which in turn the enhances the accumulation and retention duration in the tumour. The hydrodynamic diameter of the polymer is about 4 to 50 times smaller than the tumor pores and interendothelial junctions in cancerous tissue. It is also about the size of the largest interendothelial junctions in healty tissue, but in contrast to cancerous tissue, polymers are quickly removed from healthy tissues and returned to the blood compartment by the lymphatic system.

## 6.2. Polymer degradation and drug release

The degradation mechanism of PLA derivatives is believed to occur mainly through random chain scissions, causing a gradual decrease in the molecular weight. Recent studies show, however, that the degradation mechanism and the kinetics are strongly influenced by the nature of the chain end. Oligolactides with free hydroxyl chain ends degrade predominantly by chain end scission via a backbiting mechanism with a pseudo first-oder rate constant of $k_{bb} = 2.7\ \mathrm{h}^{-1}$ (aqueous buffer, pH 7.2, 37 °C). Once the hydroxyl groups are protected, e.g. by acylation, random chain scission becomes the predominant degradation mechanism with a much lower rate constant of $k_r = 0.022\ \mathrm{h}^{-1}$ (aqueous buffer, pH 7.2, 37 °C)[88]. It was concluded that at a pH of 2 or lower, the ultimate ester bond is the most labile, while the penultimate ester bond is preferentially hydrolysed in neutral or alkaline pH, resulting in the stepwise removal of lactoyllactate, due to the so called backbiting mechanism (see fig. 6.5).

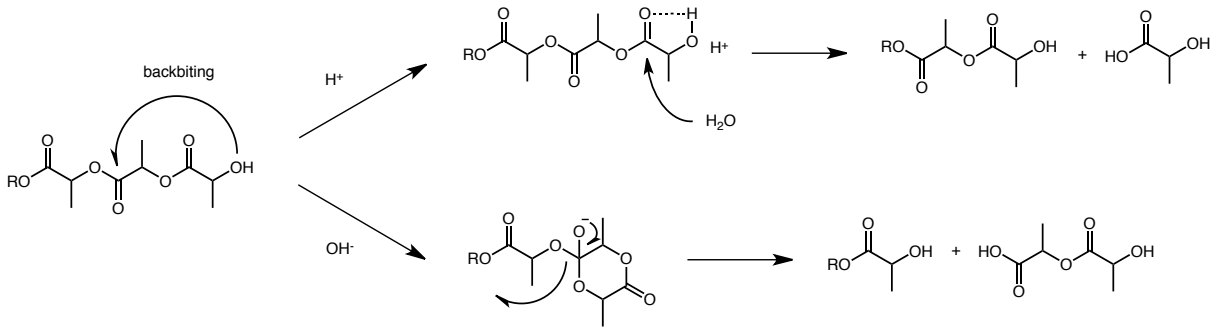


Figure 6.5.: Degradation of oligo(lactic acid) by chain end scission. Backbiting is catalysed by hydroxyl ions.[88]

The first order reaction rates for lactides with a hydroxyl chain end or a derivatised chain end can be calculated, as thoroughly investigated and described in the work of van Nostrum *et al.*[88] In case of a HPMA initialised lactide, the degradation of the ester bond between HPMA and lactic acid (with a rate constant of $k_{HPMA} = 0.0056\ \mathrm{h}^{-1}$ at pH 7.2, aqueous buffer, 37 °C) has to be taken into account, since it is considerably slower than that of the ester bond between two lactic units. Furthermore, the free hydroxyl endgroup allows degradation by backbiting, which also has to be included in the calculations.

$$k = (n-2) * k_r + k_{HPMA} + k_{bb} \tag{6.1}$$

In contrast, derivatised polylactides are degraded by random chain scission since initial backbiting is impossible, resulting in a considerably slower degradation rate.

$$k = (n-1) * k_r + k_{HPMA} \tag{6.2}$$

The degradation half lives $t_{1/2}$ can be calculated according to the equation for first order reaction kinetics.

$$t_{1/2} = \frac{ln2}{k} \tag{6.3}$$

An overview of the scission rate constants as well as the calculated degradation rate constants and degradation half lives for some examples of the prepared carrier systems are shown in table 6.1.

Table 6.1.: Calculated reaction rate constants and half life times for the hydrolysis of the lactide side chains in HPMA copolymers (aqueous buffer at pH 7.2 and 37 °C)

| | **rate constant** $k(h^{-1})$ | **half life** $t_{1/2}(h)$ |
|---|---|---|
| $k_{HPMA}$ | 0.0056 | 123.8 |
| $k_r$ | 0.022 | 31.5 |
| $k_{bb}$ | 2.7 | 0.26 |
| HPMA-co-HPMA$(PLA)_4$-OH | 2.75 | 0.25 |
| HPMA-co-HPMA$(PLA)_{10}$-OH | 2.93 | 0.24 |
| HPMA-co-HPMA$(PLA)_{20}$-OH | 3.10 | 0.22 |
| HPMA-co-MA$(PLA)_4$-O-$CH_2(C_5H_4N)$ | 0.088 | 7.88[a] |
| HPMA-co-MA$(PLA)_{10}$-O-$CH_2(C_5H_4N)$ | 0.22 | 3.15[a] |
| HPMA-co-MA$(PLA)_{20}$-O-$CH_2(C_5H_4N)$ | 0.44 | 1.56[a] |

[a] calculated with $k = (n) * k_r$

Chains that are degradable by backbiting, which is the fastest degradation step, have a degradation half life of only about 15 minutes, whereas polymers without the possibility of initial backbiting are degraded much slower, taking hours to degrade. The calculations stress the fact that longer lactide chains are degraded faster, since there are more scission sites, which results in faster drug release. Once initial cleavage of the side chain has occurred and backbiting is made possible, the polylactides degrade very rapidly. This is quite useful, as it enables fast degradation of the carrier upon drug release, leaving the bare polymethacrylate backbone small enough to be excreted.

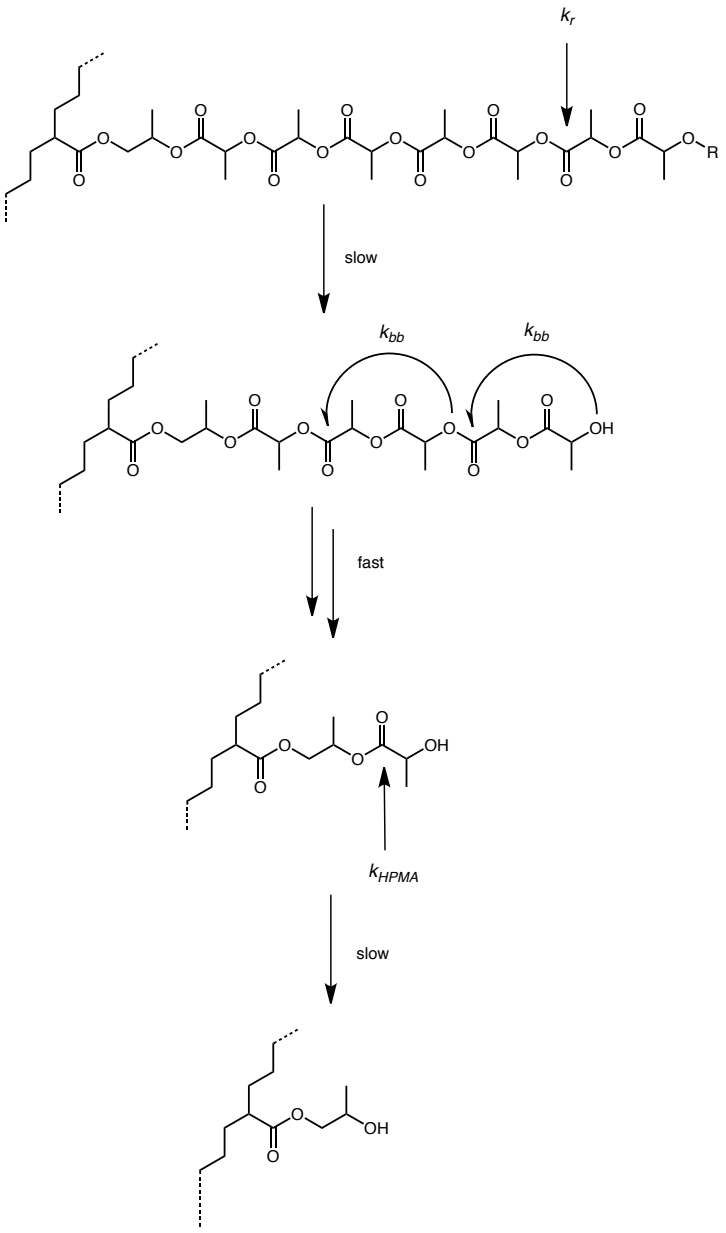


Figure 6.6.: Reaction scheme showing the possible degradation of a polymeric carrier with HPMA backbone bearing protected lactide side chains.

A bare poly-HPMA backbone with an average number of 250 repeating units has an average molecular weight of 36 kDa, which is a useful molecular weight of non-degradable polymers for in vivo application, because it does not accumulate in the tumour tissue after drug release, is diffused back to the bloodstream and can be readily excreted by the kidneys. Average molecular weights, degradation rates and the amount of released drug of carrier systems using this backbone were calculated.

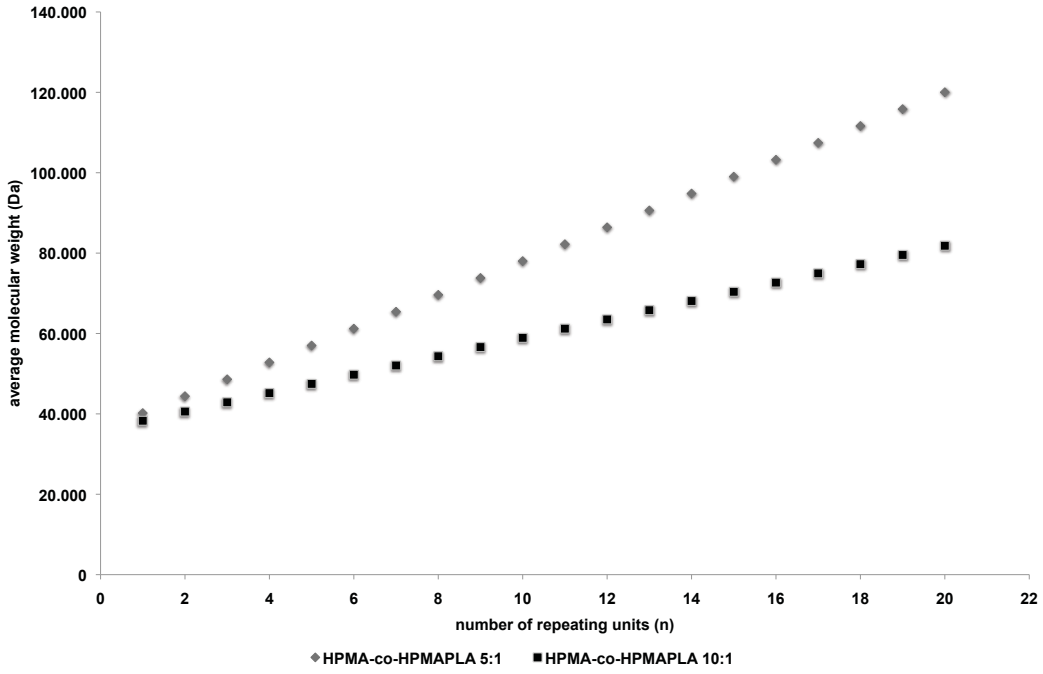


Figure 6.7.: Average molecular weight vs side chain length of HPMA-co-HPMAPLA

Two cases were differentiated - one lactide side chain for either every five or for every ten HPMA units. The resulting average molecular weights with increasing lactide chain lengths (with a maximum of 20 repeating units) were calculated (see fig. 6.7).

This way, copolymers of up to 120 kDa can be obtained in case of a 5:1 ratio and 82 kDa in case of a 10:1 ratio. Subsequent derivatisation with ligands and attachment of the drug molecules increases the average molecular weight further. The carrier systems with lactide side chains on every sixth backbone repeating unit can bind up to 42 drug molecules per macromolecule, the carrier systems with lactide side chains on every eleventh repeating unit up to 23. The degradation half life of these polymers can be calculated as described above and the results are depicted in fig. 6.9.

By choosing the drug loading per polymer as well as selecting lactide chain length, drug release can be fine-tuned. A high dose of active drug can be released over a short period of time, when a high drug loading is chosen and cleavable side chains are long, whereas a low dose of active drug can be released over a longer period of time when a low drug loading is combined with short lactide side chains.

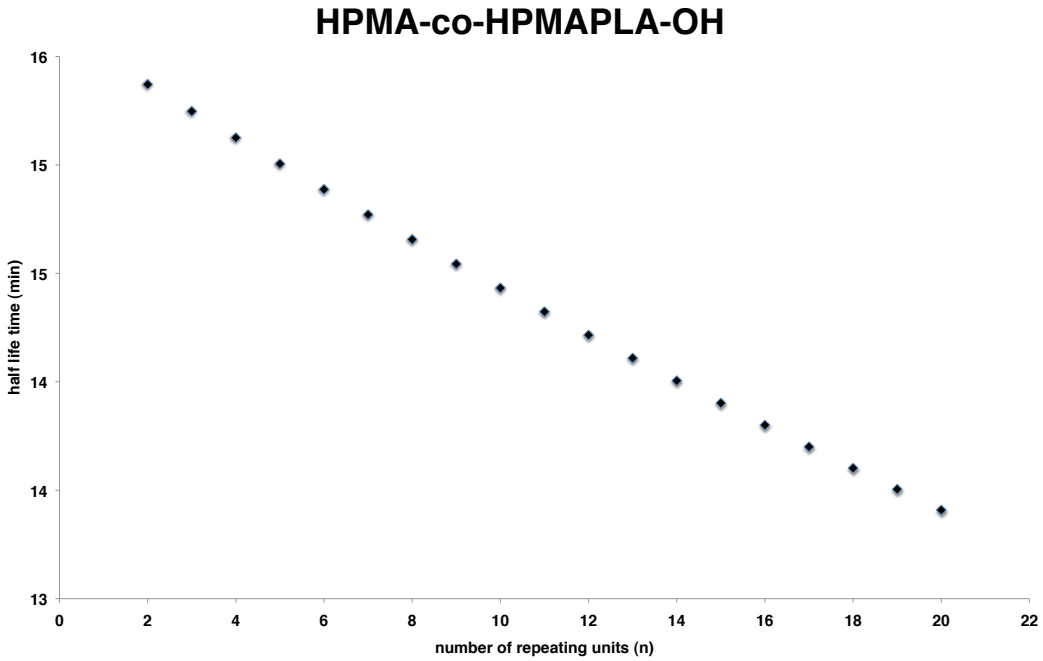


Figure 6.8.: Degradation half life vs lactide chain length of hydroxy functionalised polymers at pH 7.2 and 37 °C.

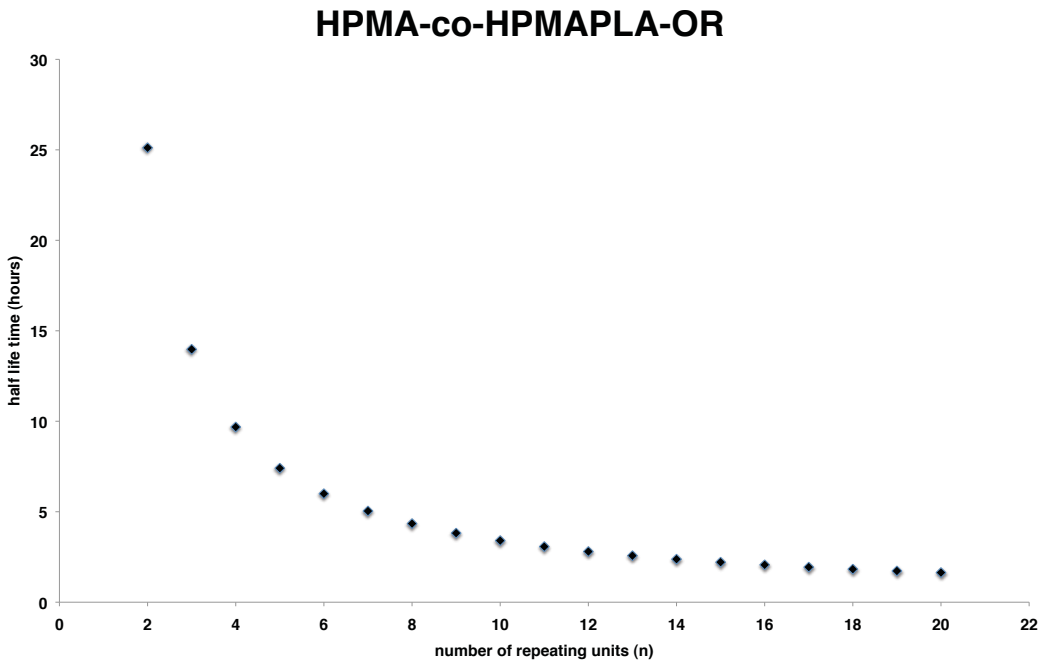


Figure 6.9.: Degradation half life vs lactide chain length of ligand functionalised polymers or polymer conjugates at pH 7.2 and 37 °C.

In order to calculate drug release and resulting plasma levels, a degradation profile of the selected drug conjugate can be created using the equation for first order reaction kinetics.

$$[A]_t = [A]_0 * e^{-kt} \tag{6.4}$$

The concentration of undegraded polymer conjugate is a function of the concentration of the polymer conjugate at the beginning, of the rate constant $k$ and the time $t$. For the calculations, polymer concentration was defined as 1, time was calculated in increments of one hour (up to 20 hours) and the rate constant for derivatised polymers of $k_r = 0.022$ $h^{-1}$ was used. The rate constants of backbiting and scission of the ester bond between HPMA and lactide are not needed in the calculation, because drug release occurs upon initial chain cleavage, which is random chain scission. Degradation profiles of polymer conjugates with side chain lengths of 2, 4, 6, 10 and 20 repeating units are shown in fig. 6.10.

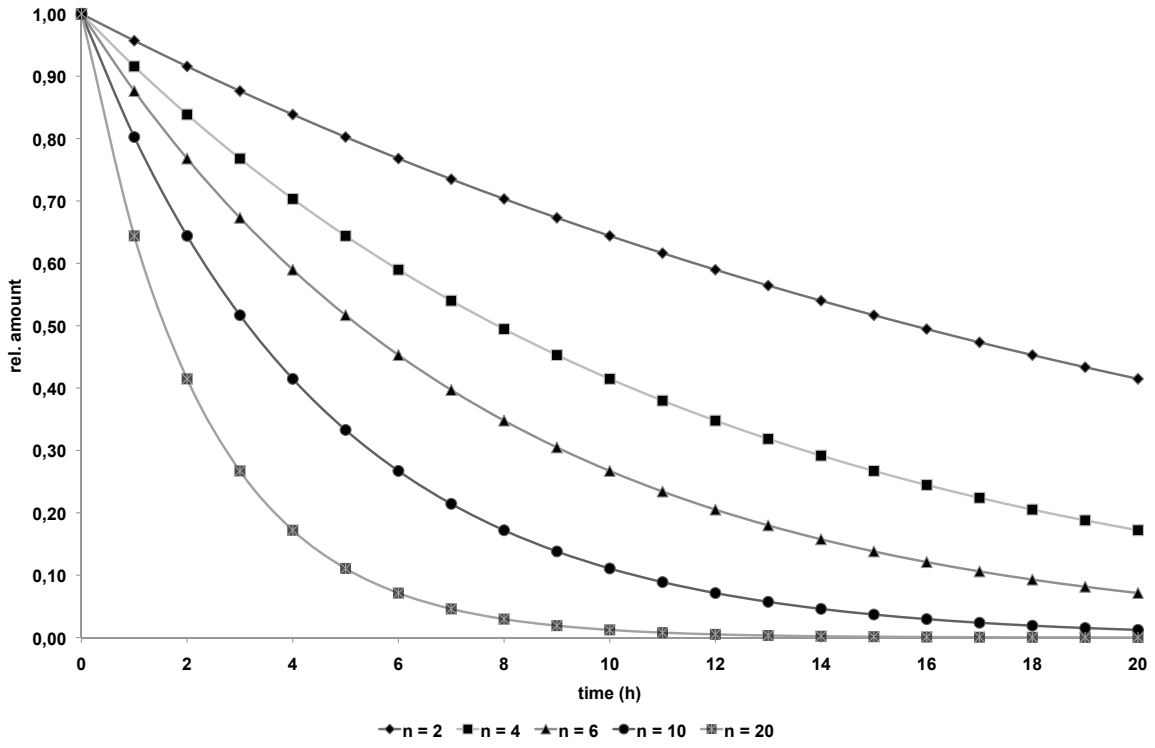


Figure 6.10.: Relative amounts of HPMA-$(PLA)_n$-OR during degradation at pH 7.2 and 37 °C.

Tumour accumulation and blood clearance are molecular weight dependent. While polymers with molecular weights below 20 kDa pass through the kidneys and are excreted

rapidly and polymers with molecular weights of below 40 kDa do not accumulate but diffuse back to the bloodstream, higher molecular weight polymers significantly accumulate in the tumour. These polymers show levels of 2.5 to 3.0 % of the applied dose, in the tumour tissue compared to the initial dose, only one hour after intravenous injection. After the first hour, the levels remain almost stable, only slightly increasing to 3.0 to 3.5 % over the course of the next five hours[83].

Using this distribution equilibrium to our advantage, slow releasing polymeric carrier systems make the most sense. Of those carriers that bear lactide side chains of two to four repeating units, about 95 to 90 % remain intact over the course of the first hour. It seems reasonable to assume that carrier systems, which have released the active drug inside the tumour tissue are diffused back to the bloodstream if the remaining backbone has a molecular weight of less than 40 kDa. The distribution of the polymer drug conjugate should then equilibrate again to 3.0 to 3.5 % in the tumour tissue compared to the total applied dose. This would lead to further influx of conjugate into the tumour tissue. That way the amount of drug released at the tumour site in contrast to the blood compartment could be increased as much as possible under these conditions.

To take a concrete example, in chapter 4.5.3, the preparation of the polymer conjugate HPMA-co-MA-PLA-[HMP-$Re(CO)_3$(bipy)]OTf **PC2** is presented. This conjugate bears rhenium tricarbonyl bisimine on every sixth repeating unit on average. A backbone length of 250 methacrylate units translates to about 42 active drugs per conjugate, with an average molecular weight of 76.6 kDa. If the cleavable side chain consists of 4 lactide units, endfunctionalised with a pyridyl ligand to coordinate the rhenium tricarbonyl moiety, the free complex [$Re(CO)_3$(bipy)(HMP)]OTf **2a** is released comparatively slowly. About 50 % are released ten hours after application and about 83 % after twenty hours (in contrast, i.v. injection of low molecular drugs is usually a bulk release of a defined dose and inherently instantaneous; often substantial excretion begins minutes after application[89]). This is very interesting for tumour diagnostics, as well, because it reduces the signal from compound accumulated in the bladder and enhances the signal in the tumour tissue at the same time. It also opens up a larger time slot for the actual computer tomography. Following degradation of the conjugate, the remaining methacrylate backbone is readily excreted by the glomerular system due to its molecular weight of about 31.8 kDa. For the gold conjugates, the same reasoning applies accordingly. The prepared carrier systems and resulting conjugates would thus be useful in terms of targeted drug release and *in vivo* diagnostics.

## 6.3. Physiological stability

An important requirement for the *in vivo* application is physiological stability for at least the duration of drug effect. Following injection into the bloodstream, the compounds have to be inert against ligand exchange. Typical competing ligands are N- and S-functional groups in proteins, e.g. nitrogen donor ligands like histidines or thioles like cyteines[90, 91].

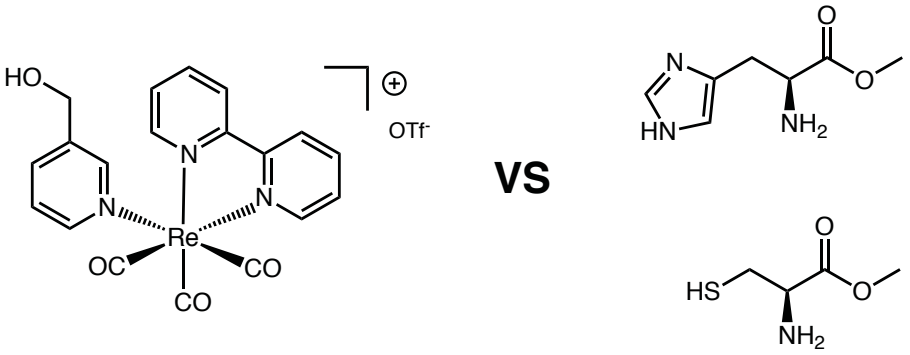


Figure 6.11.: The inertness of $[Re(CO)_3(bipy)(3\text{-}HMP)]OTf$ was tested against histidine methylester (top right) and cysteine methylester (bottom right).

In order to test the complex inertness, two ligand-challenge $^1H$ NMR studies were carried out, in which the tridentate ligands histidine methylester and cysteine methylester were added in tenfold excess to $[Re(CO)_3(bipy)(3\text{-}HMP)]OTf$ in DMSO-$d_6$ (the methylesters are chosen for solubility reasons). $^1H$ NMRs were measured in decreasing time intervals up to a total of seven days.

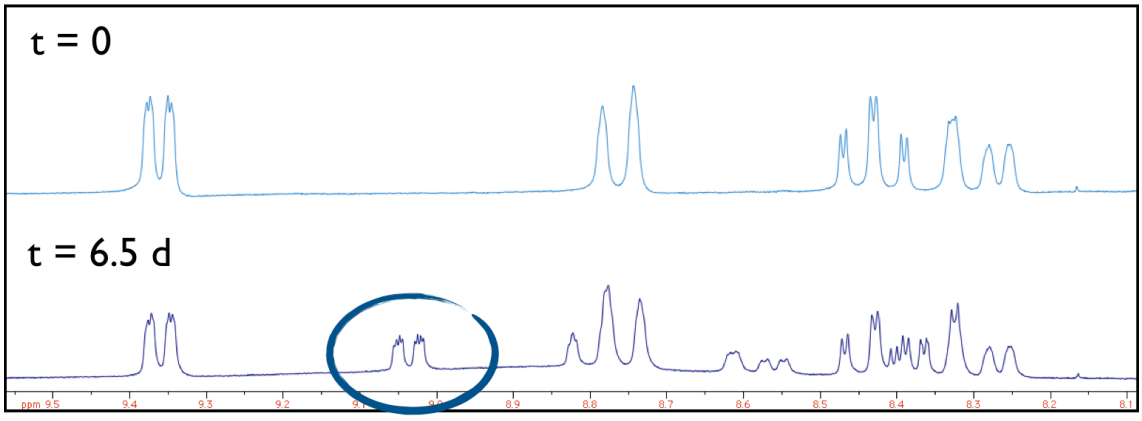


Figure 6.12.: $^1H$ NMR spectra of $[Re(CO)_3(bipy)(3\text{-}HMP)]OTf$ during ligand challenge with histidine methylester in DMSO-$d_6$.

A baseline separated signal of uncoordinated ligand was chosen as the analytical probe to monitor the decomposition of the complex (see fig. 6.12). After about 24 hours, the signal becomes large enough to be distinguishable from the baseline. The remaining relative amount of the complex was calculated by dividing the ratio of the area under the curve of uncoordinated ligand by the sum of coordinated and uncoordinated ligand.

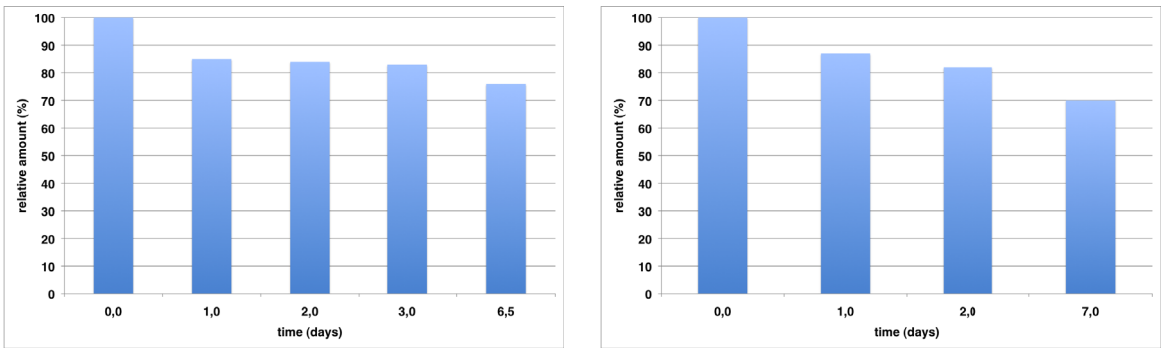


(a) histidine methylester (b) cysteine methylester

Figure 6.13.: Relative amount of $[Re(CO)_3(bipy)(3\text{-HMP})]OTf$ during ligand challenge with (a) histidine methylester and (b) cysteine methylester in DMSO-$d_6$.

In case of histidine methylester as the competing ligand, no decomposition was observed within the first four hours. After 24 h about 15 % and after a week about 24 % were decomposed (see fig. 6.13a). In case of cysteine methylester, again, no decomposition was observed within the first four hours. After 24 h about 13 % and after a week about 30 % were decomposed (see fig. 6.13b). Therefore, the polymer conjugate is sufficiently inert towards ligand exchange, as accumulation of macromolecules in the tumour tissue mainly occurs within the first hour.[83]

# 7. Fluorescence spectroscopy

The rhenium tricarbonyl polymer conjugates were developed to serve three purposes: passive targeting (made possible by a suitable polymeric carrier system), coordination and release of a bioactive agent ($^{188}$Re as the intended radiopharmaceutical or $^{99m}$Tc as a radiotracer for real time imaging) and functioning as a fluorescent tag for optical imaging (using the $^{3}$MLCT transition of Re(I)bisimine complexes).

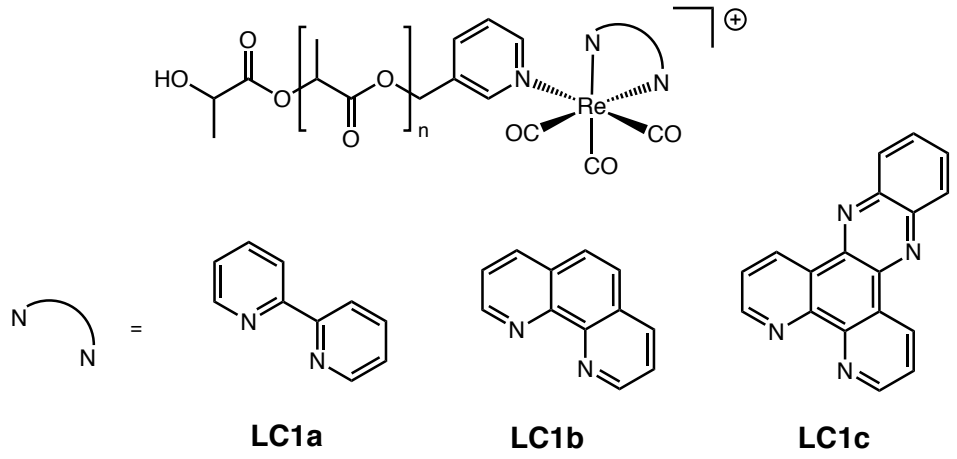


Figure 7.1.: Lactide conjugates with fluorescent Re(bisimine) cores (**LC1a-c**).

Combining *in vivo* and *in vitro* imaging is an interesting concept because nuclear imaging offers high-detection sensitivity, but neither positron emission tomography (PET) nor single photon emission computed tomography (SPECT) can localise radiotracers at the cellular level because of low spatial resolution[91, 92]. A multimodal (fluorescent and radioactive) imaging probe would allow elucidation of the pathway of the compound inside the cell, while imaging with scintigraphy would localise the compound inside the human body. This makes it possible to validate *in vivo* imaging findings using *in vitro* fluorescent microscopic examinations.

To evaluate the usefulness of the polymers as dyes for optical imaging, the fluorescence properties of the polymer bound rhenium bisimines PLA-HMP-Re(CO)$_3$(bipy)OTf, PLA-HMP-Re(CO)$_3$(phen)OTf and PLA-HMP-Re(CO)$_3$(dppz)OTf were studied. The large Stokes shifts, which are typical for Re(bisimines), are especially interesting for fluorescence imaging in medicinal context, as they overcome the challenge of differentiating the fluorescence of the dye from the endogenous fluorescence in cells and tissues (fig. 2.3).

Table 7.1.: Fluorescence and IR spectroscopic data of the fluorescent polymers

| | $\lambda_{max}$ **abs** [nm][a] | $\lambda_{max}$ **em** [nm][a] | **Stokes shift** [$cm^{-1}$] | $\nu$**(CO)** [$cm^{-1}$][b] |
|---|---|---|---|---|
| **LC1a** | 350 | 572 | 11100 | 2035, 1929 |
| **LC1b** | 340 | 560 | 11550 | 2035, 1926 |
| **LC1c** | -[c] | -[c] | | 2034, 1912 |
| **1a** | 370[d] | 575[d] | 9640 | 2012, 1905 |
| **1b** | 370[d] | 570[d] | 9480 | 2017, 1930 |
| **1c** | 425[d] | 520[d] | 4300 | 2026, 1927 |

[a] In acetone solution.
[b] KBr pellets.
[c] no notable fluorescence observed.
[d] published in [50].

The absorption and fluorescence properties of the three synthesised polylactide-rhenium(I) bisimine complexes were measured in aerated acetone solution. As expected, the polymers carrying 2,2'-bipyridine and 1,10-phenanthroline complexes show large Stokes shifts resulting from the metal-to-ligand-charge-transfer (MLCT) $d\pi(Re) \rightarrow \pi^*$(bisimine).[93] The absorption wavelengths of **LC1a** and **LC1b** are at 350 and 340 nm, respectively, and the corresponding emission wavelengths are significantly blue shifted to 572 and 560 nm. The difference in wavelengths in both cases is almost exactly 220 nm. To represent the Stokes shifts, they have to be converted into the wavenumbers between absorption and emission. The Stokes shifts are thus about 11100 $cm^{-1}$ for **LC1a** and 11550 $cm^{-1}$ for **LC1b**, which makes them easily distinguishable from background autofluorescence in the tissue.

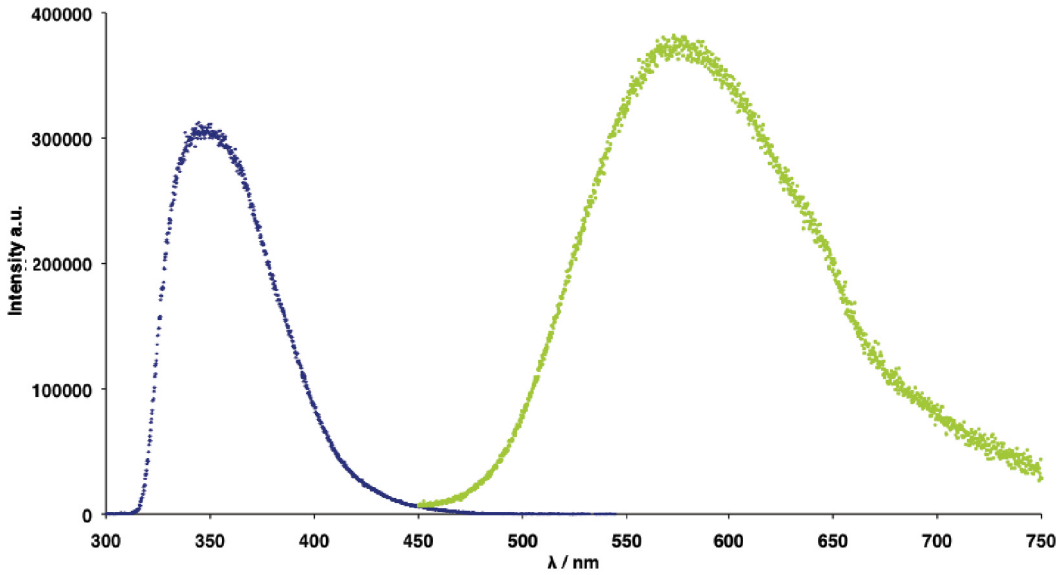


Figure 7.2.: Absorption and emission spectra of [PLA-HMP-$Re(CO)_3$(bipy)]OTf.

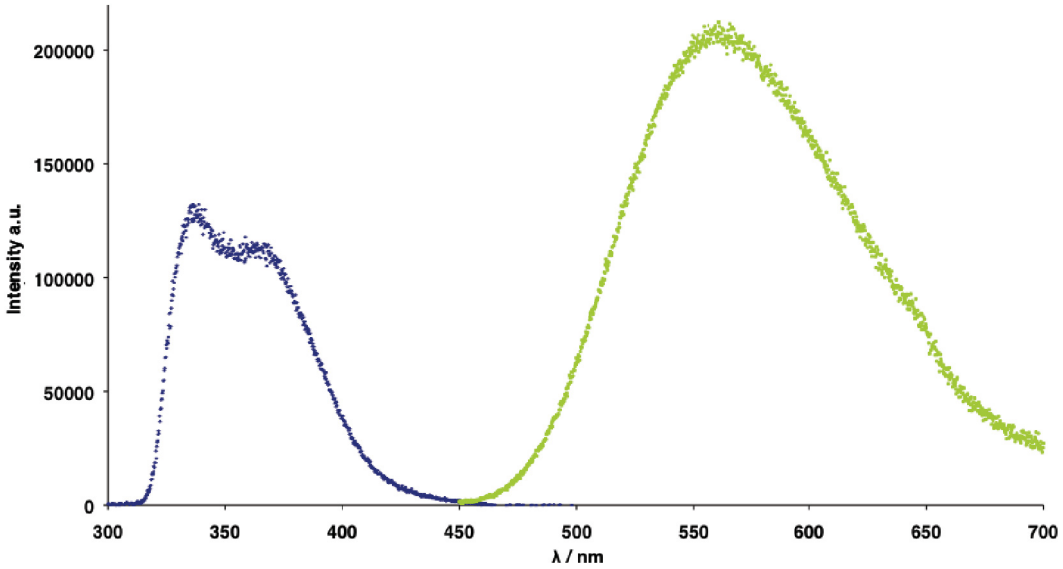


Figure 7.3.: Absorption and emission spectra of [PLA-HMP-Re(CO)$_3$(phen)]OTf.

No notable fluorescence was detected from the polymer bound Re(CO)$_3$(dppz) complex, however. It is known that dppz complexes of Ru(II) serve as light switches for non-aqueous environments because hydrogen bonding with water quenches the luminescence.[94] To investigate whether something similar applies to the Re(I) complex or whether this can be attributed to an effect of the polymer, the free complex was also investigated.

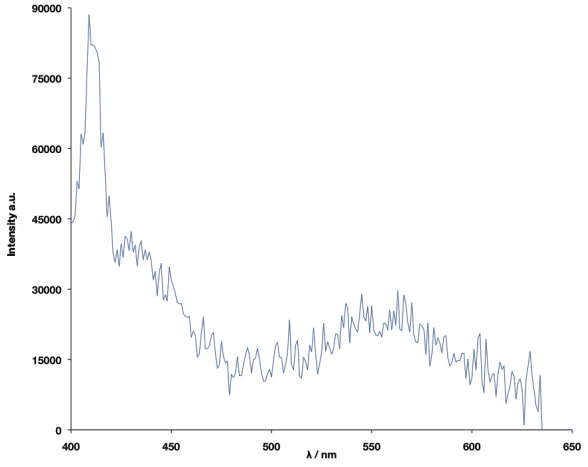


Figure 7.4.: Absorption spectrum of the free complex Re(CO)$_3$(dppz)Br (**1c**). The signal at 410 nm is a result of Stokes scattering.

Hereto, fluorescence spectra of the free complex Re(CO)$_3$(dppz)Br in acetone, dichloromethane and DMF were recorded. Fluorescence was observed solely in DMF and only in very low quantum yields. Looking at the spectrum, the most intense signal (at about 410 nm) can be attributed to Stokes scattering (see fig. 7.4), making absorption and fluorescence intensity insignificant in comparison. Absorption and emission values found for the dppz complex are in accordance to the findings of Kurz et al.[50] Comparing the fluorescence data of the free complexes to the polymer bound Re(CO)$_3$(bisimine) cores (see table 7.1) shows that the complexes retain their absorption and emission properties when attached to the polylactide carrier system.

Even though **LC1c** does not fluoresce in non-aqueous solution, it might still be useful for imaging as well as targeting purposes. It can actively target the radiopharmaceutical to the DNA because dppz is known to strongly bind to DNA by intercalation to the major groove of the helix. Studies into dppz binding mode and affinity towards DNA have been done by Talib *et al.*[95] As a result, in aqueous solution, the dppz complexes luminesce brightly only when bound to DNA or otherwise protected from water through binding to folded RNAs, or association with membranes or other macromolecular structures.[94] An experiment could be done to intercalate the described dppz complexes and conjugates into the DNA and measure the resulting fluorescence. This is outside of the scope of this work, but it would be an interesting experiment to be realised in the future.

# 8. Cell culture experiments

The A2780 human ovarian cancer cell line was used to conduct the *in vitro* experiments concerning membrane integrity, viability and cytotoxicity as well as for confocal fluorescence microscopy experiments.

## 8.1. Confocal fluorescence microscopy

Depending on the structure and make-up of $d^6$ metal bisimine complexes, the cellular targets vary. As can be seen in the overview published by Fernandez-Moreira *et al.* (see fig. 8.1), complexes bearing nuclear localising ligands, which are mostly strong DNA intercalators, accumulate in the nucleus. Other complexes target mitochondria, endosomes, the ER and Golgi apparatus or the cellular membranes. The localisation of such complexes can be determined by confocal fluorescence microscopy, as all of these complexes are fluorescent dyes. Rhenium tricarbonyl complexes with a 2,2' bipyridine and a picolylchloride ligand were found to be targeting mitochondria, Rhenium tricarbonyl complexes with long aliphatic chains were found to accumulate in cellular membranes. It stands to reason that the prepared polymer **LC1b** and the corresponding free complex **2b** localise similarly. In order to determine their cellular localisation, confocal microscopy experiments were undertaken.

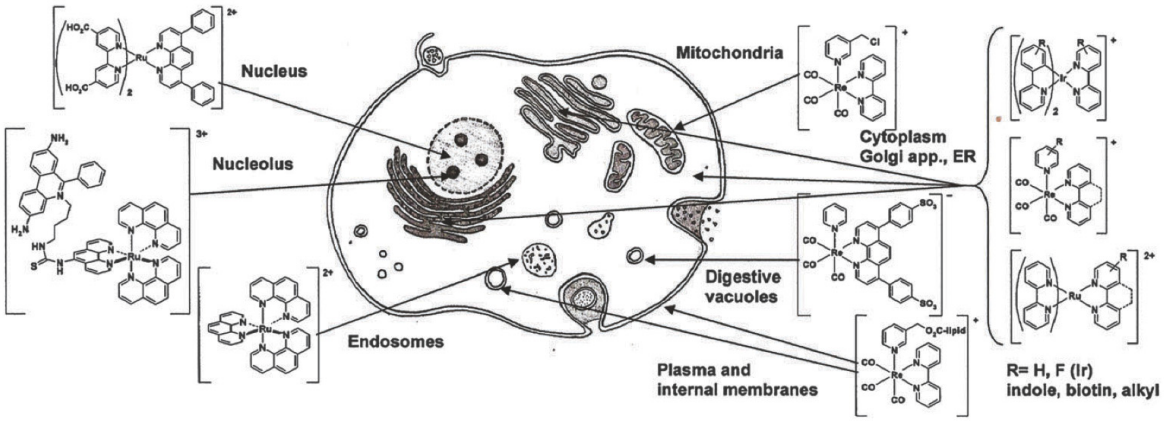


Figure 8.1.: Localisation of different $d^6$ metal complexes in cells and membranes.[96]

Confocal fluorescence microscopy was used to take images of high spatial resolution without interference from diffracted light. Several images were recorded of polymer **LC1b** and its corresponding free complex **2b** after an incubation period of two hours with 10 $\mu$M solutions of the respective compound. Optical slices stacked on top of each other, so called z-stacks, were combined to generate a 3D image to determine the localisation of the fluorescent polymer **LC1b**.

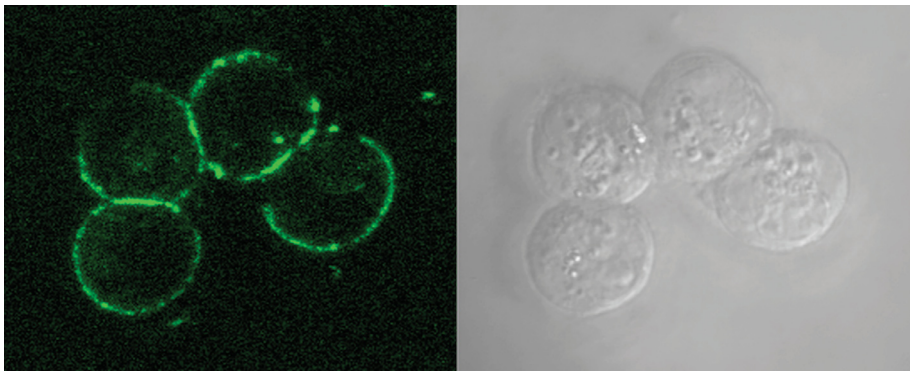

Figure 8.2.: Confocal fluorescence and bright field images of A2780 cells incubated for two hours with **LC1b**.

The images in fig. 8.2 show the accumulation of the polymer bound complex within the plasma membranes, which was expected due to the lipophilic nature of the polylactide and corresponds to the findings reported by Fernandez-Moreira *et al* for PEGylated analogues.[96] The images taken of A2780 after incubation with complex **2b** confirm the assumption, that the free complex (analogous to $[Re(CO)_3(bipy)(picolylchloride)]^+$) accumulates within the cells, as shown in fig. 8.3.

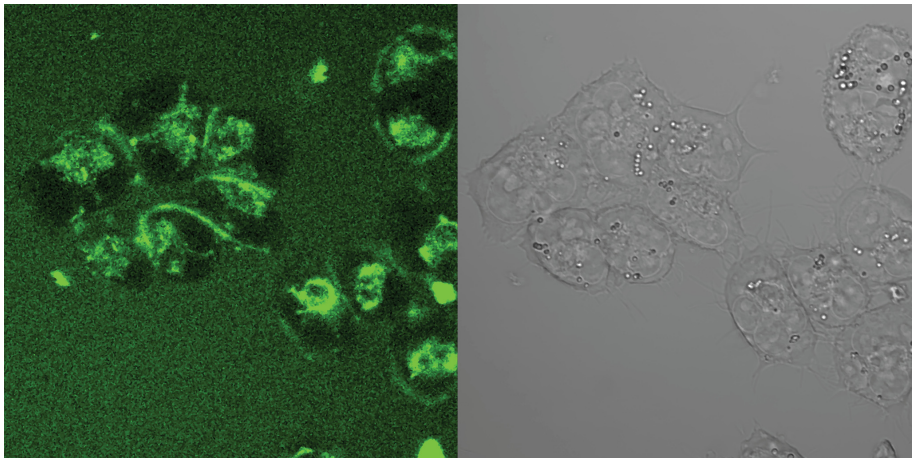

Figure 8.3.: Confocal fluorescence and bright field images of A2780 cells incubated for two hours with **2b**.

Further experiments were done using a mitotracker (Red CMXRos) as a co-locator to determine whether the free complex in fact targets the mitochondria. These experiments were unfortunately unsuccessful, because the fluorescence properties of the employed mitotracker were too similar to those of complex **2b**. Excitation of the free complex **2b** resulted in cross fluorescence as well as in direct excitation of the mitotracker. The very intense fluorescence of CMXRos overlaid the emission of the complex, making a distinction of the two compounds and a qualified conclusion impossible. The possibility remains to use other types of mitotrackers and solve this problem in the future.

Theoretically, hydrolytic degradation of the oligolactide chain of **LC1b** should release the fluorophore **2b** and enable it to pass through cellular membranes, enter the cells and accumulate inside. To test that theory, confocal images as well as z-stacks of A2780, incubated with polymer **LC1b** for 72 h, were done. The images show increased fluorescence inside the cell and less fluorescence in the cell membranes, indicating the hydrolytic degradation of the oligolactide and release of the complex. However, there was still reasonably intense fluorescence from the compound in the membranes, which is probably due to the fact that the hydrolysis is hampered when the polymer is located within the hydrophobic environment of the lipid bilayer.

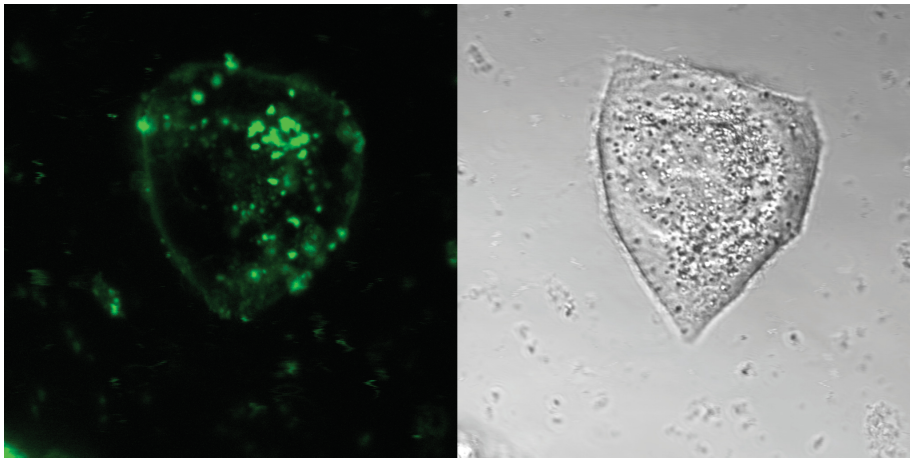

Figure 8.4.: Confocal fluorescence and bright field images of A2780 cells incubated for 72 hours with PLAPHEN.

The degradation kinetics of these oligolactides in aqueous environment have been calculated (see chapter 6.2) and predict a degradation half life of about 15 minutes at 37 °C and pH 7.2 (lactide chains with a number of 20 repeating units and a free hydroxyl chain end group). This means that hydrolysis would take place fairly quickly upon i.v. injection, giving the polymer little time to accumulate in the tumour. This problem can be solved by integrating the lactides as side chains into larger polymeric carrier systems because esterification of the hydroxyl end group leads to the much larger degradation half life time of about 1.5 hours (as discussed previously in chapter 6.2), which is enough for the polymer to accumulate in the tumour tissue.[83]

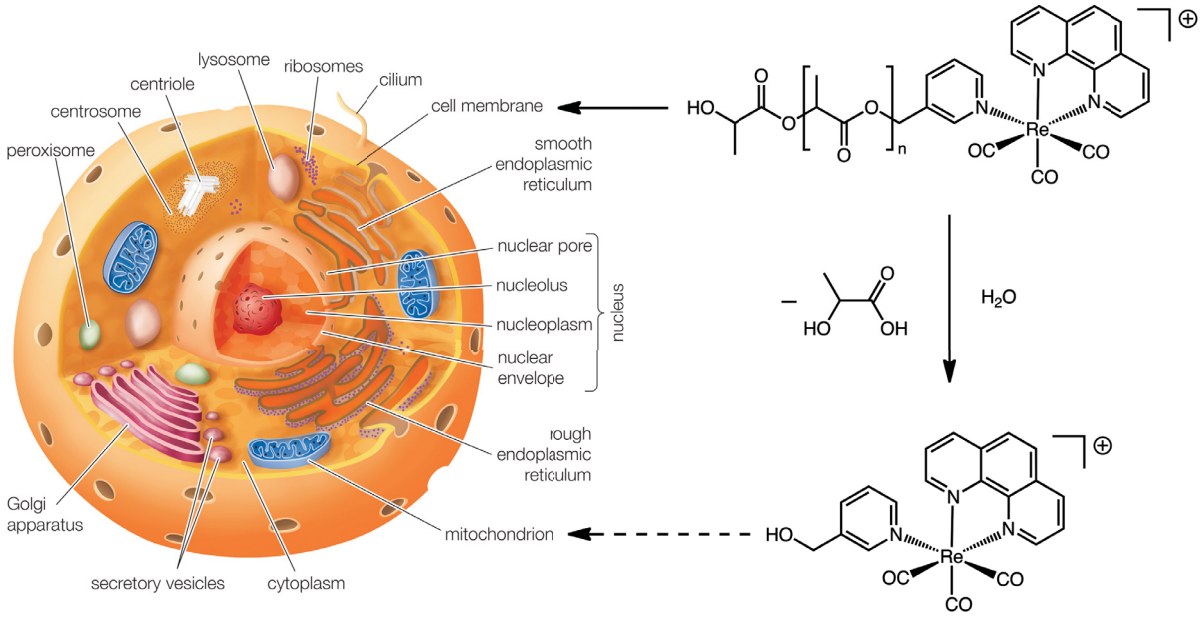


Figure 8.5.: Localisation of polymer **LC1b** and probable target of complex **2b** inside the cell as determined by confocal images. Image of eukaryote cell by Encyclopedia Britannica 2010.

## 8.2. Cell membrane integrity (trypan blue exclusion method)

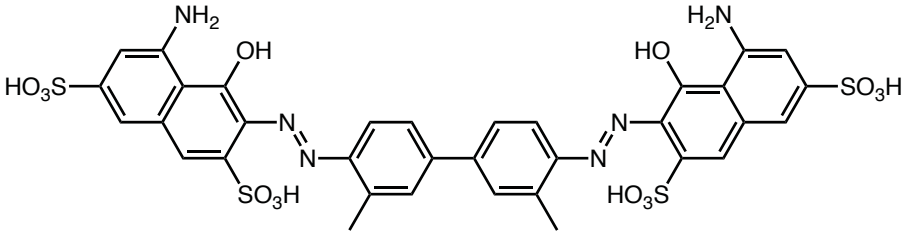


Figure 8.6.: Diazo dye trypan blue.

Accompanying the confocal microscopy, a trypan blue test was done in A2780 cells to determine whether the fluorescent polymer disrupts cell membrane integrity. Trypan blue is a blue diazo dye which is used as a probe for membrane integrity. Trypan blue is not absorbed into viable cells and cannot pass through intact cell membranes, only damaged and dead cells are stained and can thus be distinguished from viable cells.

There was no notable trypan blue uptake in the cells after two hours of incubation with a 10 $\mu$M solution of **LC1b** (containing no more than 0.5 % DMSO). Therefore, it can be concluded that the conjugates to not desintegrate cellular membranes, as some polymers and detergents are known to do. A2780 were incubated under the same conditions with 0.5 % DMSO as the negative control and 30 % DMSO as a positive control.

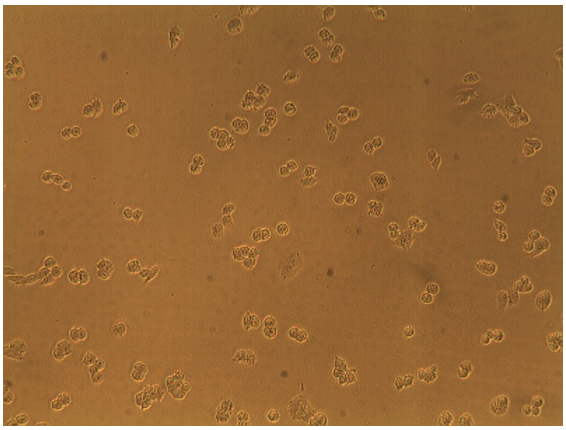

(a) **LC1b**

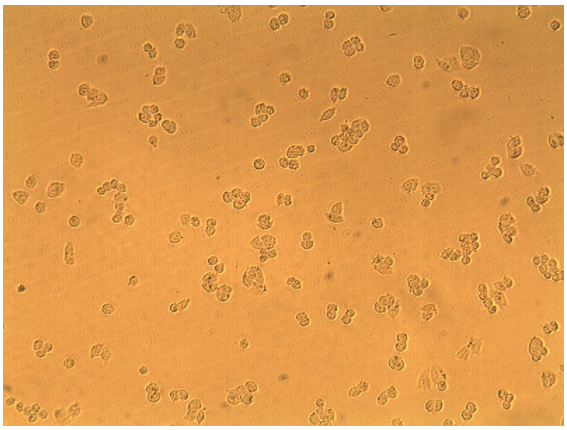

(b) negative control

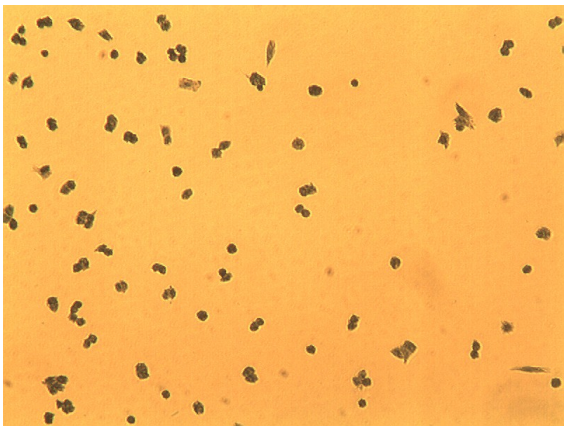

(c) positive control

Figure 8.7.: Microscope images of A2780 incubated with **LC1b** and trypan blue for the cell membrane integrity test, as well as negative and positive control. Incubation time was two hours at 37 °C.

## 8.3. Cell viability (eosin staining)

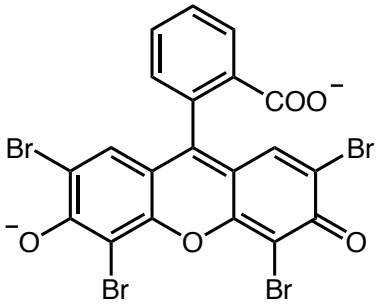


Figure 8.8.: Red eosin dye, a tetrabromo fluorescein derivative.

Eosin is a derivative of fluorescein, which is often used in histology to stain so-called eosinophilic structures. Among those eosinophilics are cytoplasm, collagen and muscle fibres. Here, it was used in conjunction with the confocal microscopy experiments and the trypan blue test as a control for cellular viability. The eosin dye stains dead cells red, while leaving viable cells uncoloured. The dye was added after two hours of incubation with a 10 $\mu$M solution of **LC1b**. The negative control was done adding 0.5 % DMSO instead of **LC1b** ceteris paribus. As can be seen in the images, there was no deep red staining of the cells. Under the chosen reaction conditions, no premature apoptosis or necrosis is caused by **LC1b**.

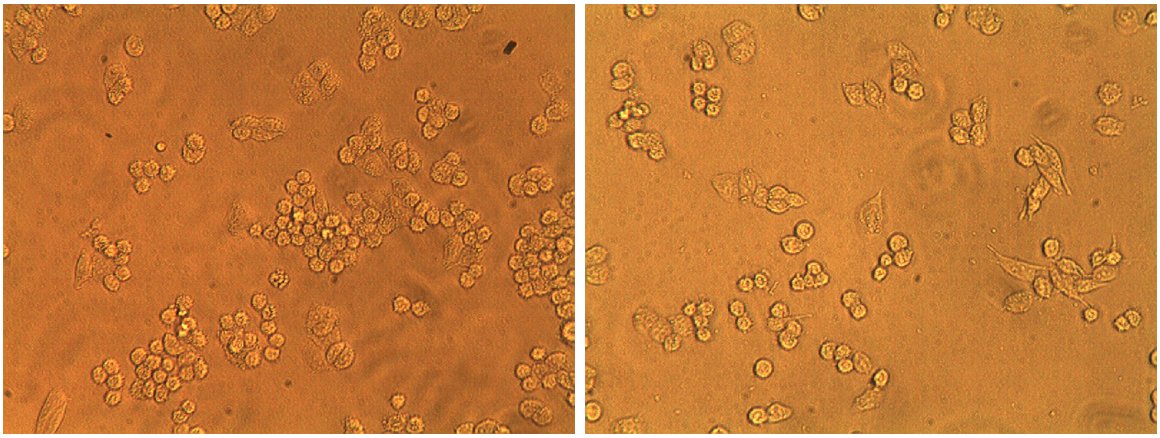

(a) negative control (b) **LC1b**

Figure 8.9.: Microscopy images of the cell viability test. A2780 incubated with **LC1b** for two hours at 37 °C and negative control.

## 8.4. Cytoxicity (MTT assay)

A MTT assay was conducted to test the cytotoxicity of $[Re(CO)_3(phen)(3\text{-HMP})]OTf$ **2b** and the corresponding conjugate **LC1b**. MTT (3-(4,5-dimethylthiazol-2-yl)-2,5-diphenyltetrazolium bromide) is a water-soluble yellow tetrazolium salt, which undergoes enzymatic reduction to the corresponding insoluble blue formazan dye. The reduction takes place only in viable cells by mitochondrial dehydrogenases. Dead cells cannot transform the yellow tetrazolium into the blue formazan. The absorbance is measured by a spectrophotometer and compared to a negative and positive control.

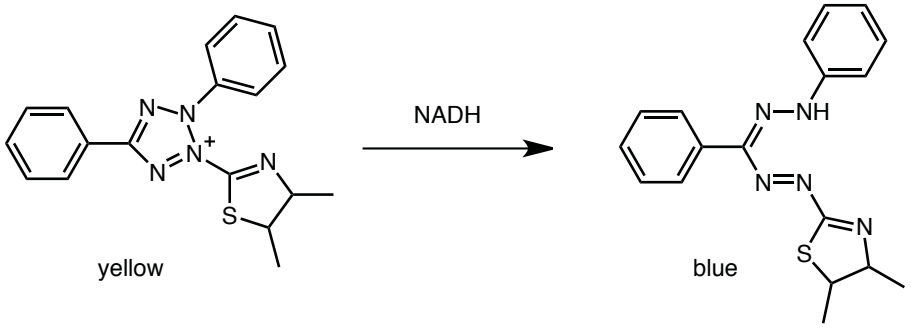


Figure 8.10.: Reduction of yellow MTT dye to blue formazan in viable cells by NADH.

After incubation for 72 hours with increasing concentrations of **LC1b** and **2b**, the $IC_{50}$ was found to be 6 $\mu$M for the polymer and 12 $\mu$M for the free complex ($pIC_{50}$: $5.2 \pm 0.04$ (mean $\pm$ SEM) and $4.9 \pm 0.03$ respectively) (see fig. 8.11). For comparison, the $IC_{50}$ of cisplatin is 1.7 $\mu$M ($pIC_{50}$: 5.8).[97] **LC1b** and the free complex $[Re(CO)_3(phen)(3\text{-HMP})]Br$ show some cytotoxicity *in vitro* (compared to cisplatin) but the cytotoxicity should be low enough to be suitable for diagnostic purposes *in vivo*.

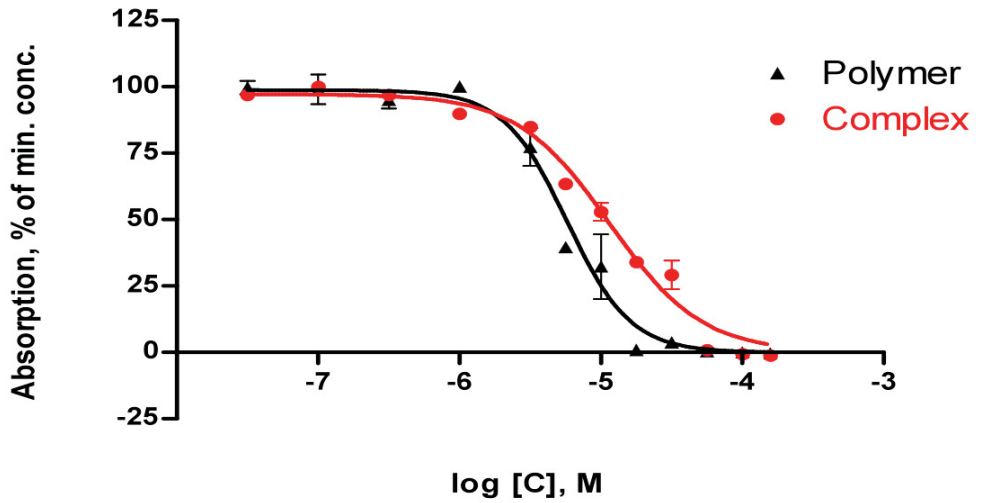


Figure 8.11.: MTT assay of polymer **LC1b** and the corresponding complex **2b**.

# Part III.

# Conclusion

# 9. Summary and Outlook

The aim of this thesis was to develop new polymer-drug conjugates, focussing on using metallodrugs as the active substance. Fluorescent rhenium tricarbonyl bisimines (fig. 9.1a, shown: bipy; not shown: phen, dppz) as well as phosphane and phosphinite gold complexes (fig. 9.1b) were successfully attached to a polymeric carrier system.

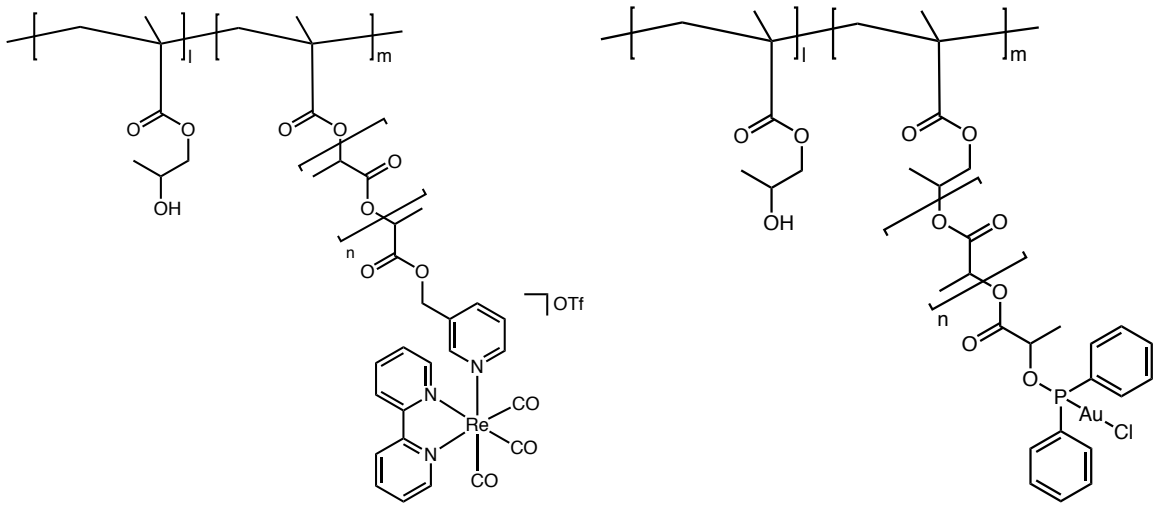


(a) (b)

Figure 9.1.: Polymeric carrier systems with metallodrugs: (a) HPMA-rhenium conjugate (b) HPMA-gold conjugate

The rhenium tricarbonyl complexes serve as model complexes for radioactive rhenium and technetium cores. The component in itself was shown to have *in vitro* imaging properties useful for fluorescence microscopy, which could improve tumour diagnosis by histological analysis of tissue samples. Choosing radioactive rhenium instead of the non radioactive isomer, results in conjugates that can be used to treat cancer by radiotherapy, while producing imaging data for it's detection at the same time. Alternatively, the radioactive technetium $^{99m}$Tc can be selected to combine real-time *in vivo* imaging using computer tomography such as SPECT with the *in vitro* imaging capabilities of the bisimine complex. This can increase the probability to detect tumours very early on. Early cancer diagnosis can help save many lives, because the treatment can start when the cancer is still in the early stages, making complete remission much more likely.

The gold conjugates should have promising anticancer potential, because these types of phosphane gold complexes have already proven to show antitumour activity. The polymeric carrier system improves the drug's potential by targeting the active compound to the malignant tissue and reducing side effects. Upon release, the gold complexes should show the same activity as their small molecular counterparts. Unfortunately, their ability to inhibit cathepsin, as an indicator of antitumour activity, could not be successfully determined, so far. Further experiments and enzyme assays have to be done to generate the data needed to draw any conclusions.

A versatile carrier system was developed as well, to which different ligands can be attached via esterification. With this carrier system, other metallodrugs or cancer therapeutics can be passively transported to the tumour site. It is conceivable to modify this system even further by using two different ligand macromonomers for terpolymerisation with HPMA. This would lead to carrier systems transporting two different drugs for combination therapy and/or personalised therapy purposes. Especially in cancer therapy, drug cocktails are often used to gain synergistic effects. Using such carrier systems would ensure different drugs to be transported to the area of drug effect, even if the drugs have quite different pharmacokinetic properties.

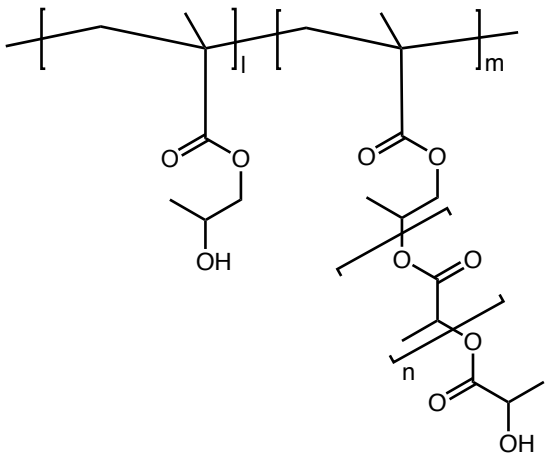

Figure 9.2.: Hydroxy functionalised polymeric carrier system.

The polymeric carrier systems were prepared with molecular weights of more then 60 kDa with hydrodynamic diameters in a magnitude of about 10 nm, which is useful for passive targeting of drugs to tumour tissue. It was shown that molecular weights and polymer constitution can be tailored to suit different needs. Larger carrier systems, for example, carry more active metallodrugs, to be released at the tumour site. Also, the amount of ligand side chains per polymer can be varied to increase or decrease drug loading. Side chains length can be chosen to suit release kinetics: shorter chains for a slower release over time, longer chains for faster drug release. This is due to the fact that the number of cleavable ester bonds increases with the chain length. The non degradable backbone must not exceed molecular weights of 50 kDa, so that it remains excretable and will not be retained the body. The lactide side chain is degraded into lactic acid *in vivo*, which is nontoxic and easily metabolised. Possible combinations of monomer ratios and polymer constitutions were presented and their molecular weights, as well as release kinetics calculated (see chapter 6.2). Degradation half lives are in a range of 25 hours for cleavable linkers with two repeating units to about 90 minutes for cleavable linkers with twenty repeating units. A release profile for carriers with 2, 4, 6, 10 and 20 repeating units was calculated as well, showing the release profiles of polymers with the respective side chains.

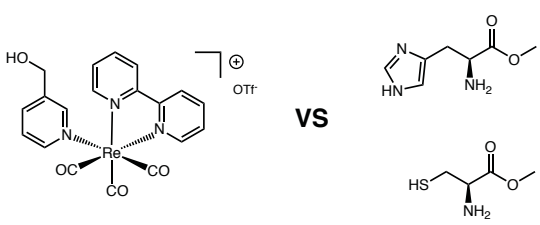


Figure 9.3.: Complex inertness

Furthermore, the inertness of the $d^6$ rhenium tricarbonyl complexes was determined with a ligand challenge NMR experiment. $[Re(CO)_3(bipy)(3\text{-HMP})]OTf$ was added to a tenfold excess of histidine methylester and cysteine methyl ester in $CDCl_3$. Both amino acid derivatives are competing chelating ligands of the kind ubiquitous in enzymes and proteins. Over the course of a week, 24 % of the complex were decomposed when subjected to histidine methyl ester, and 30 % were degraded when subjected to cysteine methyl ester. There was hardly any ligand exchange within the first few hours. It was concluded that the monodentate coordination of the organometallic fluorophore to the polymer is sufficiently inert for in vivo application, since it takes about an hour for polymer conjugates to accumulate in the tumour tissue.

The fluorescence properties of the lactide bound rhenium bisimines **LC1a-c** were evaluated to determine their usefulness for diagnostic imaging purposes. The emission and absorption wavelengths of the 2,2'-bipyridine rhenium tricarbonyl conjugate **LC1a** as well as the 1,10'-phenanthroline rhenium tricarbonyl conjugate **LC1b** differ only slightly from those of the corresponding free complexes $[Re(CO)_3(bisimine)Br]$ **1a,b**. The absorption and emission maxima of the complexes $[Re(CO)_3(bipy)Br]$ and $[Re(CO)_3(phen)Br]$ are at 370 and 575 nm, and at 370 and 570 nm, respectively. Absorption and emission maxima of the corresponding lactide conjugates are at 350 and 572 nm, and at 340 and 560 nm. Coordination of the pyridyl ligand of the polymer carrier only results in a slight blue shift of absorption and emission. This leads to the conclusion that the fluorescence properties do not change significantly upon coordination to the lactide chain. Most importantly, the large Stokes shift of the fluorophores of about 11100 $cm^{-1}$ helps to easily identify the conjugates, even within the diverse environment of cells and tissues. The dppz conjugate **LC1c** as well as the corresponding free complex **1c** showed no notable fluorescence, probably due to fluorescence quenching in hydrophilic environments or hydrogen bonding. It is known, that Ru(II) dppz complexes serve as light switches that show no fluorescence in hydrophilic environments, but fluoresce intensively within hydrophobic environments. Dppz is a strong DNA intercalator, which can still be useful as an active targeting moiety to the nucleus. Therefore, the liberated complex $Re(CO)_3(dppz)(3\text{-HMP})]OTf$ **2c** should show a strong affinity to the DNA and could serve as a light switch upon intercalation of the complex to the DNA. Since $^{186/188}Re$ is a $\beta$ emitter and is used to degrade DNA in radiotherapy, this is still well worth investigating.

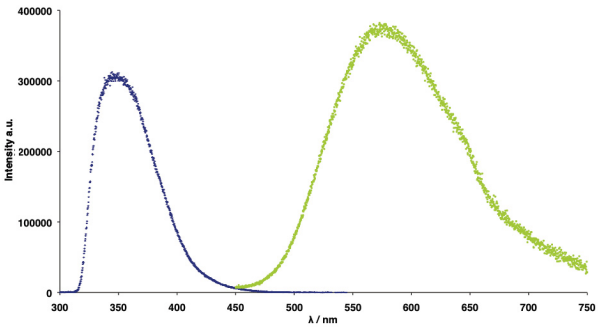


Figure 9.4.: Absorption and emission of **LC1a**.

Confocal fluorescence microscopy was used to record images of high spatial resolution in order to determine cellular localisation of the conjugates as well as of the released metallodrugs.

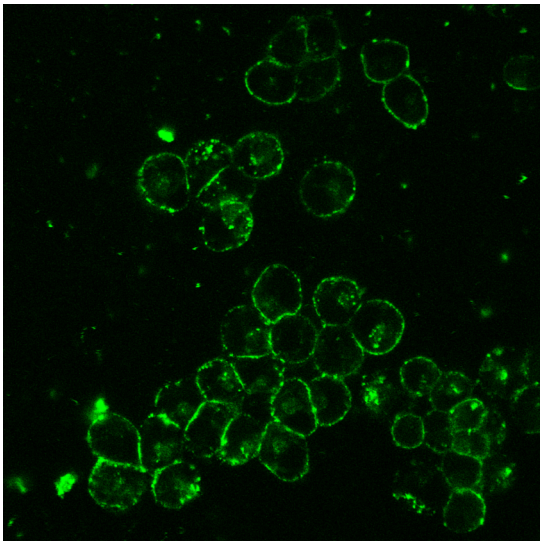

Figure 9.5.: Confocal image of **LC1b** in the membranes of A2780 cells.

Optical slices stacked on top of each other, so-called z-stacks, were combined to generate rotating 3D images to ensure correct interpretation of the images concerning the localisation of the fluorophores within the cells, on cellular membranes and outside the cells. Several images of A2780 cells incubated with conjugate **LC1b** and its corresponding free complex [Re(CO)3(phen)(3-HMP)]OTf were recorded after an incubation period of two hours. The images show accumulation of the polymer-bound complex in the plasma membranes, which was expected with regard to the lipophilic nature of the polylactides. In contrast, the free complex is able to pass cellular membrane and accumulate within the cells. Confocal images of A2780 incubated with **LC1b** after an incubation period of 72 hours showed increased fluorescence inside the cell and less fluorescence in the cell membranes. Proving hydrolysis of the polymer and subsequent release the free complex, which can then enter the cells. Hydrolysis kinetics suggest that the polylactide side chains should be entirely degraded over the course of 72 hours, but there was still reasonably intense fluorescence from the compound in the membranes. It was concluded that the polymer cannot be degraded as quickly, since the lactide is located in the hydrophobic environment of the lipid bilayer, resulting in a kind of depot effect with slower release kinetics.

Accompanying the confocal microscopy, a trypan blue test was performed in A2780 cells to determine whether the fluorescent polymers disrupt cell membrane integrity. No notable trypan blue uptake in the cells was found after two hours of incubation with the lactide conjugate **LC1b**, which leads to the conclusion that the membranes are not desintegrated by the polymer. The cytotoxicity of **LC1b** as well as that of the free complex [Re(CO)3(phen)(3-HMP)]Br **2b** towards the human ovarian carcinoma cell line A2780 have been evaluated by MTT assay, showing $IC_{50}$ values of 6 $\mu$M for the polymer and 12 $\mu$M for the free complex. The compounds are fairly cytotoxic, but the toxicity should still be low enough for the conjugates to be suitable for pharmaceutical purposes.

In summary, it can be stated that both polymer-metallodrug conjugates are suitable for therapeutic and/or diagnostic purposes, because molecular weight as well as release properties fulfill the criteria needed for passive transport and drug release. Similar carrier systems with multiple drugs for combination or personalised therapy could still be investigated. Several studies remain to be done concerning the antitumour efficacy of

the gold complexes. The fluorescence properties of the rhenium bisimine conjugates are useful for histological fluorescence imaging and thus suitable for diagnostic applications. The usefulness of the intercalating bisimine ligand dppz for nuclear targeting with an integrated light switch remains to be investigated. The complex inertness towards ligand exchange ensures transport of the rhenium core to the target site. After intravenous injection, the conjugates should accumulate within the cellular membranes of the tumour cells, releasing the active metallodrugs. Upon release, the small molecules are taken up by the tumour cells, which are the intended target for both therapeutic and diagnostic measures. Additional investigations can be undertaken using the radioactive $d^6$ metals $[^{186/188}Re(I)(CO)_3]^+$ and $[^{99m}Tc(I)(CO)_3]^+$ as the active metallodrug. Injection of the conjugates into mice and subsequent computer tomography of the technetium compound would yield insight into the distribution patterns of the conjugate within a living system and it's real-time imaging properties. Concurrently, samples of mouse tumour tissue could be taken to confirm the findings of the *in vivo* imaging using fluorescence microscopy. Both the radioactive rhenium conjugate as well as the gold conjugate could be studied in mice, in order to determine their *in vivo* therapeutic efficacy. Again, samples of the fluorescent rhenium conjugate could be taken for concurrent *in vitro* imaging.

# Part IV.

# Experimentals

# 10. Materials and Methods

All chemicals were purchased from Aldrich, Acros, VWR and Fluka and used as received unless mentioned otherwise. $[Re(CO)_3(dmso)_3]OTf$[49] and $[Re(CO)_3(H_2O)]Br$[41] were synthesised according to literature procedures. Dipyrido[3,2-a:2',3'-c]phenazine was a generous donation from Dr. U. Schatzschneider, University of Bochum. Reactions carried out under inert conditions were done using standard Schlenk techniques.

$^1H$ NMR spectra were recorded with a Bruker AM 200 at 200.13 MHz at 20 °C, the $^{31}P\{^1H\}$ NMR spectra were recorded with the same spectrometer at 81.02 MHz. The spectra were calibrated against the residual proton signals of the solvents as internal references. The coupling constants J are given as their absolute values in Hertz (Hz). The multiplicity of individual peaks is indicated as singlet (s), doublet (d), doublet of a doublet (dd), doublet of a triplet (dt), triplet of a doublet (td), quartet (q) or multiplet (m).

The ESI mass spectra were recorded with an Ion-Trap-API mass spectrometer Finnigan LCQ Deca. MALDI-TOF mass spectra were recorded with a Bruker Ultraflex TOF mass spectrometer. For GC/MS analyses, a Thermo Finnigan Trace DSQ system was used.

IR spectra were recorded with a Bruker IFS 66 FT-IR spectrometer. Positions of the absorption bands are given in wavenumbers ($\tilde{\nu}$).

Fluorescence spectra were recorded with a Fluoromax-3. Imaging of preincubated cells was performed on an Olympus FV1000 Confocal Laserscanning micoscope (Olympus GmbH, Hamburg, Germany) equipped with a 60x water immersion objective, NA 1.2. The fluorescent polymer was excited at 405 nm using a diode laser at an output power of 10 %. The fluorescence signal was detected between 540 and 640 nm using a spectral detector.

UV/Vis-spectra for the MTT assay was measured using a FLUOstar (bmg, Offenburg) microplate reader. GraphPadPrism© 4.0 software (San Diego, CA, USA) was used to calculate the sigmoidal dose-response curves using the four-parameter logistic equation with variable Hill slope for non-linear regression.

Gel permeation chromatography (GPC) analyses were carried out on a GPC system from PSS with PSS-WIN-GPC software 4.01, 6.1 with DMF as eluent. The flow rate was

1mL/min and the column temperature was maintained at 60 °C. The number-average molecular weight (Mn) and the polydispersity (PD) were calculated by a calibration curve generated by polystyrene standards with a molecular weight range from 374 Da to 1000 kDa.

DLS experiments were carried out with a Malvern HPPS-ET apparatus at a temperature value of 25 °C. The particle size distribution was derived from a deconvolution of the measured intensity autocorrelation function of the sample by the general purpose mode algorithm included in the DTS software. Each experiment was performed five times to obtain statistical information.

# 11. Synthesis of rhenium tricarbonyl complexes

## 11.1. $Re(CO)_3$(bisimine)Br

The rhenium bisimine bromides were prepared as published with minor modifications[50, 51] .

**$Re(CO)_3$(bipy)Br** $[Re(CO)_3(H_2O)_3]Br$ (0.10 mg, 0.25 mmol) and 2,2'-bipyridine (58 mg, 0.37 mmol) were dissolved in THF (20 mL) and refluxed for 0.5 h, during which the product precipitated as a bright yellow solid. The solution was concentrated in vacuo, whereupon more product precipitated. The collected solids were washed with THF and ether successively and dried under high vacuum (0.10 mg, 82 % yield).

$^1$H NMR ($CDCl_3$, 200 MHz), $\delta$ = 9.06 (d, 2H, bipyC6-H, $^3J_{HH}$ = 5.30), 8.80 (d, 2H, bipyC3-H, $^3J_{HH}$ = 8.17), 8.37 (m, 2H, bipyC5-H), 7.79 (m, 2H, bipyC4-H). ESI-MS (MeOH/H2O) m/z: 869 ($[(Re(CO)_3(bipy))_2H_2O]^+$), 445.0 ($[Re(CO)_3(bipy)(H_2O)^+$). IR (KBr): $\tilde{\nu}$ = 2012, 1905

**$Re(CO)_3$(phen)Br** $[Re(CO)_3(H_2O)_3]Br$ (0.13 mg, 0.33 mmol) and 1,10-phenanthroline (91 mg, 0.48 mmol) were added to 25 mL of THF and refluxed for about 15 minutes. The yellow precipitate was filtered out, washed twice with THF and dried under high vacuum (123 mg, 70 % yield). Note: Prolonged refluxing can result in the formation of dimers whereupon the bright yellow solution turns orange.

$^1$H NMR (DMSO-$d_6$, 200 MHz), $\delta$ = 9.48 (dd, 2H, phenC2/9-H, $J_{HH}$ = 5.0, 1.3), 9.00 (dd, 2H, phenC4/7-H, $J_{HH}$ = 8.3, 1.3), 8.36 (s, 2H, phenC5/6-H), 8.14 (m, 2H, phen C3/8-H). EI-MS m/z: 530 ($M^+$), 502, 474, 446, 366. IR (KBr): $\tilde{\nu}$ = 2017, 1930

**$Re(CO)_3$(dppz)Br** $Re(CO)_5Br$ (60 mg, 15 mmol) and dipyridophenazine (40 mg, 15 mmol) were put in a Schlenk flask with reflux-condenser and overpressure valve. The reactants were dissolved in n-heptane and refluxed for 1 hr under a nitrogen atmosphere.

The product precipitated as a bright yellow powder, was filtered off, washed with hexane and dried under high vacuum. (78 mg, 86 % yield).

$^1$H NMR (DMSO-$d_6$, 200 MHz), $\delta$ = 9.83 (m, 2H), 9.59 (m, 2H), 8.51 (m, 2H), 8.29 (m, 2H), 8.19 (m, 2H). ESI-MS, (MeOH/$H_2O$) m/z: 631 ($M^+$), 571 ([$Re(CO)_3$(dppz)($H_2O$)]$^+$). IR (KBr): $\tilde{\nu}$ = 2026, 1927

## 11.2. [Re(CO)$_3$(bisimine)(3-HMP)]OTf

**[Re(CO)$_3$(bipy)(3-HMP)]OTf** Re(CO)$_3$(bipy)Br (0.10 g, 0.20 mmol) and silver triflate (52 mg, 0.20 mmol) were dissolved in degassed acetone (10 mL) under a nitrogen atmosphere. The solution was refluxed for 1 hr, precipitated silver bromide was filtered out and the solution added to a solution of 3-(hydroxymethyl)pyridine (0.11 g, 1.1 mmol) in acetone. The solution was refluxed for another hour. The solvent was removed at the rotatory evaporator and the product recrystallised from ethanol / diethyl ether (89 mg, 67 % yield).

$^1$H NMR ($CDCl_3$, 200 MHz), $\delta$ = 9.15 (m, 2H, bipyC6-H), 8.63 (d, 2H, bipyC3-H, $^3J_{HH}$ = 8.24), 8.34 (m, 1H, pyC2-H), 8.32 (m, 2H, bipyC5-H), 7,89 (s, 1H, pyC6-H), 7.78 (m, 2H, bipyC4-H), 7.68 (d, 1H, pyC4-H, $^3J_{HH}$ = 7.83), 7.24 (m, 1H, pyC5-H), 4.53 (s, 2H, py-$CH_2$-). ESI-MS, (MeOH/$H_2O$) m/z: 536 ($M^+$), 445 ([$Re(CO)_3$(bipy)($H_2O$)]$^+$). IR (KBr): $\tilde{\nu}$ = 2031, 1917

**[Re(CO)$_3$(phen)(3-HMP)]OTf** [Re(CO)$_3$(phen)Br] (70 mg, 0.13 mmol) and silver triflate (34 mg, 0.13 mmol) were dissolved in degassed acetone (10 mL) under a nitrogen atmosphere. The solution was refluxed for 1 hr, precipitated silver bromide was filtered out and the solution added to a solution of 3-(hydroxymethyl)pyridine (63 mg, 0.58 mmol) in acetone. The solution was refluxed for another hour. The solvent was removed at the rotatory evaporator. The residue was dissolved in little dicloromethane and the complex precipitated and subsequently washed with diethyl ether. The product was obtained as bright yellow crystals (76 mg, 82 % yield).

$^1$H NMR (DMSO-$d_6$, 200 MHz), $\delta$ = 9.80 (m, 2H, phenC2/9-H), 9,07 (m, 2H, phenC4/7-H), 8.38 (m, 1H, pyC2-H), 8.34-8.24 (m, 5H, phenC5/6-H, pyC6-H, phenC3/8), 7.78 (m, 1H, pyC4-H), 7.30 (m, 1H, pyC5-H), 4.34 (s, 2H, py-$CH_2$). MALDI-TOF m/z: 560 ($M^+$), 532, 450, 423. IR (KBr): $\tilde{\nu}$ = 2031, 1916

# 12. Synthesis of functionalised polylactides

## 12.1. Ligand functionalisation

**PLA-HMP** Synthesis modified from[30]. 3-(hydroxymethyl)pyridine (0.10 g, 0.92 mmol) and (3S)-cis-3,6-dimethyl-1,4-dioxane-2,5-dione (2.4 g, 17 mmol) were added to 50 mL of dry toluene under a nitrogen atmosphere. The solution was heated to 120 °C and 50 $\mu$L of stannous octoate were added. The solution was refluxed for 3 hours at 120 °C. The solvent was removed in vacuo and the residue dissolved in dichloromethane, which was extracted with dilute HCl, brine and $H_2O$. The organic layer was separated, dried with $Na_2SO_4$ and concentrated to approx. 3 mL. The polymer was precipitated and washed with diethyl ether. The product was obtained as a white powder, which was dried under high vacuum (1.7 g, 66 % yield).

$^1$H NMR ($CDCl_3$, 200 MHz), $\delta$ = 8.65 (s, 2H, pyC2-H, pyC6-H), 7.73 (d, 1H, pyC4-H, $^3J_{HH}$ = 7.9), 7.37 (m, 1H, pyC5-H), 5.20 (q, PLA-CH, $^3J_{HH}$ = 7.10), 1.62 (d, PLA-$CH_3$, $^3J_{HH}$ = 7.10). MALDI-TOF, m/z: 615, 686, 758, 830, 902, 974, 1046, 1118, 1190, 1262, 1334, 1406, 1478, 1551, 1623, 1695, 1767, 1839, 1911, 1983, 2055, 2127, 2199, 2271, 2343, 2415, 2487, 2559, 2631, 2703, 2775, 2847, 2919, 2991, 3064, 3136, 3279, 3423. IR (KBr): $\tilde{\nu}$ = 3507, 2998, 2948, 1759, 1457, 1386, 1360

**PLA-tppa** 3,3,3-Tris(pyrazol-1-yl)propanol (0.12 g, 0.47 mmol) and (3S)-cis-3,6-dimethyl-1,4-dioxane-2,5-dione (1.2 g, 8.3 mmol) were dissolved in dry toluene (15 mL) and stannous octoate (30 $\mu$L) was added. The reaction mixture was stirred for 3 h at 120 °C and the solvent subsequently removed. The resulting polymer was then redissolved in 15 mL dichloromethane and washed with HCl (10 mL, 0.1 M), saturated brine and water. The solvent was dried over anhydrous $Na_2SO_4$, filtered, and reduced in volume to 5 mL. The product was precipitated as a white powder, washed with diethyl ether and dried under high vacuum (1.0 g, 75 % yield).

$^1$H NMR ($CDCl_3$, 500 MHz), $\delta$ = 7.62 (m, pzC5-H), 6.70 (m, pzC3-H), 6.25 (m, pzC4-H), 5.10 (q, PLA-CH, $^3J_{HH}$ = 7.10), 4.50 (m, -$OCH_2CH_2C(pz)_3$), 4.29 (q, $CH_3CHOH$, $^3J_{HH}$ = 7.1 Hz), 3.61 (m, -$OCH_2CH_2C(pz)_3$), 1.51 (d, PLA-$CH_3$, $^3J_{HH}$ = 7.10). MALDI-TOF,

m/z: 2131, 2275, 2420, 2492, 2636, 2780, 2924, 3068, 3212, 3356, 3501, 3645, 3789, 3934, 4078, 4222, 4366, 4510, 4655, 4799, 4943, 5088.

**PLA-EtPPh$_2$** $Ph_2PEtOH$ (0.20 g, 0.87 mmol) and (3S)-cis-3,6-dimethyl-1,4-dioxane-2,5-dione (1.6 g, 11 mmol) were added to 50 mL of dry toluene under a nitrogen atmosphere. The solution was heated to 120 °C and 50 $\mu$L of stannous octoate were added. The solution was refluxed for 3 hours at 120 °C. The solvent was removed in vacuo and the residue dissolved in dichloromethane, which was extracted with dilute HCl, brine, and $H_2O$. The organic layer was separated, dried with $Na_2SO_4$ and concentrated to approx. 3 mL. The polymer was precipitated and washed with diethyl ether. The product was obtained as a white powder, which was dried under high vacuum (0.52 g, 29 % yield).

$^1$H NMR ($CDCl_3$, 200 MHz), $\delta$ = 7,83-7,32 (m, 10H, Ph), 5.20 (q, PLA-CH,$^3J_{HH}$ = 7.10), 3.6 (m, 2H, O-$CH_2$-), 2.7 (m, 2H, -$CH_2$-P), 1.61 (d, PLA-$CH_3$, $^3J_{HH}$ = 7.10). $^{31}P\{^1H\}$ NMR ($CDCl_3$, 81 MHz), $\delta$ = 29.51 ($Ph_2$-P(O)-R), -21.65 ($Ph_2$-P-R). MALDI-TOF, m/z, excerpt: ($M^+$), (M+$Na^+$), (M-oxide$^+$), (M-oxide+$Na^+$) 1887, 1903, 1909, 1927. IR (KBr): $\tilde{\nu}$ = 3432, 2998, 2947, 1759, 1457, 1385, 1361, 755, 697

**MeO-PLA** Methanol (67 mg, 2.1 mmol) and (3S)-cis-3,6-dimethyl-1,4-dioxane-2,5-dione (3.0 g, 21 mmol) were added to 50 mL of dry toluene under a nitrogen atmosphere. The solution was heated to 120 °C and 50 $\mu$L of stannous octoate were added. The solution was refluxed for 3 hours at 120 °C. The solvent was removed in vacuo and the residue dissolved in dichloromethane, which was extracted with dilute HCl, brine, and $H_2O$. The organic layer was separated, dried with $Na_2SO_4$ and concentrated to approx. 3 mL. The polymer was precipitated and washed with diethyl ether. The product was obtained as a white powder, which was dried under high vacuum (1.9 g, 63 % yield).

$^1$H NMR ($CDCl_3$, 200 MHz), $\delta$ = 5.20 (q, PLA-CH, $^3J_{HH}$ = 7.10), 3.70 (s, 3H, O-$CH_3$), 1.62 (d, PLA-$CH_3$, $^3J_{HH}$ = 7.10). MALDI-TOF, m/z: 1279, 1351, 1423, 1495, 1568, 1640, 1712, 1784, 1856, 1928, 2000, 2072, 2144, 2216,2288, 2360, 2432, 2504, 2576, 2648, 2720, 2792, 2864, 2936, 3008, 3080, 3152, 3224, 3296, 3368, 3440. IR (KBr): $\tilde{\nu}$ = 2998, 2948, 1759

**MeO-PLA-PPh$_2$** MeO-PLA (0.60 g, 0.43 mmol) was dissolved in dry dichloromethane under a nitrogen atmosphere. Triethyl amine (47 mg, 0.47 mmol) was added dropwise to the solution. Chlorodiphenylphosphane was added by syringe. The solution was stirred at room temperature for 8 hours. The solution was washed with 0.2 M HCl and water, dried over $Na_2SO_4$ and the solvent removed in vacuo. The polymer was precipitated from a few mL dichloromethane with diethyl ether, washed with diethyl ether and dried under high vacuum (0.56 g, 80 % yield).

$^1$H NMR ($CDCl_3$, 200 MHz), $\delta$ = 7,96-7,45 (m, 10H, Ph), 5.20 (q, PLA-CH, $^3J_{HH}$ = 7.09), 3.78 (s, 3H, O-$CH_3$), 1.61 (d, PLA-$CH_3$, $^3J_{HH}$ = 7.09). $^{31}$P{$^1$H} NMR ($CDCl_3$, 81 MHz), $\delta$ = 116 ($Ph_2$-P-), 34 ($Ph_2$-P(O)-O). MALDI-TOF, m/z: (M-oxide+$Na^+$) 1912, 1984, 2056, 2127, 2200, 2272, 2344, 2416, 2488, 2560, 2632, 2704, 2776, 2848, 2920, 2992, 3064, 3136, 3208, 3352, 3424, 3496, 3568, 3640, 3702, 3784, 3856, 3928 IR (KBr): $\tilde{\nu}$ = 2997, 2947, 1759, 1456, 1385, 1360, 755

## 12.2. Lactide macromonomers

**MA-PLA-HMP** PLA-HMP (0.90 g, 1.9 mmol) and triethyl amine (0.20 g, 2.0 mmol) were dissolved in dichloromethane and a methacryloyl chloride solution (0.21 g, 2.0 mmol) in dicloromethane was added dropwise at 45 °C. The solution was stirred for three hours at 45 °C. The solvent was evaporated to a volume of 10 mL and the concentrated solution was washed with 10 mL of 0.1M HCl, brine and $H_2O$, respectively. The aqueous phases were reextracted with dichloromethane and the combined organic phases dried over anhydrous $Na_2SO_4$. The solvent was removed at the rotary evaporator and the resulting clear oil was dried under high vacuum (0.94 g, 88 % yield).

$^1$H NMR ($CDCl_3$, 200 MHz), $\delta$ = 8.66 (s, 2H, pyC2-H, pyC6-H), 7.73 (d, 1H, pyC4-H, $^3J_{HH}$ = 7.9), 7.37 (m, 1H, pyC5-H), 6.24 (s, 1H, vinylH), 5.67 (s, 1H, vinylH), 5.20 (q, PLA-CH, $^3J_{HH}$ =7.10), 1.99 (s, 3H MA-$CH_3$), 1.60 (d, PLA-$CH_3$, $^3J_{HH}$ = 7.10). MALDI-TOF, m/z: 250, 322, 394, 466, 538, 610, 682, 754, 826, 898, 970, 1041, 1114, 1186, 1258, 1330, 1402, 1474. IR (KBr): $\tilde{\nu}$ = 2997, 2947, 1756, 1457, 1385, 1360, 756, 713

**HPMAn-PLA** Synthesis modified from[82]. N-(2-Hydroxypropyl)methacrylamide (1.0 g, 7.0 mmol) and (3S)-cis-3,6-dimethyl-1,4-dioxane-2,5-dione (3.0 g, 21 mmol) were put in a Schlenk tube and subjected to three vacuum/nitrogen cycles. The monomers were molten at 110 °C and 60 mg $Sn(oct)_2$ in 0.5 mL of dry toluene was added. The mixture was allowed to polymerise under vigorous stirring at 110 °C for two hours. The congealed polymer was dissolved in THF (20 mL) and poured into ice-water, whereupon the polymer separated from the aqueous layer. The water was decanted and the polymer dissolved in ethyl acetate. The organic solution was dried with $Na_2SO_4$, the solvent removed in vacuo and the resulting clear oil dried under high vacuum (3.1 g, 78 % yield).

$^1$H NMR ($CDCl_3$, 200 MHz), $\delta$ = 6.33 (1H, -NH), 5.74 (d, 1H, vinylH), 5.36 (s, 1H, vinylH), 5.20 (q, PLA-CH, $^3J_{HH}$ = 7.10), 3.8-3.2 (m, 3H, HPMA-$CH_2$, HPMA-CH), 1.89 (s, 3H, HPMA-$CH_3$), 1.62 (d, PLA-$CH_3$, $^3J_{HH}$ = 7.10), 1.20 (d, 3H, HPMA-$CH_3$, $^3J_{HH}$ = 6.5). MALDI-TOF, m/z: (M+$Na^+$) 454, 526, 598, 670, 742, 814, 886, 958, 1030, 1102, 1174, 1246, 1318, 1394, 1462. IR (KBr): $\tilde{\nu}$ = 2991, 2943, 1754

**HPMAo-PLA** (2-hydroxypropyl)methacrylate (0.50 g, 3.5 mmol) and (3S)-cis-3,6-dimethyl-1,4-dioxane-2,5-dione (2.5 g, 18 mmol) were added to 50 mL of dry toluene under a nitrogen atmosphere. The solution was heated to 120 °C and 50 $\mu$L of stannous octoate were added. The solution was refluxed for 3 hours at 120 °C. The solvent was removed in vacuo and the residue dissolved in dichloromethane, which was extracted with dilute HCl, brine,and $H_2O$. The organic layer was separated, dried with $Na_2SO_4$ and the solvent removed in vacuo. The resulting clear oil was dried under high vacuum (2.6 g, 87%).

$^1$H NMR ($CDCl_3$, 200 MHz), $\delta$ = 6.13 (1H, vinylH), 5.61 (s, 1H, vinylH), 5.20 (q, PLA-CH, $^3J_{HH}$ = 7.10), 4.45-4.15 (m, 3H, HPMA-$CH_2$, HPMA-CH), 2.0 (s, 3H, HPMA-$CH_3$), 1.62 (d, PLA-$CH_3$, $^3J_{HH}$ = 7.10), 1.28 (m, 3H, HPMA-$CH_3$). MALDI-TOF, m/z: (M+$Na^+$) 600, 671, 743, 815, 887, 959, 1031, 1103, 1175, 1247, 1319, 1391, 1463, 1535, 1607, 1679, 1751, 1823, 1895 IR (KBr, excerpt): $\tilde{\nu}$ = 2997, 2947, 1759

# 13. Polylactide-metallodrug conjugates

## 13.1. Rhenium conjugates

**PLA-HMP-Re(CO)$_3$(bipy)OTf** $Re(CO)_3$(bipy)Br (90 mg, 0.18 mmol) and silver triflate (51 mg, 0.20 mmol) were dissolved in dry acetone under a nitrogen atmosphere and refluxed for 1 hour. Silver bromide precipitate was filtered out and the filtrate added to an acetone solution of PLA-HMP (0.17 mg, 0.090 mmol). The mixture was refluxed for 2 hours and stirred at room temperature for 72 hours. The solvent was removed in vacuo and the residue dissolved in minimal dichloromethane. To this was added approx. 80 mL diethyl ether to precipitate the product. The product was filtered out and washed twice with diethyl ether (0.17 g, 72 % yield).

$^1$H NMR ($CDCl_3$, 200 MHz), $\delta$ = 9.13 (d, 2H, bipyC6-H), 8.78 (d, 2H, bipyC3-H, $^3J_{HH}$ = 8.22), 8.34 (m, 2H, bipyC5-H), 8.26 (d, 1H, pyC2-H, $J_{HH}$ = 1.72), 8.08 (m, 1H, pyC6-H), 7.78 (m, 3H, bipyC4-H, pyC4-H), 7.41 (m, 1H, pyC5-H), 5.19 (q, PLA-CH- $^3J_{HH}$ = 7.10), 1.60 (d, PLA-$CH_3$, $^3J_{HH}$ = 7.10). MALDI-TOF, m/z: 830, 968, 1112, 1256, 1400, 1544, 1688, 1833, 1977, 2121, 2265, 2409, 2553, 2697, 2840, 2986. IR (KBr): $\tilde{\nu}$ = 3445, 2999, 2948, 2035, 1929, 1759, 1457, 1386, 1361

**PLA-HMP-Re(CO)$_3$(phen)OTf** $Re(CO)_3$(phen)Br (0.10 mg, 0.19 mmol) and silver triflate (52 mg, 0.19 mmol) were dissolved in degassed acetone under a nitrogen atmosphere. The solution was refluxed for 1 hour. The precipitated silver bromide was filtered out and the filtrate was added to a solution of PLA-HMP (0.18 g, 0.095 mmol) in acetone. The solution was refluxed for an hour and stirred for five days at room temperature. The solvent was removed in vacuo and the residue dissolved in a few mL of dichloromethane. The product was precipitated with diethyl ether and washed twice with diethyl ether. The polymer was dried under high vacuum (91 mg, 40 % yield).

$^1$H NMR ($CDCl_3$, 200 MHz), $\delta$ = 9.64 (m, 2H, phenC1/10-H), 8.86 (m, 2H, phenC3/8-H), 8.38 (m, 1H, pyC2-H), 8.27-8.18 (m, 5H, phenC5/6-H, pyC6-H, phenC2/9), 7.73 (m, 1H, pyC4-H), 7.39 (m, 1H, pyC5-H), 5.14 (q, PLA-CH- $^3J_{HH}$ = 7.10), 1.62 (d, PLA-$CH_3$, $^3J_{HH}$ =7.10). MALDI-TOF, m/z: 1424, 1496, 1568, 1640, 1712, 1785, 1857, 1929, 2001, 2073, 2145, 2217, 2289, 2361, 2433, 2505, 2577, 2721, 2865. IR (KBr): $\tilde{\nu}$ = 2035, 1926, 1759

**PLA-HMP-Re(CO)$_3$(dppz)OTf** [Re(CO)$_3$(dppz)Br] (1 eq) and silver triflate (1 eq) were dissolved in dry methanol under a nitrogen atmosphere and refluxed for 3 hours. Silver bromide precipitate was filtered out with celite and the filtrate added to an acetone solution of PLA-HMP (0.5 eq). The mixture was refluxed for 2 hours and stirred at room temperature for 72 hours. The solvent was removed in vacuo and the residue dissolved in minimal dichloromethane. The product precipitated upon addition of diethyl ether. The product was washed twice with diethyl ether and dried under high vacuum. Coordination of the lactide was incomplete, resulting in an overlap of the NMR-signals in the aromatic region.

MALDI-TOF, m/z: 1118, 1190, 1262, 1335, 1406, 1479, 1526, 1550, 1623, 1670, 1695, 1767, 1815, 1839, 1910, 1959, 1983, 2102, 2127, 2270, 2414, 2558. IR (KBr, excerpt): $\tilde{\nu}$ = 2034, 1912, 1758

## 13.2. Gold conjugates

**PLA-EtPPh$_2$-AuCl** Ph$_2$P(EtOH)-AuCl (0.23 mg, 0.50 mmol) and (3S)-cis-3,6-dimethyl-1,4-dioxane-2,5-dione (1.0 g, 7.5 mmol) were added to 50 mL of dry toluene under a nitrogen atmosphere. The solution was heated to 120 °C and 50 $\mu$L of stannous octoate were added. The solution was refluxed for 3 hours at 120 °C. The solvent was removed in vacuo and the residue dissolved in dichloromethane, which was extracted with dilute HCl, brine and water. The organic layer was separated, dried with sodium sulfate and concentrated to a few mL. The polymer was precipitated with diethyl ether, filtered out and washed with diethyl ether. The product was dried under high vacuum (0.56 g, 47 % yield).

$^1$H NMR (CDCl$_3$, 200 MHz), $\delta$ = 7,84-7,51 (m, 10H, Ph), 5.20 (q, PLA-CH, $^3J_{HH}$ = 7.09), 3.6 (m, 2H, O-CH$_2$-), 2.90 (m, 2H, -CH$_2$-P), 1.61 (d, PLA-CH$_3$,$^3J_{HH}$ = 7.09). $^{31}$P{$^1$H} NMR (CDCl$_3$, 81 MHz), $\delta$ = 23.84 MALDI-TOF, m/z: (M+Na$^+$, M-Cl$^-$) 1493, 1579, 1637, 1723,1782, 1866, 1926, 2012, 2070,2156,2214,2300, 2358, 2444, 2502, 2588, 2646, 2732, 2790, 2862, 2934, 3006, 3078, 3150, 3222, 3367 IR (KBr): $\tilde{\nu}$ = 2998, 2947, 1759

**MeO-PLA-PPh$_2$-AuCl** MeO-PLA (0.37 g, 0.18 mmol) and triethylamine (33 mg, 0.32 mmol) were dissolved in dry dichloromethane under a nitrogen atmosphere. Chlorodiphenylphosphane (74 mg, 0.32 mmol) was added dropwise and the solution was stirred at room temperature for 3 hours, whereupon (tht)AuCl (101 mg, 0.32 mmol) was added and the solution stirred for another hour. The solution was extracted with 10 mL 0.1 M HCl, brine and water, respectively. The aqueous phases were reextracted with dichloromethane and the combined organic phases subsequently dried over anhydrous sodium sulfate. The solvent was evaporated to a few mL and the polymer was precipi-

tated with diethyl ether, filtered out and washed with diethyl ether. The product was dried under high vacuum (0.38 g, 86 % yield).

$^1$H NMR ($CDCl_3$, 200 MHz), $\delta$ = 7,85-7,49 (m, 10H, Ph), 5.20 (q, PLA-CH, $^3J_{HH}$ = 7.10), 3.78 (s, 3H, O-$CH_3$), 1.61 (d, PLA-$CH_3$, $^3J_{HH}$ = 7.10). $^{31}$P{$^1$H} NMR ($CDCl_3$, 81 MHz), $\delta$ = 114.58 MALDI-TOF, m/z: (M+$Na^+$) 1709, 1781, 1853, 1925, 1997, 2069, 2142, 2214, 2286, 2358, 2430, 2502, 2574, 2646, 2718, 2790, 2862, 2934, 3006, 3078, 3150, 3222, 3294, 3366, 3438, 3510, 3582, 3654, 3726

**HPMAn-PLA-$PPh_2$-AuCl** HPMAn-PLA (2.0 g, 0.91 mmol) and triethylamine (0.11 g, 1.1 mmol) were dissolved in dry dichloromethane under a nitrogen atmosphere. Chlorodiphenylphosphane (0.25 g, 1.1 mmol) was added dropwise and the solution was stirred at room temperature for 3 hours, whereupon (tht)AuCl (0.35 g, 1.1 mmol) was added and the solution stirred for another hour. The solution was extracted with 10 mL 0.1 M HCl, brine and $H_2O$, respectively. The aqueous phases were reextracted with dichloromethane and the combined organic phases subsequently dried over sodium sulfate. The solvent was evaporated to a few mL and the polymer was precipitated with diethyl ether, filtered out and washed with diethyl ether. The product was dried under high vacuum (2.1 g, 87 % yield)

$^1$H NMR ($CDCl_3$, 200 MHz), $\delta$ = 7,84-7,48 (m, 10H, Ph), 6.30 (1H, -NH), 5.73 (d, 1H, vinylH-trans), 5.34 (s, 1H, vinylH-cis), 5.19 (q, PLA-CH, $^3J_{HH}$ = 7.10), 3.76-3.18 (m, 3H, HPMA-$CH_2$, HPMA-CH), 1.98 (s, 3H, HPMA-$CH_3$), 1.61 (d, PLA-$CH_3$, $^3J_{HH}$ = 7.10), 1.24 (d, 3H, HPMA-$CH_3$). $^{31}$P{$^1$H} NMR ($CDCl_3$, 81 MHz), $\delta$ = 114.56 MALDI-TOF, m/z: (M+$H^+$) 2003, 2147, 2219, 2291, 2363, 2435, 2507, 2579, 2651, 2723, 2795, 2867,2939, 3011, 3083, 3155, 3227, 3299, 3371, 3443, 3515, 3587, 3659, 3731, 3803, 3875. IR (KBr): $\tilde{\nu}$ = 2998, 2947, 1759, 1457

# 14. RAFT polymerisation of methacrylates

**Dithiobenzoyldisulfide** Synthesis adapted from [62]. A solution of sodium methoxide (54 g in 400 mL methanol, 1.0 mol) was added to the flask via cannula, followed by rapid addition of elememtal sulfur (32 g, 1.0 mol). Benzyl chloride (63 g, 0.50 mol) was then added dropwise over a period of 1 h under a dry nitrogen atmosphere. The reaction mixture was heated in an oil bath at 70 °C for 10 h. After this time, the reaction mixture was cooled to 0 °C using an ice bath. The precipitated salt was removed by filtration and the solvent removed in vacuo. To the residue 0.5 L of deionized water were added and the solution was filtered a second time and then transferred to a 2 L separatory funnel. The sodium dithiobenzoate solution was washed three times with 200 mL of diethyl ether. 200 mL diethyl ether and 500 mL 1.0 M HCl were added, and dithiobenzoic acid was extracted into the ethereal layer. 300 mL Deionized water and 600 mL 1.0 M NaOH were added whereupon sodium dithiobenzoate was extracted to the aqueous layer. This washing process was repeated two more times to finally yield a, aqueous solution of sodium dithiobenzoate. Potassium ferricyanide(III) solution was added dropwise to the sodium dithiobenzoate via an addition funnel over a period of 1 h under vigorous stirring until no further precipitation occured. The red precipitate was filtered and washed with deionized water until the washings became colorless. The solid was dried in vacuo at room temperature overnight. (53 g, 68 % yield).

**2-Cyanoisopropyl dithiobenzoate** Synthesis adapted from [60]. 2,2'-Azobis(2-methylpropionitrile) (0.55 g) and bis(thiobenzoyl) disulfide (0.68 g) were dissolved in 30 mL ethyl acetate and the solution was heated at reflux for 18 hours. After removal of the solvent in vacuo, the crude product was subjected to column chromatography (Kieselgel-60, 70-230 mesh) with ethyl acetate/n-hexane 1:9 as eluent, to afford 2-cyanoisopropyl dithiobenzoate as a red oil. On keeping in a freezer at −20 °C, the product turned into a red solid.

$^1$H NMR ($CDCl_3$, 200 MHz), $\delta = 7.9$ (m, 2H, ArH), 7.6 (m, 1H, ArH), 7.4 (m, 2H, ArH), 1.98 (s, 6H, $CH_3$). GC-MS, RT 9.05 min, m/z: 221 [$M^+$], 153 [Ph-$CS_2^+$], 121 [Ph-$CS^+$], 77 [$Ph^+$]

**HPMAn - N-(2-Hydroxypropyl)methacrylamide** Synthesis modified from[24, 98]. 1-Aminopropanol-2 (21 g, 0.21 mol) was dissolved in methanol (120 mL). The solution was cooled to 0 °C and potassium hydroxide (2 M, aqueous) added until the pH was 8-9. Methacryloyl chloride (15 g, 0.20 mol) in THF (120 mL) were slowly added to the solution. Potassium hydroxide was added throughout the reaction to maintain the solution pH at 8-9. The solution was stirred for 4 hours at room temperature. The solvent was evaporated at room temperature under high vacuum. 200 mL of ethanol were added to the residue, the potassium chloride salts were filtered out and the solvent evaporated. The product was dissolved in dichloromethane, polymeric byproducts are filtered out. The product crystallizes from dichloromethane at −20 °C (20 g, 72 % yield).

$^1$H NMR ($CDCl_3$, 200 MHz), $\delta$ = 6.51 (s, 1H, -NH), 5.76 (s, 1H, vinylH-trans), 5.38 (s, 1H, vinylH-cis), 3.98 (m, 1H, -CH), 3.51 (m, 1H -$CH_2$), 3.08 (m, 1H -$CH_2$), 1.99 (s, 3H, $H_2C$=C-$CH_3$), 1.23 (d, 3H, $^3J_{HH}$ = 6.30). GC-MS, RT 5.42 min, m/z: 128 [$M^+ - CH_3$], 99 [$M^+ - C_2H_4OH$], 85 [$M^+ - C_3H_5OH$], 69 [$M^+ - NHC_3H_6OH$]

**HPMA-co-HPMA-PLA** Synthesis modified from[57]. A Schlenk tube was charged with HPMA-PLA (2.4 g, 2.8 mmol) and (2-hydroxypropyl)methacrylate (2.0 g, 14 mmol) under a nitrogen atmosphere, 10 mL of degassed acetone, 15 mg AIBN and 40 mg 2-cyanoisopropyl dithiobenzoate were added. The system was heated to 60 °C for a duration of 24 hours. The solvent volume was subsequently reduced to a few mL and the product precipitated by adding the polymeric solution to a solution of acetone/diethyl ether (25:75, v/v). The polymer was washed with diethyl ether and dried under high vacuum (2.0 g, 45 % yield).

$^1$H NMR (acetone-$d_6$, 200 MHz), $\delta$ = 5.20 (m, PLA-CH), 4.4-3.6 (m, 3H, HPMA-$CH_2$, HPMA-CH), 2.0 (3H, HPMA-$CH_3$), 1.60 (m, PLA-$CH_3$), 0.8-1.4 (m, 5H, backbone-$CH_2$-, backbone-$CH_3$). GPC: Mw 67.7 kDa, Mn 52.5 kDa, Mz 82.0 kDa, Mp 70.5 kDa, PD 1.29. DLS (acetone, material RI: 1,50, material absorption: 0.01): z-average (d.nm): 9.60, PdI: 0.179. IR (KBr): $\tilde{\nu}$ = 3453, 2991, 2945, 1761, 1729

**HPMA-co-MA-PLA-HMP** A Schlenk tube was charged with MA-PLA-HMP (1.3 g, 2.8 mmol) and (2-hydroxypropyl)methacrylate (2.0 g, 14 mmol) under a nitrogen atmosphere. 10 mL of degassed acetone, 15 mg AIBN and 40 mg 2-cyanoisopropyl dithiobenzoate were added. The system was heated to 60 °C for a duration of 24 hours. The solvent volume was subsequently reduced to a few mL and the product precipitated by adding the polymeric solution to a solution of acetone/diethyl ether (25:75, v/v). The polymer was washed with diethyl ether and dried under high vacuum (2.4 g, 73 % yield). $^1$H NMR (acetone-$d_6$, 200 MHz), $\delta$ = 8.66 (m, 2H, pyC2-H, pyC6-H), 7.90 (s, 1H, pyC4-H), 7.49 (s, 1H, pyC5-H), 5.20 (m, PLA-CH), 4.5-3.6 (m, 3H, HPMA-$CH_2$, HPMA-CH), 2.1 (3H, HPMA-$CH_3$), 1.60 (m, PLA-$CH_3$), 0.8-1.4 (m, 5H, backbone-$CH_2$-, backbone-$CH_3$). IR (KBr): $\tilde{\nu}$ = 3446, 2983, 2943, 1730, 749, 712

# 15. Methacrylate-metallodrug conjugates

**HEMA-co-MA-PLA-HMP-Re(CO)$_3$(bipy)OTf** [Re(CO)$_3$(bipy)]Br (63 mg, 0.12 mmol) and silver triflate (31 mg, 0.12 mmol) were dissolved in degassed acetone under a nitrogen atmosphere. The solution was stirred for 1 hour at 60 °C . The precipitated silver bromide was filtered out and the filtrate was added to a solution of HPMAo-co-MA-PLA-HMP (71 mg, 0.059 mmol lactide sidechain) in acetone. The solution was stirred for another hour at 60 °C and subsequently stirred at room temperature for 5 days. The solvent volume was subsequently reduced to a few mL and the product precipitated by adding the polymeric solution to a solution of acetone/diethyl ether (25:75, v/v). The polymer was washed with diethyl ether and dried under high vacuum (67 mg, 69 % yield).

$^1$H NMR (acetone-d$_6$, 200 MHz), $\delta$ = 9.55 (d, 2H, bipyC6-H), 8.80 (d, 2H, bipyC3-H), 8.7-8.5 (m, 4H, bipyC5-H, pyC2-H, pyC6-H), 8.1 (m, 3H, bipyC4-H, pyC4-H), 7.58 (m, 1H, pyC5-H), 5.2 (m, PLA-CH), 4.5-3.6 (m, 3H, HPMA-CH$_2$, HPMA-CH), 2.1 (3H, HPMA-CH$_3$), 1.6 (m, PLA-CH$_3$), 0.8-1.4 (m, 5H, backbone-CH$_2$-, backbone-CH$_3$). IR (KBr): $\tilde{\nu}$ = 3450, 2981, 2942, 2035, 1937, 1728

**HPMAo-co-HPMAo-PLA-PPh$_2$-AuCl** HPMAo-co-HPMAo-PLA (0.50 g, 0.23 mmol lactide sidechain) and triethylamine (50 mg, 0.50 mmol) were dissolved in dry dichloromethane (20 mL) under a nitrogen atmosphere. Chlorodiphenylphosphane (0.10 g, 0.46 mmol) in dry dichloromethane (20 mL) was added dropwise and the solution was stirred at room temperature for three hours. (tht)AuCl (0.15 g, 0.46 mmol) was added and the solution stirred for another hour. The solvent volume was subsequently reduced to a few mL and the product precipitated by adding the polymeric solution to a solution of acetone/diethyl ether (25:75, v/v). The polymer was washed with diethyl ether and dried under high vacuum (0.44 g, 63 % yield).

$^1$H NMR (acetone-d$_6$, 200 MHz), $\delta$ = 7.84-7.48 (m, Ph), 5.2 (m, PLA-CH), 4.5-3.6 (m, HPMA-CH$_2$, HPMA-CH), 2.0 (HPMA-CH$_3$), 1.6 (m, PLA-CH$_3$), 0.8-1.4 (m, backbone-CH$_2$-, backbone-CH$_3$). $^{31}$P{$^1$H} NMR (CDCl$_3$, 81 MHz), $\delta$ = 114.56 GPC: Mw 71.4 kDa, Mn 64.6 kDa, Mz 78.2 kDa, Mp 74.0 kDa, PD 1.104, IR (KBr): $\tilde{\nu}$ = 3440, 2985, 2943, 1761, 1729, 1457, 1384, 749, 692

# Bibliography


[1] Y. Matsumura, H. Maeda, *Cancer Res.*, **1986**, 46, 6387–6392.

[2] H. Maeda, J. Wu, T. Sawa, Y. Matsumura, K. Hori, *J. Control. Release*, **2000**, 65, 271–284.

[3] S. J. Berners-Price, C. K. Mirabelli, R. K. Johnson, M. R. Mattern, F. K. McCabe, L. F. Faucette, C.-M. Sung, S.-M. Mong, P. J. Sadler, S. T. Crooke, *Cancer Res.*, **1986**, 46, 5486–5493.

[4] M. Fox, F. Szoka, J. Fréchet, *Acc. Chem. Res.*, **2009**, 42, 1141–1151.

[5] T. M. Allen, *Nat. Rev. Cancer*, **2002**, 750–763.

[6] http://bit.ly/d9GOpG.

[7] L. D. D'andrea, A. Romanelli, R. D. Stasi, C. Pedone, *Dalton Trans.*, **2010**, in press.

[8] E. Calhoun, E. Welshman, S.Brown, *Poster: Taxane-Induced Alopecia: A Historical Review of Patients with Ovarian or Breast Cancer.*

[9] E. Neuse, *Met.-Based Drugs*, **2008**, 1–19.

[10] H. Maeda, *Bioconjugate Chem*, **2010**, 21, 797–802.

[11] R. Haag, F. Kratz, *Angew. Chem. Int. Ed.*, **2006**, 45, 1198–1215.

[12] H. Ringsdorf, *J. Polym. Sci., Part A: Polym. Chem.*, **1975**, 135–153.

[13] L. Gros, H. Ringsdorf, H. Schupp, *Angew. Chem. Int. Edn. Engl.*, **1981**, 20, 305–325.

[14] P. Adiseshaiah, J. Hall, S. McNeil, *WIREs Nanomed. Nanobiotechnol.*, **2009**, 2, 99–112.

[15] R. Duncan, *Nat. Rev. Cancer*, **2006**, 6, 688–701.

[16] C. Khemtong, C. Kessinger, J. Gao, *Chem. Commun.*, **2009**, 24, 3497–3510.

[17] R. Duncan, *Nat. Rev. Drug Discovery*, **2003**, 2, 347–360.

[18] P. Rejmanova, J. Kopecek, R. Duncan, J. Lloyd, *Biomaterials*, **1985**, 6, 45–48.

[19] S. Broochini, *Encyclopedia of Controlled Drug Delivery*, Wiley, New York, **1999**.

[20] R. Chandra, R. Rustgi, *Prog. Polym. Sci.*, **1998**, 23, 1273–1335.

[21] M. Garnett, *Adv. Drug Delivery Rev.*, **2001**, 53, 171–216.

[22] T. Etrych, M. Jelínková, B. Říhová, K. Ulbrich, *J. Control. Release*, **2001**, 73, 89–102.

[23] J. Kopecek, *Eur. Polymer J.*, **1973**, 9, 7–14.

[24] J. Strohalm, J. Kopecek, *Angew. Makromol. Chem.*, **1978**, 70, 109–118.

[25] A. Nori, J. Kopecek, *Adv. Drug Delivery Rev.*, **2005**, 57, 609–636.

[26] R. Duncan, J. Kopeček, *Adv. Polymer Sci.*, **1984**, 57, 51–101.

[27] R. Duncan, L. Seymour, K. O'Hare, P. Flanagan, S. Wedge, I. Hume, K. Ulbrich, J. Strohalm, V. Subr, F. Spreafico, M. Grandi, M. Ripamonti, M. Farao, A. Suarato, *J. Control. Release*, **1992**, 19, 331–346.

[28] B. Rihova, M. Bilej, V. Vetvicka, K. Ulbrich, J. Strohalm, J. Kopecek, R. Duncan, *Biomaterials*, **1989**, 10, 335–342.

[29] T. Yeung, J. Hopewell, R. Simmonds, L. W. Seymour, R. Duncan, O. Bellini, M. Grandi, F. Spreafico, J. Strohalm, K. Ulbrich, *Cancer Chemother. Pharmacol.*, **1991**, 29, 105–111.

[30] K. Saatchi, U. Häfeli, *Dalton Trans.*, **2007**, 4439–4445.

[31] U. Menon, I. Jacobs, *Curr. Opin. Obstet. Gynecol.*, **2000**, 12, 39–42.

[32] S. Nie, Y. Xing, G. Kim, J. Simons, *Annu. Rev. Biomed. Engl.*, **2007**, 257–88.

[33] M. Bartholomä, J. Valliant, K. Maresca, J. Babich, *Chem. Commun.*, **2009**, 5, 493–512.

[34] M. Bowen, C. Orvig, *Chem. Commun.*, **2008**, 5077–5091.

[35] O. Sogbeit, J. Vaillant, *Metallotherapeutic Drugs and Metal-Based Diagnostic Agents: The Use of Metals in Medicine*, Wiley, New York, **2005**.

[36] S. Liu, *Chem. Soc. Rev.*, **2004**, 33, 445–461.

[37] R. Alberto, *Top. Curr. Chem.*, **2005**, 252, 1–44.

[38] R. Schibli, A. Schubiger, *Eur. J. Nucl. Med.*, **2002**, 29, 1529–1542.

[39] R. Alberto, R. Schibli, R. Waibel, U. Abram, *Coord. Chem. Rev.*, **1999**, 901–919.

[40] R. Alberto, K. Ortner, N. Wheatley, R. Schibli, A. Schubiger, *J. Am. Chem. Soc.*, **2001**, 123, 3135–3136.

[41] N. Lazarova, S. James, J. Babich, J. Zubieta, *Inorg. Chem. Commun.*, **2004**, 7, 1023–1026.

[42] R. Schibli, R. Schwarzbach, R. Alberto, K. Ortner, H. Schmalle, C. Dumas, A. Egli, A. Schubiger, *Bioconjugate Chem.*, **2002**, 13, 750–756.

[43] N. Billinton, A. Knight, *Anal. Biochem.*, **2001**, 291, 175–197.

[44] A. J. Amoroso, M. P. Coogan, J. E. Dunne, V. Fernández-Moreira, J. B. Hess, A. J. Hayes, D. Lloyd, C. Millet, S. J. A. Pope, C. Williams, *Chem. Commun.*, **2007**, 3066–3068.

[45] A. Gillenwater, R. Jacob, R. Richards-Kortum, *Head Neck*, **1998**, 20, 556–562.

[46] A. Juris, V. Balzani, F. Barigelletti, S. Campagna, P. Belser, A. von Zelewsky, *Coord. Chem. Rev.*, **1988**, 84, 85–277.

[47] T. J. Henly, *Coord. Chem. Rev.*, **1989**, 93, 269–274.

[48] S. Mundwiler, M. Kündig, K. Ortner, R. Alberto, *Dalton Trans.*, **2004**, 9, 1320–1328.

[49] M. Casanova, E. Zangrando, F. Munini, E. Iengo, *Dalton Trans.*, **2006**, 5033–5045.

[50] P. Kurz, B. Probst, B. Spingler, R. Alberto, *Eur. J. Inorg. Chem.*, **2006**, 15, 2966–2974.

[51] E. Abel, P. Heard, K. Orrell, *Inorg. Chim. Acta*, **1997**, 255, 65–71.

[52] C. M. Thomas, *Chem. Soc. Rev.*, **2010**, 39, 165–173.

[53] P. Kunz, M. Berghahn, N. E. Brückmann, M. Dickmeis, M. Kettel, B. Spingler, *Z. Anorg. Allg. Chem.*, **2009**, 635, 471–478.

[54] S. Penczek, A. Duda, A. Kowalski, *Macromol. Symp.*, **2000**, 157, 61–70.

[55] G. Schwach, J. Coudane, R. Engel, M. Vert, *J. Polym. Sci., Part A: Polym. Chem.*, **1997**, 35, 3431–3440.

[56] J. Clayden, N. Greeves, S. Warren, P. Wothers, *Organic Chemistry, Oxford University Press*, **2007**.

[57] M. Yanjarappa, K. Gujraty, A. Joshi, A. Saraph, R. Kane, *Biomacromolecules*, **2006**, 7, 1665–1670.

[58] J. Chiefari, Y. Chong, F. Ercole, J. Krstina, J. Jeffery, T. Le, R. Mayadunne, G. Meijs, C. Moad, G. Moad, *Macromolecules*, **1998**, 31, 5559–5562.

[59] G. Moad, E. Rizzardo, S. H. Thang, *Acc. Chem. Res.*, **2008**, 41, 1133–1142.

[60] S. Thang, Y. Chong, R. Mayadunne, *Tetrahedron Lett.*, **1999**, 40, 2435–2438.

[61] M. Benaglia, E. Rizzardo, A. Alberti, M. Guerra, *Macromolecules*, **2005**, 38, 3129–3140.

[62] Y. Mitsukami, M. Donovan, A. Lowe, *Macromolecules*, **2001**, 34, 2248–2256.

[63] I. Lorenzen, *Ann. Clin. Res.*, **1975**, 7, 195–201.

[64] J. R. Ward, *Am. J. Med.*, **1988**, 85, 39–44.

[65] T. Giraldi, G. Sava, L. Perissin, S. Zorbet, *Anticancer Res.*, **1984**, 4, 221–224.

[66] T. M. Simon, D. H. Kunishima, G. J. Vibert, A. Lorber, *Cancer*, **1979**, 44, 1965–1975.

[67] C. K. Mirabelli, R. K. Johnson, D. T. Hill, L. F. Faucette, G. R. Girard, G. Y. Kuo, *J. Med. Chem.*, **1986**, 29, 218–223.

[68] C. F. Shaw, *Chem. Rev.*, **1999**, 99, 2589–2600.

[69] E. R. T. Tiekink, *Crit. Rev. Onc. Hem.*, **2002**, 42, 225–248.

[70] S. S. Gunatilleke, A. M. Barrios, *J. Med. Chem.*, **2006**, 49, 3933–3937.

[71] G. F. Rush, P. F. Smith, G. D. Hoke, D. W. Alberts, R. M. Snyder, C. K. Mirabelli, *Toxicol. Appl. Pharmacol.*, **1987**, 90, 391–400.

[72] E. Im, A. Kazlauskas, *Exp. Eye Res.*, **2007**, 84, 383–388.

[73] M. Niedergethmann, B. Wostbrock, J. Sturm, F. Willeke, S. Post, R. Hildenbrand, *Pancreas*, **2004**, 29, 204–211.

[74] P. Lipton, *Physiol. Rev*, **1999**, 79, 1431–1568.

[75] S. S. Gunatilleke, C. A. F. Oliveira, J. A. McCammon, A. M. Barrios, *J. Biol. Inorg. Chem.*, **2008**, 13, 555–561.

[76] A. Bianchi, A. Bernardi, *J. Org. Chem*, **2006**, 71, 4565–4577.

[77] H. R. Kricheldorf, I. Kreiser-Saunders, *Makromol. Chem.*, **1990**, 191, 1057–1066.

[78] K. Issleib, H. Roloff, *Chemische Berichte*, **1965**, 98, 2091–2098.

[79] G. Muller, D. Sainz, *J. Organomet. Chem.*, **1995**, 495, 103–111.

[80] S. Grim, W. McFarlane, *Nature*, **1965**, 208, 995–996.

[81] D. Couch, S. Robinson, J. Wingfield, *J. Chem. Soc., Dalton Trans.*, **1974**, 1309–1313.

[82] D. Neradovic, M. V. Steenbergen, L. Vansteelant, Y. Meijer, C. van Nostrum, W. Hennink, *Macromolecules*, **2003**, 36, 7491–7498.

[83] Y. Noguchi, J. Wu, R. Duncan, J. Strohalm, K. Ulbrich, T. Akaike, H. Maeda, *Jpn. J. Cancer Res.*, **1998**, 89, 307–314.

[84] Y. Takakura, M. Hashida, *Pharm. Res.*, **1996**, 13, 820–831.

[85] P. KUNZ, N. BRÜCKMANN, B. SPINGLER, *Eur. J. Inorg. Chem.*, **2007**, 394–399.

[86] D. Venturoli, B. Rippe, *Am. J. Physiol. Renal. Physiol.*, **2005**, 288, 605–613.

[87] K. Ulbrich, V. Šubr, *Advanced Drug Delivery Reviews*, **2010**, 62, 150–166.

[88] C. van Nostrum, T. Veldhuis, G. Bos, W. Hennink, *Polymer*, **2004**, 45, 6779–6787.

[89] L. L. Brunton, J. S. Lazo, K. L. Parker, *Goodman and Gilman's - The Pharmacological Basis of Therapeutics*, McGraw-Hill, 11th edition, **2005**.

[90] R. Herrick, T. Brunker, C. Maus, K. Crandall, *Chem. Commun.*, **2006**, 4330–4331.

[91] N. Agorastos, L. Borsig, A. Renard, P. Antoni, G. Viola, B. Spingler, P. Kurz, R. Alberto, *Chem. Eur. J.*, **2007**, 13, 3842–3852.

[92] C. Xiong, W. Lu, R. Zhang, M. Tian, W. Tong, J. Gelovani, C. Li, *Chem. Eur. J.*, **2009**, 15, 8979–8984.

[93] P. Barbazán, R. Carballo, B. Covelo, C. Lodeiro, J. C. Lima, E. M. Vázquez-López, *Eur. J. Inorg. Chem.*, **2008**, 17, 2713–2720.

[94] C. Puckett, J. Barton, *J. Am. Chem. Soc*, **2009**, 131, 8738–8739.

[95] J. Talib, D. Harman, C. Dillon, J. Aldrich-Wright, *Dalton Trans.*, **2009**, 504–513.

[96] V. Fernández-Moreira, F. L. Thorp-Greenwood, M. P. Coogan, *Chem. Commun.*, **2010**, 1–26.

[97] J. Zisowsky, S. Koegel, S. Leyers, K. Devarakonda, M. Kassack, M. Osmak, U. Jaehde, *Biochem. Pharmacol.*, **2007**, 73, 298–307.

[98] J. Song, E. Saiz, C. Bertozzi, *J. Am. Chem. Soc.*, **1999**, 125, 1236–1243.

Herewith, I affirm that this dissertation thesis was written by myself without using any unauthorised means. Neither this dissertation nor any similar documents have been submitted to any other faculty. No unsuccessful dissertation attempts have been undertaken.